

T-4061

FABRICATION OF ALUMINUM NITRIDE
CRUCIBLES FOR MOLTEN SALT AND
PLUTONIUM COMPATIBILITY
STUDIES

by

Jeffrey Allen Phillips

ProQuest Number: 10783731

All rights reserved

INFORMATION TO ALL USERS

The quality of this reproduction is dependent upon the quality of the copy submitted.

In the unlikely event that the author did not send a complete manuscript and there are missing pages, these will be noted. Also, if material had to be removed, a note will indicate the deletion.



ProQuest 10783731

Published by ProQuest LLC (2018). Copyright of the Dissertation is held by the Author.

All rights reserved.

This work is protected against unauthorized copying under Title 17, United States Code
Microform Edition © ProQuest LLC.

ProQuest LLC.
789 East Eisenhower Parkway
P.O. Box 1346
Ann Arbor, MI 48106 – 1346

T-4061

A thesis submitted to the Faculty and the Board of Trustees of the Colorado School of Mines in partial fulfillment of the requirements for a degree of Master of Science (Materials Science).

Golden, Colorado

Date July 24, 1991

Signed:

Jeffrey Allen Phillips
Jeffrey Allen Phillips

Approved:

Gerald L. DePoorter
Dr. Gerald L. DePoorter
Thesis Advisor

Golden, Colorado

Date July 24, 1991

William D. Copeland
Dr. William D. Copeland
Professor and Coordinator,
Materials Science Department

ABSTRACT

Aluminum nitride crucibles have been fabricated utilizing an isostatic pressing technique and subsequent high temperature sintering. These crucibles were pressed from a commercial spray dried powder using calcium carbonate as a sintering additive. The crucibles were exposed at 850°C to various molten chloride salts (e.g., NaCl, KCl, and CaCl₂) and evaluated for salt release and corrosion of the ceramic crucible. Data are presented which show the effects of the salt exposure to the aluminum nitride microstructure. Additionally, the predicted high temperature exposure of aluminum nitride to plutonium oxide and plutonium metal in a chloride salt medium, as estimated by a Solgasmix computer modeling program, is detailed. Brief overviews of the direct oxide reduction (DOR) and electrorefining (ER) processes for plutonium processing are discussed. Sintering mechanisms applicable for aluminum nitride processing are also presented.

TABLE OF CONTENTS

	<u>Page</u>
ABSTRACT	iii
TABLE OF CONTENTS	iv
LIST OF FIGURES	vi
LIST OF TABLES	viii
ACKNOWLEDGEMENTS	ix
CHAPTER 1: INTRODUCTION	1
1.1 Scope of Research	2
1.2 Objective of Research	4
1.3 Research Conducted	5
1.4 Thesis Organization	7
CHAPTER 2: LITERATURE REVIEW	8
2.1 Direct Oxide Reduction	8
2.2 Ceramic Materials	13
2.2.1 Magnesium Oxide	15
2.2.2 Aluminum Oxide	16
2.2.3 Zirconium Oxide	17
2.2.4 Silicon Carbide and Silicon Nitride	18
2.2.5 Aluminum Nitride	19
2.3 Physical Properties of Aluminum Nitride	20
2.3.1 Thermal Conductivity	20
2.3.2 Thermal Coefficient of Expansion	26
2.3.3 Corrosion Resistance	27
2.4 Sintering	29
2.4.1 Solid State Sintering	33
2.4.2 Liquid Phase Assisted Sintering	35
2.4.3 Sintering of Aluminum Nitride	35
2.4.3.1 Sintering with Yttrium Oxide	37
2.4.3.2 Sintering with Calcium Carbonate ...	41
CHAPTER 3: THERMODYNAMIC CALCULATIONS	43
3.1 Solgasmix Computer Modeling	43
3.2 Ceramic Materials	46
3.2.1 Magnesium Oxide	47
3.2.2 Aluminum Oxide	49
3.2.3 Zirconium Oxide	51
3.2.4 Silicon Carbide	53

TABLE OF CONTENTS (continued)

	<u>Page</u>
3.2.5 Silicon Nitride	55
3.2.6 Aluminum Nitride	58
CHAPTER 4: EXPERIMENTAL PROCEDURES	65
4.1 Raw Materials	65
4.2 Isostatic Pressing	66
4.3 Sintering	68
4.3.1 Binder Burnout	69
4.3.2 Sintering	71
4.4 Analytical Techniques	72
4.4.1 X-ray Diffraction	73
4.4.2 Scanning Electron Microscopy	74
4.5 Molten Salt Exposure	75
4.5.1 DOR Salt Exposure	75
4.5.2 ER Salt Exposure	80
CHAPTER 5: DISCUSSION OF RESULTS	84
5.1 Fabrication Techniques	84
5.1.1 Isostatic Pressing	85
5.1.2 Sintering	85
5.2 DOR Salt Exposure	91
5.2.1 Calcium Chloride Salt	94
5.2.2 Calcium Metal/Calcium Chloride Salt	102
5.2.3 Evaluation of Corrosion	108
5.3 ER Salt Exposure	115
5.3.1 Sodium-Potassium Chloride Salt	115
5.3.2 Evaluation of Corrosion	119
CHAPTER 6: CONCLUSION	121
6.1 Enumerated Conclusions	121
6.2 Recommendations for Further Study	124
BIBLIOGRAPHY	126
APPENDICES	135
Appendix A: Solgasmix Data Files	136
Appendix B: JC-PDS X-ray Cards	148
Appendix C: X-ray Diffraction Data	175

LIST OF FIGURES

<u>Figure</u>	<u>Description</u>	<u>Page</u>
2.1	DOR vessel	9
2.2	Wetting of a liquid on a solid	14
2.3	Wurtzite crystal structure	21
2.4	Depiction of neck formation due to diffusion of matter to the contact region	34
2.5	Yttria-Alumina phase diagram	38
2.6	Parallel/Series thermal conductivity models...	40
2.7	Calcia-Alumina phase diagram	42
3.1	Gibbs free energy vs. temperature of silicon nitride and plutonium nitride	57
3.2	Gibbs free energy vs. temperature of aluminum nitride and plutonium nitride	60
4.1	Green aluminum nitride crucible dimensions ...	67
4.2	TGA results in nitrogen and air of spray dried aluminum nitride powder	70
4.3	Sybron furnace setup for DOR salt exposure ...	78
4.4	Photograph of ER salt test furnace	82
5.1	Photograph of sintered aluminum nitride crucible	86
5.2	XRD pattern of aluminum nitride powder	88
5.3	XRD pattern of spray dried aluminum nitride powder	89
5.4	XRD pattern from sintered aluminum nitride ...	90
5.5	SEM micrographs of sintered aluminum nitride at 500X and 2,000X	92
5.6	SEM micrographs of sintered aluminum nitride at 5,000X and 10,000X	93
5.7	Photographs of crucible/salt cross section ...	95
5.8	SEM micrographs of calcium chloride salt exposed aluminum nitride at 33X	96
5.9	SEM micrographs of calcium chloride salt exposed aluminum nitride at 500X	97
5.10	XRD pattern of virgin calcium chloride salt ..	100
5.11	XRD pattern of molten calcium chloride salt ..	101
5.12	XRD pattern of molten calcium metal/calcium chloride salt	103
5.13	SEM micrographs of calcium metal/calcium chloride exposed aluminum nitride at 33X	105

LIST OF FIGURES (continued)

<u>Figure</u>	<u>Description</u>	<u>Page</u>
5.14	SEM micrographs of calcium metal/calcium chloride exposed aluminum nitride at 500X and 5,000X	106
5.15	SEM micrographs of calcium metal/calcium chloride exposed aluminum nitride at 500X and 5,000X	107
5.16	XRD pattern of calcium chloride exposed aluminum nitride	111
5.17	XRD pattern of calcium chloride exposed aluminum nitride	112
5.18	SEM micrographs of sodium-potassium chloride exposed aluminum nitride at 500X and 5,000X	116
5.19	SEM micrographs of sodium-potassium chloride exposed aluminum nitride at 500X and 5,000X	117

LIST OF TABLES

<u>Table</u>	<u>Description</u>	<u>Page</u>
2.1	Physical properties of common ceramic materials	26
3.1	Thermodynamic modeling of DOR process in a magnesium oxide crucible	48
3.2	Thermodynamic modeling of DOR process in an aluminum oxide crucible	50
3.3	Thermodynamic modeling of DOR process in a zirconium oxide crucible	52
3.4	Thermodynamic modeling of DOR process in a silicon carbide crucible	54
3.5	Thermodynamic modeling of DOR process in a silicon nitride crucible	56
3.6	Thermodynamic modeling of DOR process in an aluminum nitride crucible	59
3.7	Thermodynamic modeling #1 of ER process in an aluminum nitride crucible	62
3.8	Thermodynamic modeling #2 of ER process in an aluminum nitride crucible	64
4.1	Dow Chemical spray dried aluminum nitride powder formulation	65
5.1	EDX results from calcium chloride salt exposed aluminum nitride crucible	98
5.2	EDX results from calcium metal/calcium chloride salt exposed aluminum nitride crucible	104
5.3	EDX results from sodium chloride-potassium chloride salt exposed aluminum nitride crucible	119

ACKNOWLEDGEMENTS

I want to express my sincere gratitude to my thesis advisor, Dr. Gerald DePoorter, for his guidance on this project. I also want to thank the committee members, Dr. Don Williamson, Dr. Dennis Readey, and Dr. Dave Wirth for their time spent in evaluating this work. Special thanks go to Dave for supporting and encouraging me in pursuing the Master's Degree during my employment at Coors Ceramics Company.

The Materials Development and Technology Development/Waste Chemistry departments at EG&G Rocky Flats provided financial support for this project as salary, tuition reimbursement, supplies, and time allotment. Special thanks go to Wendy Sticka, Nat Quick, Hiroko Akima, and Rowena Olsen at Rocky Flats for their assistance and support. Coors Ceramics Company also provided additional funding as salary, time allotment, and tuition reimbursement. Thanks go to Jim Stephan, Jim Collins, Rob Lucernoni, Earl Lyon, and Dean Recla at Coors Ceramics Company for their friendship, support, and assistance.

It is a pleasure to acknowledge the assistance of Dr. Jack Enloe at W.R. Grace & Company who provided aluminum nitride powder samples and Dr. Sam Khoury and Dr. Arne Knudsen

at Dow Chemical Company who aided in sintering samples for this study. Thanks go to Keith Axler and Peter Lopez at Los Alamos National Laboratory for their help in the molten salt compatibility studies, to Bob McGrew and Bob Klug at Mines for their help with the SEM, to Dr. Gerard Martins for his helpful insights in our informal discussions, and to Jae-Ho Lee for his help in photography.

I extend my thanks and love to my parents, Don and Mary Lou, who have always been supportive in my education endeavors as well as my personal life, and to my brother, Mike, for being a special friend. I also extend my thanks and love to Marley for being supportive, especially during the tougher times.

I finally want to acknowledge my wife, Karen, for her love, support, and assistance (even though she got her degree before I got mine). We have experienced some rough roads together and spent many an evening alone because of the others pursuit of this "elusive" degree, but I feel that we will be brought closer together because of this. Karen has made me a stronger person because of her determination and strong will, and I love her very much.

CHAPTER 1
INTRODUCTION

Direct oxide reduction, or DOR, is one of several methods utilized to fabricate plutonium metal from a non-metallic source material. Plutonium oxide (PuO_2) is reduced in the DOR process with the aid of a reducing agent to form plutonium metal. Reduction is typically performed in a chloride salt, or mixture of chloride salts. These salts have sufficiently low melting temperatures, are inert to the plutonium metal, and serve as a solvent for the reducing agent. Calcium metal is commonly used to reduce plutonium oxide due to its affinity for oxygen.

The ultimate goal in the direct oxide reduction process is to produce an ingot of plutonium metal from an oxide precursor. Plutonium metal is typically refined and purified in a ceramic crucible at elevated temperatures and under a non-oxidizing atmosphere. During this refinement process, the crucible must withstand a corrosive environment of molten chloride salts at temperatures of 800°C to 1050°C ; not react with the molten plutonium metal; and have sufficient thermal shock resistance to prevent failure during the thermal cycling. Potential ceramic materials for the DOR process include magnesium oxide (MgO), aluminum oxide (Al_2O_3),

zirconium oxide (ZrO_2), silicon carbide (SiC), silicon nitride (Si_3N_4), and aluminum nitride (AlN).

Aluminum nitride has recently received attention for electronic and structural applications due to its superior electrical, mechanical, and thermal properties. Aluminum nitride displays superior corrosion resistance and is typically utilized as a crucible material in processing molten aluminum. To be effective in these applications, aluminum nitride should be sintered to near-theoretical density. Sintering may produce minimal amounts of secondary phases in the grain boundaries of the microstructure. These secondary phases result from the addition of sintering additives; the sintering additives react with trace amounts of aluminum oxide in aluminum nitride to form a liquid phase. This liquid phase produces a capillary pressure between the aluminum nitride particles, drawing the particles into better contact. Sintering is enhanced by the presence of the liquid phase, and the aluminum nitride matrix is purified by the removal of aluminum oxide from the structure.

1.1 Scope of Research

Ceramic materials are used in applications ranging from electronic substrates and electronic/ionic conductors to ballistic armor. These uses are possible due to the wide

range of properties that result from the processing conditions. Processing affects the microstructure which in turn affects the final properties of the ceramic. Factors that affect the microstructure and final properties include phases present, particle size of the green and fired components, and processing temperatures.

Magnesium oxide is commonly utilized as the ceramic containment vessel in the DOR process due to its inertness to the molten chloride salt and plutonium metal; a higher purity ingot results. Magnesium oxide, however, is prone to thermal shock. The thermal shock potential limits the cycle times as the heating and cooling rates must be controlled to minimize crucible failure during the reduction operation. The chloride salt also adheres strongly to the magnesium oxide crucible on cooling. The crucible must be broken to separate the salt and metal from the ceramic; the ceramic becomes a radioactive waste material due to the exposure to plutonium metal.

Aluminum nitride is a strong covalently bonded material. It does not naturally occur. In sintering aluminum nitride, additives such as calcium carbonate or yttrium oxide are typically added to aluminum nitride powder in quantities ranging from one to eight weight percent. These additives promote liquid phase sintering; fabricated shapes may be sintered to near-theoretical density at temperatures of 1700°C

to 1800°C. Aluminum nitride has superior thermal shock resistance in comparison to magnesium oxide, thus allowing for more rapid DOR processing. Salt release from a crucible will permit multiple cycles per crucible in the DOR process and reduce the generation of radioactive wastes.

1.2 Objectives of Research

The overall objective of this research was to fabricate a calcium oxide sinter-aided aluminum nitride crucible and determine the compatibility of this crucible with molten chloride salts and plutonium metal in the DOR process. Calcium oxide sinter-aided aluminum nitride was preferred over yttrium oxide sinter-aided aluminum nitride because of 1) the presence of calcium chloride, calcium oxide, and calcium metal in the molten salts utilized in the DOR process, and 2) the higher volatility of the secondary phases formed compared with phases resulting from the addition of yttrium oxide during the aluminum nitride sintering process. The calcium oxide system may yield a higher purity crystal structure with fewer secondary phases present than in the yttrium oxide system. The secondary phases that are present in the grain boundaries may be unreactive with the calcium chloride salt due to the presence of calcium in the secondary phases.

Producing aluminum nitride powder was not an objective of

this research. A number of companies currently synthesize and formulate aluminum nitride for use as a dry pressed powder, for tape casting substrates, and for isostatically pressing large blocks. One such commercial powder was utilized to fabricate shapes to be sintered for further study. Likewise, it was not a goal of this study to fabricate shapes with maximum thermal conductivity as is desired for electronic substrate applications; high crucible thermal conductivity, however, would allow the system to cool faster through more efficient heat transfer. The objective was to provide samples with sufficient thermal shock and corrosion resistance for analysis in a corrosive chloride salt environment.

1.3 Research Conducted

Aluminum nitride crucibles were fabricated by an isostatic pressing operation. Spray dried aluminum nitride powder produced by the Dow Chemical Company, Midland, Michigan, was procured for pressing. Isostatic press and tooling equipment located at the Coors Ceramics Company, Golden, Colorado, were used for forming crucible shapes. Isostatic bag tooling controlled the green size; forming pressure controlled crucible green strength. Crucibles were pressed so that when sintered, they would be at the final size required for the molten salt studies. The crucible size (1"

diameter by 2" height) was limited by the chamber size (approximately 2" diameter by 3" to 5" height) of the furnaces used in the salt exposure testing. A seven degree taper and rounded crucible bottom were designed and pressed to permit easier salt release. Fabricated shapes were sintered at the Dow Chemical Company, Midland, Michigan.

Sintered samples were characterized by X-ray diffraction (XRD) and scanning electron microscopy (SEM), prior to exposure to the molten salt, to provide a reference point for comparison. These analyses were performed at the Colorado School of Mines, Golden, Colorado.

The molten salt compatibility studies were conducted at Los Alamos National Laboratory, Los Alamos, New Mexico. Crucibles were monitored for salt release to determine the inertness of the crucible to the salt. Corrosion determination was performed utilizing XRD and SEM. XRD was used to monitor impurity phases in the ceramic and the salt. SEM was used to investigate surface corrosion. Again, XRD and SEM analyses were performed at the Colorado School of Mines.

Plutonium compatibility studies could not be conducted during the course of this research. The furnace used for testing was being moved into a glove box for radioactive, or "hot", testing and will be operational in July, 1991. Plutonium compatibility predictions, however, were performed

with the aid of a Solgasmix computer program.

1.4 Thesis Organization

An overview of the direct oxide reduction process and aluminum nitride properties and sintering techniques are presented in Chapter 2. A brief review of the Solgasmix thermodynamic calculations used to predict reactions of the constituents is provided in Chapter 3.

The procedures used in this study to fabricate crucible shapes are discussed in Chapter 4. The procedures used to test and evaluate the material are also presented in this Chapter. A discussion of the results obtained during this research is provided in Chapter 5.

Chapter 6 contains enumerated conclusions. Additional recommendations for further study based on the experimental results obtained during this study are also presented.

CHAPTER 2

LITERATURE REVIEW

Aluminum nitride is a ceramic material that has uses in both electronic and structural applications. These applications are possible because of the material's physical properties that include high thermal conductivity (>150 W/m·K), low thermal coefficient of expansion ($4 \times 10^{-6}/^{\circ}\text{C}$), and good thermal and chemical stability in a number of environments. This chapter contains a review of the factors that influence these properties. Aluminum nitride sintering mechanisms and the direct oxide reduction (DOR) process are also discussed.

2.1 Direct Oxide Reduction

Direct oxide reduction of plutonium oxide (PuO_2) is one of several methods used in producing and refining plutonium metal. This method involves reacting plutonium oxide with a reducing agent in a chloride salt mixture. A schematic of the DOR cell is shown in Figure 2.1. Calcium metal is generally used as the reducing agent due to its affinity for oxygen with reduction performed in an inert atmosphere. The reduction reaction is listed below [Cleveland, 1970].



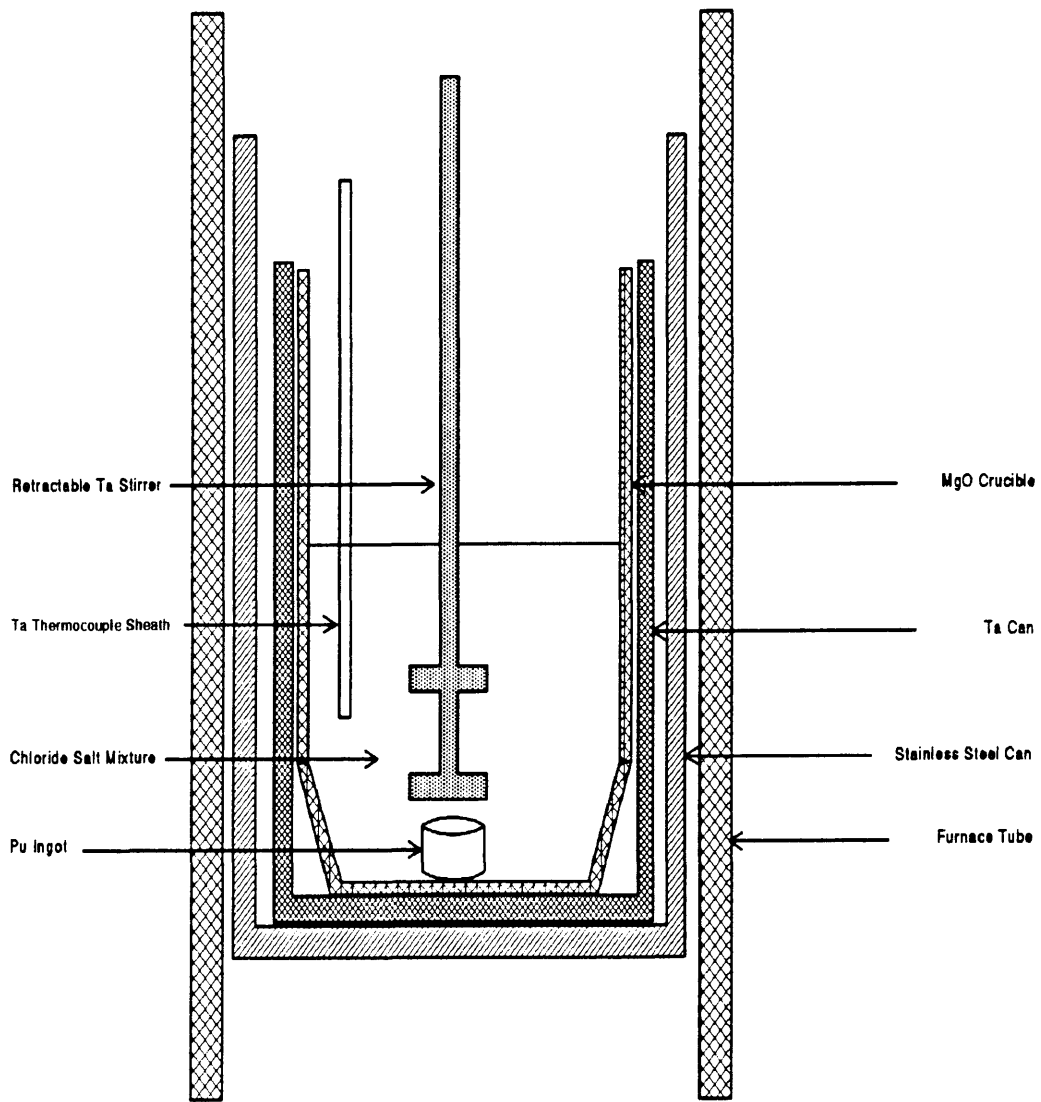


Figure 2.1: DOR vessel [Axler, 1990].

The chloride salts typically used are a mixture of potassium chloride (KCl), sodium chloride (NaCl), magnesium chloride ($MgCl_2$), and calcium chloride ($CaCl_2$). These salts are used because of their availability, high purity, low melting temperatures (below $900^\circ C$), and inertness with plutonium metal.

The DOR process is conducted in an argon purged glove box to minimize radiation exposure. The current DOR processing scheme uses a magnesium oxide crucible to melt the chloride salts. Magnesium oxide is used because of its kinetic stability in the DOR processing conditions. Raw materials are loaded into a magnesium oxide crucible and resistively heated to $850^\circ C$ to $900^\circ C$, a temperature sufficient to melt the chloride salt [Axler, 1991]. A tantalum (Ta) crucible supports the magnesium oxide containment crucible in the event of MgO crucible failure. Tantalum, a refractory metal, is capable of containing a spill of molten salt. A stainless steel can supports the tantalum crucible. When the salt is in a molten state, a retractable tantalum stirrer is lowered into the salt. The stirrer mixes the salt; the stirring action accelerates the reduction process by dispersing the calcium metal in the molten salt. The stirrer and thermocouple are retracted prior to cooling to prevent them from being frozen in the salt on cooling. The system is then held at temper-

ature to allow the plutonium metal to coalesce in the salt.

Reduced plutonium metal coalesces and settles to the bottom of the reduction crucible in the DOR process. Settling is due to the density of the plutonium metal ($\rho_{\text{Pu}} = 16.6 \text{ gm/cc}$) [Danworth, 1961] significantly exceeding that of the surrounding molten salt mixture ($\rho_{\text{KCl}} = 1.98 \text{ gm/cc}$, $\rho_{\text{NaCl}} = 2.17 \text{ gm/cc}$, $\rho_{\text{MgCl}_2} = 2.32 \text{ gm/cc}$, $\rho_{\text{CaCl}_2} = 2.15 \text{ gm/cc}$, $\rho_{\text{CaO}} = 3.30 \text{ gm/cc}$) and of the oxide precursor ($\rho_{\text{PuO}_2} = 11.5 \text{ gm/cc}$). After being extracted from the furnace, the salt and metal are removed from the crucible. The metal is physically separated from the salt for further processing (refining and machining).

After being reduced, plutonium metal is purified via an electrorefining (ER) process to remove impurities. Typical impurities include aluminum (Al), magnesium (Mg), silicon (Si), nickel (Ni), iron (Fe), and americium (Am). The ER process is also conducted in an argon purged glove box to minimize radiation exposure. The reduced plutonium and an equimolar sodium-potassium chloride salt are loaded in a two compartment magnesium oxide crucible and resistively heated to 700°C to 850°C to melt the salt [Cleveland, 1970]. The inner compartment contains the impure plutonium; the outer compartment contains the purified plutonium. A tungsten rod is immersed along the outer compartment and operates as the cathode; a tungsten lead is immersed in the impure plutonium

to serve as the anode. When the salt is in a molten state, a retractable tantalum stirrer is lowered into the salt and a d.c. voltage is applied across the circuit. Controlling the amperage across the circuit allows plutonium to plate at the cathode while impurities are isolated at the anode. Purified plutonium metal is collected at the cathode and settles to the bottom of the outer wall. The voltage is terminated when the anode salt becomes depleted in plutonium; continued operation allows impurities in the salt to electroplate at the cathode. The stirrer is retracted prior to cooling to prevent it from being frozen in the salt on cooling. The system is then held at temperature to allow the plutonium metal to coalesce in the salt.

To ease salt release and minimize plutonium contamination, the plutonium and molten salt should not wet the crucible. Wetting occurs when a material has a high solid-vapor interfacial energy (γ_{sv}) compared to the solid-liquid interfacial energy (γ_{sl}) as described by the following equations [Kingery, 1976; Hiemenz, 1986] :

$$\cos\theta = \frac{\gamma_{sv} - \gamma_{sl}}{\gamma_{lv}} \quad (2.2.1)$$

$$S_{LS} = \gamma_{sv} - (\gamma_{lv} + \gamma_{sl}) \quad (2.2.2)$$

where θ = contact angle of liquid on the solid ($^{\circ}$),
 γ_{sv} = solid-vapor interfacial energy (J/m^2),

γ_{SL} = solid-liquid interfacial energy (J/m^2),
 γ_{LV} = liquid-vapor interfacial energy (J/m^2),
and S_{LS} = spreading coefficient.

Wetting occurs when the spreading coefficient is positive and results in an increase in the overall contact surface area, as shown in Figure 2.2. The liquid (molten salt and plutonium) wets the solid (crucible) to lower the solid-vapor (crucible-argon gas) interfacial energy. Generally, liquid metals have higher surface energies than ceramic oxides. The metals, therefore, do not wet these ceramics. Non-wetting results in poor adhesion between the two [Kingery, 1976]. Non-wetting of the molten salt and plutonium metal on a ceramic crucible, therefore, will allow easier salt release from the crucible as the contact area is decreased. Minimizing the contact surface also minimizes the contamination potential of the plutonium metal from aluminum and nitrogen in the aluminum nitride crucible. Unfortunately, no data were found that would help predict the wetting behavior of the molten chloride salts and plutonium on an aluminum nitride crucible.

2.2 Ceramic Materials

Several ceramic materials may be considered for use in the direct oxide reduction process. These materials include magnesium oxide, aluminum oxide, zirconium oxide, silicon

$$\cos \theta = \frac{\gamma_{sv} - \gamma_{sl}}{\gamma_{lv}}$$

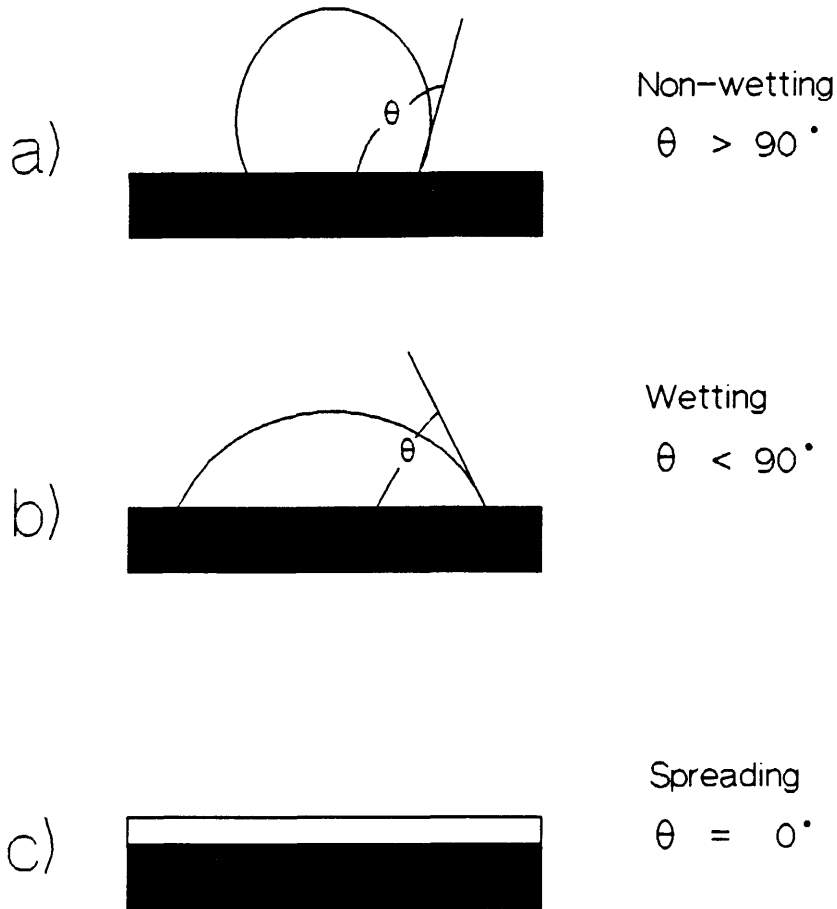


Figure 2.2: Wetting of a liquid on a solid: a) non-wetting ($\theta > 90^\circ$); b) partial wetting ($\theta < 90^\circ$); and c) spreading or complete wetting ($\theta = 0^\circ$) [Kingery, 1976; Hiemenz, 1986].

carbide, silicon nitride, and aluminum nitride. A discussion of each follows.

2.2.1 Magnesium Oxide

Magnesium oxide has been the material of choice for the direct oxide reduction of plutonium oxide. Magnesium oxide has sufficient resistance to corrosion in the molten chloride salt environment and does not react with plutonium at the DOR processing conditions. Computer modeling of this system predicts reduction of magnesium oxide. Reduction, however, is not observed in actual practice as the reaction kinetics are sufficiently slow. Computer modeling will be covered in greater detail in Chapter 3.

Magnesium oxide has a high melting temperature ($\approx 2800^{\circ}\text{C}$) and can be fabricated into crucibles with minor difficulty. Yttrium oxide is sometimes added to the magnesium oxide powder (one to five weight percent) to aid the sintering kinetics but may remain as an impurity in solid solution with magnesium oxide [Roth, 1981].

One inherent drawback of magnesium oxide is its poor thermal shock resistance. The poor thermal shock resistance is due in part to the material's high thermal expansion of $9 \times 10^{-6}/^{\circ}\text{C}$ to $13.5 \times 10^{-6}/^{\circ}\text{C}$. Rapid heating and cooling rates are infeasible due to the likelihood of crucible failure.

Slower heating and cooling rates compensate for the failure potential, but the disadvantage is reduced production capacity from the longer cycle times. The chloride salt also strongly adheres to the magnesium oxide crucible on cooling. One can conclude that this adhesion is due to the molten salt wetting the crucible. Because of the salt adhesion, the crucible must be broken to remove the salt and reduced metal [Lopez, 1991]; one crucible is used per DOR cycle and becomes a radioactive waste from the exposure to plutonium. A crucible capable of withstanding multiple DOR cycles would thus reduce the generation of this waste material.

2.2.2 Aluminum Oxide

Aluminum oxide, or alumina, is another potential ceramic material for the direct oxide reduction of plutonium oxide. Alumina is used extensively for structural and electronic applications and is available from many sources in a wide range of purities. Purity typically ranges between 85 percent and 99.9 percent with the cost varying accordingly. The melting temperature ($\approx 2020^{\circ}\text{C}$) is satisfactory to allow for adequate operation at the temperatures used in the DOR process. Alumina is also routinely used in corrosive environments. Molten carbonate salts, however, have caused extensive corrosion on aluminum oxide test samples. Ceramic

degradation increases with decreasing alumina purity. Sintering additives (e.g., SiO_2 , MgO) used in the fabrication process form glassy phases in the ceramic microstructure. The glassy phase limits the performance of the alumina as the glass softens at lower operating temperatures [Coyle, 1985]. The thermal shock resistance is superior to that of magnesium oxide. The thermal coefficient of expansion for aluminum oxide is $6.5 \times 10^{-6}/^\circ\text{C}$ to $9.0 \times 10^{-6}/^\circ\text{C}$, allowing for more rapid heating and cooling rates.

The primary drawback with aluminum oxide, as will be discussed in Chapter 3, is that it is predicted by thermodynamic modeling to degrade in the molten chloride salt. This degradation yields incomplete reduction of the plutonium oxide. The final purity of the plutonium ingot is affected as other plutonium species are predicted to form.

2.2.3 Zirconium Oxide

Zirconium oxide, or zirconia, has also recently surfaced as a leading ceramic material for various structural applications. Zirconia may be doped with magnesium oxide, yttrium oxide, or calcium oxide. These additives transform the zirconia crystalline structure from a monoclinic to a tetragonal/cubic crystal. The tetragonal/cubic crystalline structure results in improved thermal shock resistance on

heating and cooling. The transformation is also in part responsible for an improved strength by resisting crack propagation through the matrix. The high melting temperature ($\approx 2800^{\circ}\text{C}$) also gives an ample differential for the DOR operating temperatures of 800°C to 1050°C .

Like the alumina crucible, a zirconia crucible is predicted to degrade in the molten chloride salt. This degradation is estimated from the thermodynamic modeling of the reduction reaction. Thermodynamic modeling is discussed in greater detail in Chapter 3.

2.2.4 Silicon Carbide and Silicon Nitride

Silicon carbide and silicon nitride have been shown to have superior mechanical, electrical, and thermal properties when compared to many oxide ceramics. This superiority would seem to merit greater interest in these materials as potential vessels in the DOR process. These materials, however, have been shown to degrade in a molten alkali salt environment [Henager, 1989; Fox, 1989; Price, 1989]. Degradation leads to crack growth and reduced strength of the ceramic.

Silicon carbide and silicon nitride form a protective oxide coating on the surface [Henager, 1989] in a molten alkali salt. This coating forms alkali silicates which have lower operating temperatures than the silicon carbide and

nitride. The coating may fail due to a thermal expansion mismatch or from further degradation by the salt.

Silicon carbide is predicted to be stable in the DOR processing; silicon nitride is predicted to degrade in DOR conditions. Computer modeling of these materials is covered in greater detail in Chapter 3.

2.2.5 Aluminum Nitride

Aluminum nitride has received considerable attention recently as a leading ceramic for electronic and structural applications. Aluminum nitride provides excellent thermal shock resistance which allows for faster cycling and increased production. Aluminum nitride is also stable in an inert atmosphere at the DOR operating temperatures.

Aluminum nitride is a covalently bonded ceramic material. Covalently bonded materials are typically difficult to sinter; aluminum nitride sintering is aided with additions of yttrium oxide or calcium oxide (added as calcium carbonate or oxide). Aluminum nitride sintered with additions of calcium oxide is particularly attractive due to the presence of calcium oxide, calcium chloride, and calcium metal in the DOR salt mixture. Densification of aluminum nitride is assisted by the formation of a liquid phase. The liquid phase results from a chemical reaction between the sintering additive and alumina, an

impurity in aluminum nitride. The liquid phase creates a capillary pressure that draws the particles into increased contact, improving particle arrangement. Ideally, the liquid phase volatilizes at the sintering temperatures, thus purifying the structure. Typically, the phase diffuses to the grain boundaries, and subsequently to the triple points in the microstructure.

2.3 Physical Properties of Aluminum Nitride

Aluminum nitride (AlN) is a strongly bonded covalent material with the hexagonal wurtzite crystal structure [Iwase, 1984; Kurokawa, 1985] (refer to Figure 2.3). Ceramic materials with this structure typically have a high melting point (sublimation temperature $\approx 2450^{\circ}\text{C}$), high thermal conductivity ($\kappa_{\text{theoretical}} = 320 \text{ W/m}\cdot\text{K}$), low coefficient of thermal expansion ($\text{TCE} = 4.3 \times 10^{-6}$), and good corrosion resistance in oxidizing and reducing environments. When sintered to near-theoretical density of 3.26 gm/cc , a translucent ceramic material may be produced [Kuramoto, 1986a]. The translucency indicates a high purity ceramic in near-single crystalline form.

2.3.1 Thermal Conductivity

Thermal conductivity is a measure of a material's ability to conduct heat and is expressed in power (usually Watts) per

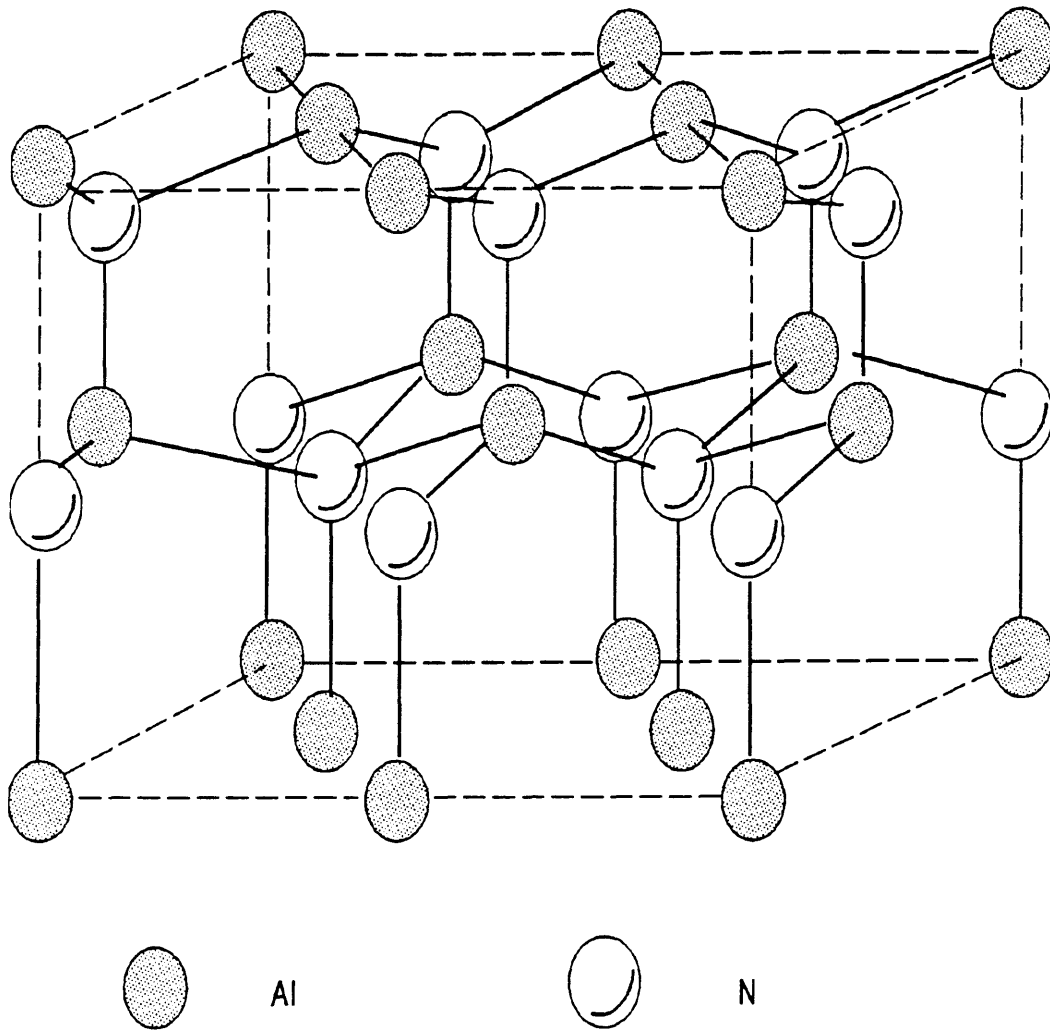


Figure 2.3: Wurtzite crystal structure [Kingery, 1976].

unit length (centimeters or meters) per unit temperature (Kelvin). Thermal conductivity may be measured with a number of techniques. The laser flash method is generally considered to be the most rapid [Dettmer, 1989]. This method involves striking one surface of the material being evaluated with a laser pulse. The temperature is measured at the opposite face either by a contact thermocouple or an optical sensor, allowing for quick determination of the thermal conductivity. This method allows a number of samples to be tested in a relatively short period of time.

Thermal conductivity is related to the structural imperfections in a crystalline lattice. In ceramic materials, phonons are primarily responsible for thermal conductivity [Slack, 1973]. As the number of phonon scattering sites increases for a particular material, the thermal conductivity decreases. Scattering may be due to lattice vacancies, impurities, or anharmonic oscillation. The thermal conductivity can be calculated from the lattice contribution due to phonon scattering. This relationship is as follows [Kittel, 1986]:

$$\kappa = \frac{1}{2}Cv\ell \quad (2.3)$$

where κ = thermal conductivity (W/m·K)
 C = heat capacity (J/m³·K),
 v = phonon velocity (m/sec), and
 ℓ = phonon mean free path (m).

As the number of scattering sites increases, the phonon mean free path decreases, thus lowering the thermal conductivity.

A material's thermal conductivity is also dependent on the atomic size and bond strength. This dependence is valid in the range from absolute zero ($T = 0$ K) to the Debye temperature ($T = \theta$ K). Thermal conductivity may be expressed by the following equation [Slack, 1973]:

$$\kappa = \frac{BM\delta^3\theta}{T\gamma^2}, \quad (2.4)$$

where

- B = a constant,
- M = average atomic mass (gm or kg),
- δ^3 = average crystal volume (cm^3 or m^3),
- θ = Debye temperature (K),
- T = absolute system temperature (K), and
- γ = Grüneisen's constant.

Materials with a higher Debye temperature will typically have higher thermal conductivities. From equation 2.4, one can deduce that crystals with large crystal volumes and comparable atomic weights (e.g., Be and O) have higher values of thermal conductivity as the term $M\delta^3\theta$ dominates the equation. The adamantine or diamond, wurtzite, and zincblende structures are examples of such crystal structures. Crystals with large differences in the atomic weights (e.g., O and U) have lower thermal conductivities due to anharmonic oscillations produced

in the crystal lattice.

There are four general conditions for predicting whether or not a crystal will have a high thermal conductivity. These conditions follow [Borom, 1972; Slack, 1973]:

- 1) low atomic mass,
- 2) strong atomic bonding,
- 3) simple crystal structure, and
- 4) anharmonicity.

According to Slack, materials with a low atomic mass and/or those strongly bonded will have a high Debye temperature and thus a high thermal conductivity. Crystalline structures with a small number of atoms per primitive crystal cell or simple crystalline structures will also tend to have a high thermal conductivity when compared to more complex structures. As the number of atoms per cell increases, so does the number of phonon scattering sites; thermal conductivity decreases with increased phonon scattering. Lattice imperfections also give rise to phonon scattering. These lattice imperfections produce anharmonic vibrations within the crystalline lattice which decrease the phonon mean free path and thermal conductivity [Kingery, 1976]. Possible sources for anharmonicity include vacant sites, dislocations, impurities in the crystalline lattice, and large differences in atomic weight and size.

As stated above, aluminum nitride has the wurtzite crystal structure and a theoretical thermal conductivity of 320 W/m·K. This value, however, is seldom observed due to defects produced in processing or those inherent to the crystal structure [Kurokawa, 1985]. Examples of inherent defects are vacant aluminum or nitrogen sites or impurities on one or more of these sites.

A typical impurity in aluminum nitride is aluminum oxide (Al_2O_3) present as $\text{Al}_{0.67}\text{O}$ [Slack, 1987]. The presence of the oxygen in the structure creates vacancies at the aluminum sites [Virkar, 1989]. The thermal conductivity is lowered due to phonon scattering from the increased disorder in the structure [Slack, 1987]. Another defect that yields similar results is porosity in the crystal structure. Porosity may result from incomplete densification during the sintering process or from inadequate pressing. Sintering will be addressed subsequently in this chapter.

Aluminum nitride competes with beryllium oxide (BeO) for high thermal conductivity. Beryllium oxide, from the data shown in Table 2.1, has a higher thermal conductivity than does aluminum nitride. Beryllium oxide, however, is toxic in nature and its use is being restricted in industrial and government applications [Werdecker, 1984; Blum, 1989]. Aluminum nitride is a likely and attractive alternative as it

does not exhibit this toxic nature.

2.3.2 Thermal Coefficient of Expansion

The thermal coefficient of expansion (TCE) is related to the bonding strength within the crystal structure. The TCE for aluminum nitride at room temperature is $4.3 \times 10^{-6}/^{\circ}\text{C}$, and closely matches that for silicon in the temperature range 0°C to 1000°C [Kuramoto, 1986a], making aluminum nitride an attractive material for electronic applications. Reported thermal conductivity and thermal expansion values for aluminum nitride and competing materials are listed in Table 2.1.

Currently, magnesium oxide is the choice crucible material in the plutonium direct oxide reduction process. Magnesium oxide is primarily an ionically bonded material comprised of Mg^{2+} and O^{2-} ions and is therefore non-directional

TABLE 2.1
Physical Properties of Common Ceramic Materials

<u>Material</u>	<u>κ (W/m·K)</u>	<u>$\alpha \times 10^6$ ($/^{\circ}\text{C}$)</u>
MgO	30-60	9-13.5
Al_2O_3	15-20	6.5-9
ZrO_2 (PSZ)	2	8.0-10.6
SiC	60-150	4.3
Si_3N_4	10-30	3.0
AlN	130-160	2.7-4.3
BeO	230-260	3.0

[American Ceramic Society, 1991; Tokuyama Soda, 1986; Keramont, 1986]

with respect to the bond strength; covalently bonded materials are directional with respect to bond strength [Kittel, 1986]. The TCE for magnesium oxide is $9 \times 10^{-6}/^{\circ}\text{C}$ to $13 \times 10^{-6}/^{\circ}\text{C}$, three times greater than that for aluminum nitride. While the bond strength and melting point are high for both materials, stresses created within the crystalline lattice from rapid heating or cooling decrease the thermal shock resistance for magnesium oxide.

2.3.3 Corrosion Resistance

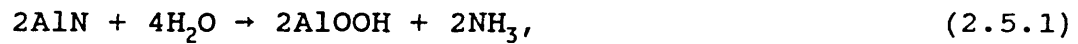
Corrosion resistance is perhaps the most important criterion concerning the direct oxide reduction process. Corrosion resistance gives an indication as to a material's ability to maintain structural and chemical integrity under harsh conditions (e.g., oxidizing or reducing atmosphere, acid exposure). Chemical breakdown of the crucible is undesirable due to potential contamination of the plutonium ingot.

Aluminum nitride is stable in an inert atmosphere to temperatures of 2200 to 2400°C at which sublimation begins to occur. Stability may vary, however, with high temperature exposure in corrosive atmospheres. In an oxidizing atmosphere, a fully dense aluminum nitride begins to oxidize at 1000°C and slowly continues to 1450°C as a protective oxide coating forms on the surface. This oxidation is termed

passive corrosion. Above 1700°C, however, oxidation proceeds rapidly due to cracking in the protective coating; a phenomenon possibly due to the thermal expansion mismatch between the oxide and nitride layers. Corrosion at these temperatures is termed active corrosion. In a reducing environment, aluminum nitride has shown good stability to 1400°C in hydrogen and to 1800°C in carbon monoxide. In a chlorine gas environment, aluminum nitride begins to decompose at 500°C as chlorine gas migrates through the structure at the grain boundaries [Werdecker, 1984; Kofstad, 1988]; higher temperatures (1500°C) yield significant sublimation. Aluminum nitride also decomposes in acidic and alkali solutions as it forms a passivating oxide layer on the surface. This passivation is similar to that observed on silicon carbide and silicon nitride [Henager, 1989]. Aluminum nitride, however, has shown good stability during exposure to molten salts and is stable with many molten metals [Marra, 1991; Werdecker, 1984].

Crucible chemical stability is critical for the DOR process. Crucible degradation may affect the purity of the plutonium ingot or cause high temperature crucible failure. There are several reports [Abid, 1986; Blum, 1989; Bowen, 1990] of a chemical reaction between aluminum nitride and water vapor at elevated temperatures. Aluminum oxide forms

from this chemical reaction as denoted by the following:



A sintered, fully dense aluminum nitride does not show such a tendency to hydrate [Werdecker, 1984]. Personal observation indicates that this reaction proceeds at room temperature as ammonia gas is commonly detectable from a container of aluminum nitride powder. Aluminum oxide is thus introduced as an impurity in the powder. Advanced Refractory Technology has developed a processing scheme that produces an aluminum nitride powder which is insensitive to moisture [Blakeley, 1990]; a higher purity powder results. This advance may make aqueous processing of aluminum nitride powders feasible. Aluminum nitride powder utilized in this study was processed in a closed loop solvent based system [Khoury, 1991]. This powder formulation will be discussed in Chapter 4.

2.4 Sintering

Sintering of ceramics may be defined as the process of forming a bond between two or more particles in contact at a temperature below the melting point [Kuczynski, 1949]. This phenomenon is associated with shrinkage, grain growth, densification, and pore removal of the compact [Reed, 1988]. The temperature dependence on the sintering kinetics is

reflected by equation 2.6 [Burke, 1958] with the mass diffusion rate exponentially dependent of the sintering temperature.

$$D = D_0 e^{-Q/RT}, \quad (2.6)$$

where D_0 = preexponential value (cm^2/sec),

Q = activation energy (J/mole),

R = gas constant ($\text{J}/\text{K}\cdot\text{mole}$), and

T = absolute temperature (K).

Sintering is typically achieved at temperatures of one-third to one-half the melting temperature for the material. Sintering is necessary to lower the total surface area of the system (a system that is not in chemical equilibrium). The thermodynamics for sintering a single phase powder is described by the following equation [Pask, 1976]:

$$\delta(G_{\text{system}}) = \delta \int \gamma_{\text{sv}} dA_{\text{sv}} + \delta \int \gamma_{\text{ss}} dA_{\text{ss}}, \quad (2.7)$$

where G = Gibbs free energy (J),

γ_{sv} = solid/vapor interface surface energy (J/m^2),

A_{sv} = solid/vapor interfacial area (m^2),

γ_{ss} = grain boundary surface energy (J/m^2), and

A_{ss} = solid/solid interfacial area (m^2).

The first term in the equation (solid-vapor) is always negative due to the decrease in surface area associated with grain growth. The second term (solid-solid) is always

positive due to an increasing grain boundary area. Sintering will continue as long as the overall equation yields a negative number, or $\delta(G_{\text{system}}) < 0$.

Other factors associated with the sintering process include the removal of organic binders or chemically attached volatile species. Chemically attached and volatile units include carbon dioxide (CO_2) and hydroxyl (OH^-) molecules that are present in many common ceramic raw materials. An example is calcium carbonate (CaCO_3) which reacts to form calcium oxide and carbon dioxide. Binders are added to the unsintered, or green, powder during a batching process. The binders give the fabricated shape adequate green strength before sintering; the green shape can be safely handled and moved from the forming area to the furnace. In removing binders, temperature control is required so that the binders decompose prior to any sufficient degree of sintering. Inadequate binder decomposition may result in entrapment of gases and subsequent porosity [Shukla, 1989].

The characteristics of the starting powder also have a strong influence on the sinterability of a material. Good sintering characteristics include a fine particle size, non-agglomerated particles, uniform powder particle size distribution, and the absence of impurities. The densification rate is inversely proportional to the particle

size [Kingery, 1976]. Therefore, small particles generally sinter with less effort than larger particles. An aggregate is a particle consisting of a number of smaller particles fused together during some processing scheme, such as calcination. Calcination is usually performed at a temperature lower than the sintering temperature with the purpose to remove organic species or initiate a chemical reaction between powders. Calcined powders, however, may undergo some degree of sintering if the reaction temperature is too high. During a subsequent sintering process, the aggregate may sinter as one unit. The tendency of the aggregate, however, to react and sinter with other particles in the matrix is reduced due to the increased particle size [Niesz, 1978]. The incomplete densification that results produces porosity in the sintered structure.

Porosity is also a function of the powder particle size distribution. A loosely packed and mono-sized powder in a close packed arrangement will have a maximum packing efficiency of 74% [Horsefield, 1934; Kingery, 1976]. The packing efficiency can be improved by filling the voids between these particles with subsequently smaller and smaller particles. If the pore volume and/or size, however, remains too high due to poor packing or an inadequate forming operation, the sintering diffusion may not be sufficient to

fill the pore space between the particles.

2.4.1 Solid State Sintering

Solid state sintering is typically modeled utilizing mono-sized spheres in contact. Sintering occurs as matter is transported to the region of contact by one of four processes: surface diffusion, lattice diffusion, grain boundary diffusion, and vapor transport [Kingery, 1976]. Grain boundary diffusion and lattice diffusion are characterized by shrinkage and neck growth. Surface diffusion and vapor transport are characterized by only neck growth. As matter is transported to a void area, the area fills, forming a neck between the particles with radius of curvature equal to $-r$ (refer to Figure 2.4). The curved surface gives rise to an accompanying pressure and vacancy differential that aids in the various diffusion mechanisms. Vacancies diffuse from regions of high concentration (e.g., neck) to regions with lower vacancy concentrations (e.g., grain boundary or lattice). Matter diffuses from the grain boundary or lattice to the neck. The particles continue to grow together so that the overall particle surface area is reduced.

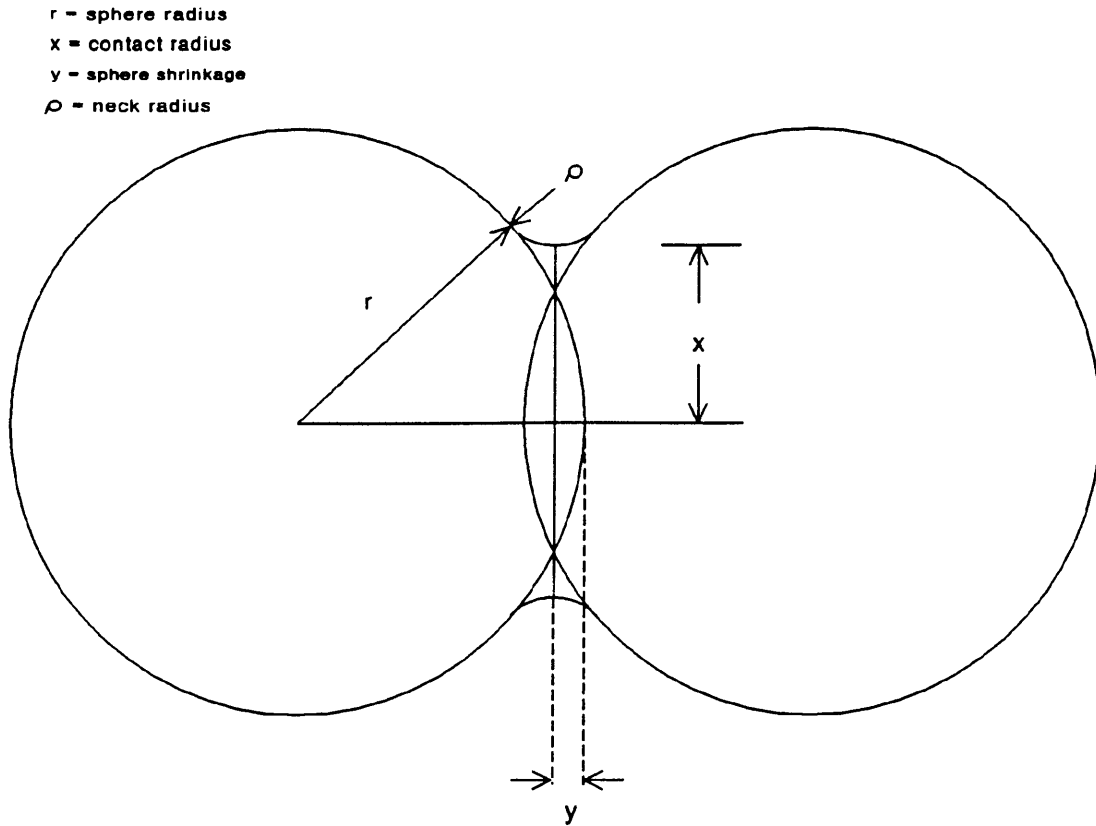


Figure 2.4: Depiction of neck formation due to diffusion of matter to the contact region [Burke, 1958].

2.4.2 Liquid Phase Assisted Sintering

The driving force behind solid state sintering is a reduction in the surface energy. The total surface energy and surface area are reduced via grain growth and diffusion of matter between particles, a process typically requiring high temperatures. Sintering with the aid of a liquid phase, however, can typically be performed at lower temperatures as the liquid tends to coat the individual grains thus forming a bonding network [Reed, 1988]. Liquid phase sintering is utilized for materials which are difficult to sinter as a single phase. One such material is aluminum nitride. The presence of the liquid draws the particles together providing for greater contact and allowing for some particle rearrangement within the matrix. The increased particle contact results in a reduced pore surface area and a higher packing efficiency. The presence of the liquid phase also aids in bonding the particles, and diffusion is enhanced due to increased contact brought about by the capillary pressure of the liquid phase [Kingery, 1958].

2.4.3 Sintering of Aluminum Nitride

As mentioned above, aluminum nitride is difficult to sinter as a single phase material. This difficulty is typical of many covalently-bonded ceramic materials including aluminum

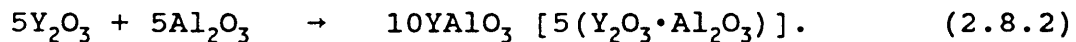
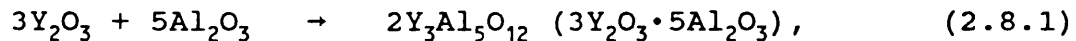
nitride, silicon nitride (Si_3N_4), silicon carbide (SiC), and boron nitride (BN) [Virkar, 1989]. A sintering aid or pressure-aided sintering technique (such as hot pressing or hot isostatic pressing) must be used to promote densification for these covalently-bonded ceramics. Hot pressing and hot isostatic pressing are more expensive alternatives than liquid-phase assisted sintering [Kingery, 1976].

In sintering aluminum nitride, a number of additives have been utilized to promote liquid-phase assisted densification. These additives include calcium carbide (CaC_2) [Kurokawa, 1986 and 1988], calcium nitrate ($\text{Ca}(\text{NO}_3)_2$) [Kuramoto, 1986a], yttrium oxide (Y_2O_3) [Kuramoto, 1986b], calcium carbonate or oxide (CaCO_3 or CaO) [Udagawa, 1990; Kuramoto, 1986b], and europium oxide (Eu_2O_3) [Van Damme, 1989]. In fact, over 30 different additives from the alkali earth oxides, lanthanum oxides, and rare earth oxides [Komeya, 1982] have proven to be successful in the liquid-phase assisted sintering of aluminum nitride. Some of these additives may improve aluminum nitride's final properties (e.g, acting as a reducing agent in removing oxygen from the structure - the thermal conductivity increases as oxygen is removed). Calcium carbide is one such additive. The sintering additive reacts with Al_2O_3 present as an impurity in the aluminum nitride powder and removes the impurity from the structure [Virkar, 1989]. The resultant

secondary phases that form from the reaction between the additive and aluminum oxide may be removed by increasing the time at the sintering temperature. Ideally, the additional soak time allows the secondary phases to volatilize and the thermal conductivity of the sintered ceramic is improved. Commonly used sintering additives include yttrium oxide and calcium carbonate.

2.4.3.1 Sintering with Yttrium Oxide

Yttrium oxide is added to aluminum nitride (up to eight weight percent) to promote densification and thereby increase the thermal conductivity [Virkar, 1989]. The impurities are diffused to the grain boundaries during the sintering process and are isolated at the triple points (grain boundary intersection of three grains forming a 120° angle at the point of contact). Two chemical reactions have been proposed and have been thermodynamically proven to occur.



The Y_2O_3 - Al_2O_3 phase diagram is shown in Figure 2.5. Excess additions (greater than 10 weight percent) of yttrium oxide degrade the thermal conductivity because a continuous coating of the secondary phase or phases forms on the aluminum nitride grains. The presence of this coating interferes with the heat

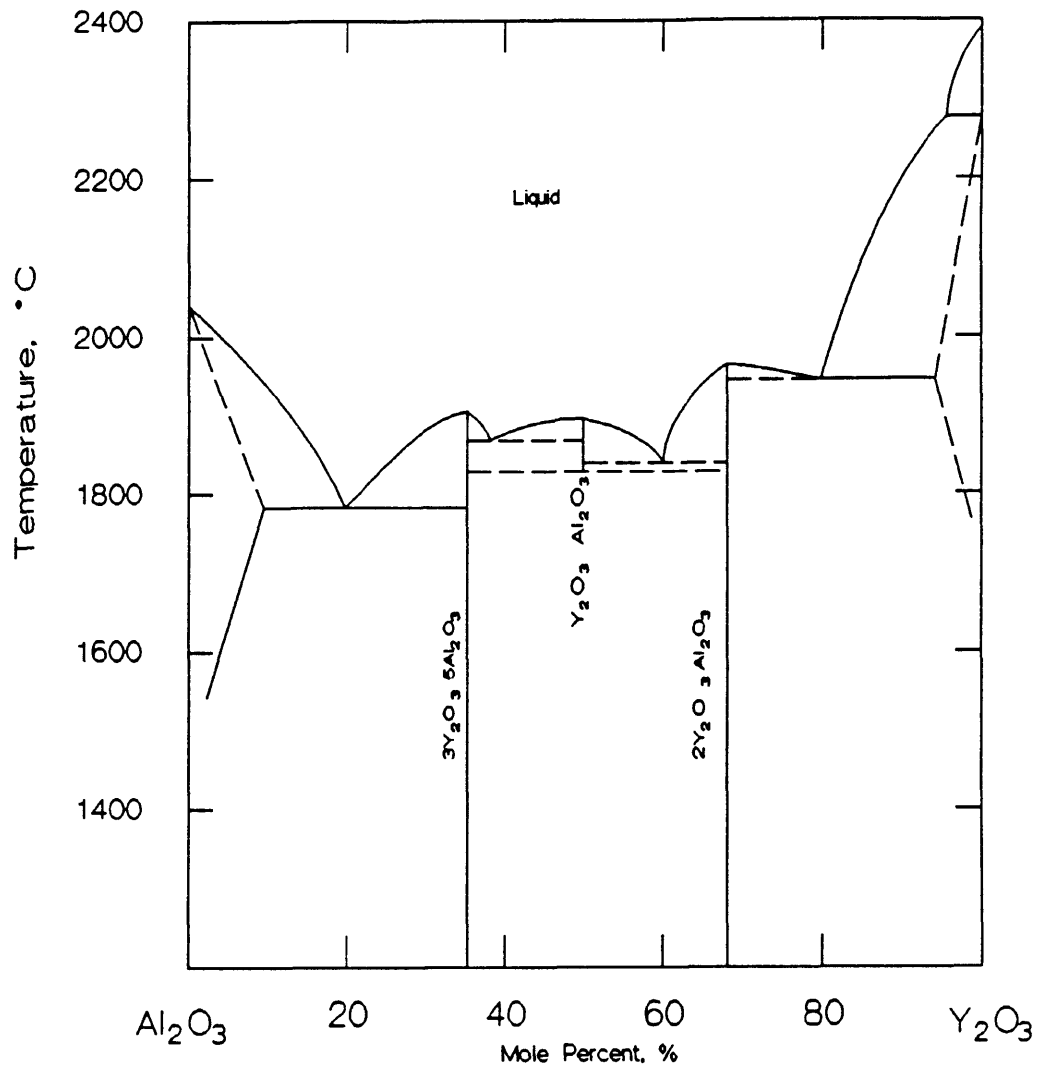


Figure 2.5: Y_2O_3 - Al_2O_3 phase diagram [Roth, 1981].

transfer through the matrix.

The overall thermal conductivity is related to the amount and location of the secondary phase. An idealized model is multi-phase ceramic with parallel and series orientations of the primary and secondary phases (refer to Figure 2.6). The total thermal conductivity is approximated by the following equations [Kingery, 1976]:

$$\kappa_{\text{parallel}} = v_1\kappa_1 + v_2\kappa_2, \text{ and} \quad (2.9)$$

$$\kappa_{\text{series}} = \frac{\kappa_1\kappa_2}{(v_1\kappa_1 + v_2\kappa_2)}, \quad (2.10)$$

where κ_1 = thermal conductivity of phase 1 (W/m·K)
 κ_2 = thermal conductivity of phase 2 (W/m·K)
 v_1 = volume fraction of phase 1 (percent), and
 v_2 = volume fraction of phase 2 (percent).

Assuming thermal conductivity values of 200 W/m·K and 10 W/m·K and volume fractions of 0.99 and 0.01 respectively for the primary and secondary phases, the overall thermal conductivity values would be 198.1 W/m·K for the parallel model and 10.1 W/m·K for the series model. The addition of the sintering additive, therefore, should be limited to promote densification and minimize the amount of secondary phases in the structure. If the amount of the secondary phase is too high (sufficient to coat the aluminum nitride grains), the thermal conductivity of aluminum nitride will be decreased.

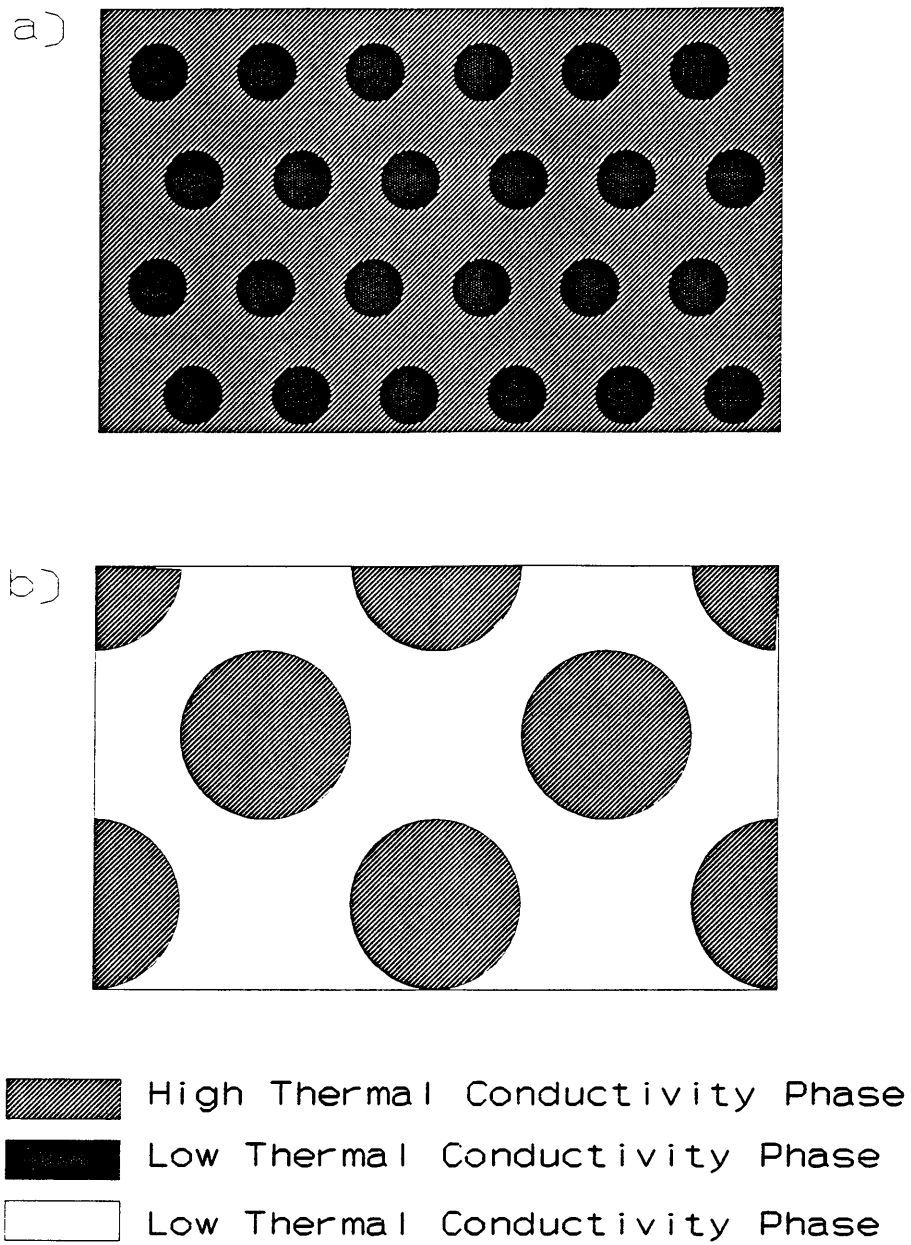
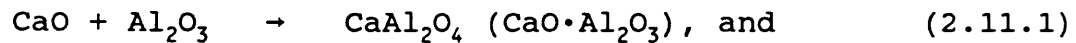


Figure 2.6: a) Parallel model, and b) series model for thermal conductivity estimation [Kingery, 1976].

Maximizing the thermal conductivity of the crucible will allow the furnace to cool more rapidly as the heat is transferred from the system. The refractory nature of the aluminum nitride will also be increased with reduced secondary phases present in the grain boundary. These phases can soften at lower operating temperatures causing the crucible to fail.

2.4.3.2 Sintering with Calcium Carbonate

Calcium carbonate is typically added to aluminum nitride in amounts that correspond to two to five weight percent of calcium oxide [Udagawa, 1990]. Calcium oxide reacts with aluminum oxide to form calcium aluminates, as shown in Figure 2.7 and listed below [Kurokawa, 1988].



Advantages in using calcium carbonate as a sintering aid over yttrium oxide are 1) lower sintering temperature, and 2) increased volatilization of the secondary phases. This is shown in Figures 2.5 and 2.7; liquid forms at a lower temperature in the CaO-Al₂O₃ system than in the Y₂O₃-Al₂O₃ system. Increasing the time at the sintering temperature may remove additional amounts of the secondary phases, further improving the physical properties of the sintered aluminum nitride from removal of the secondary phases.

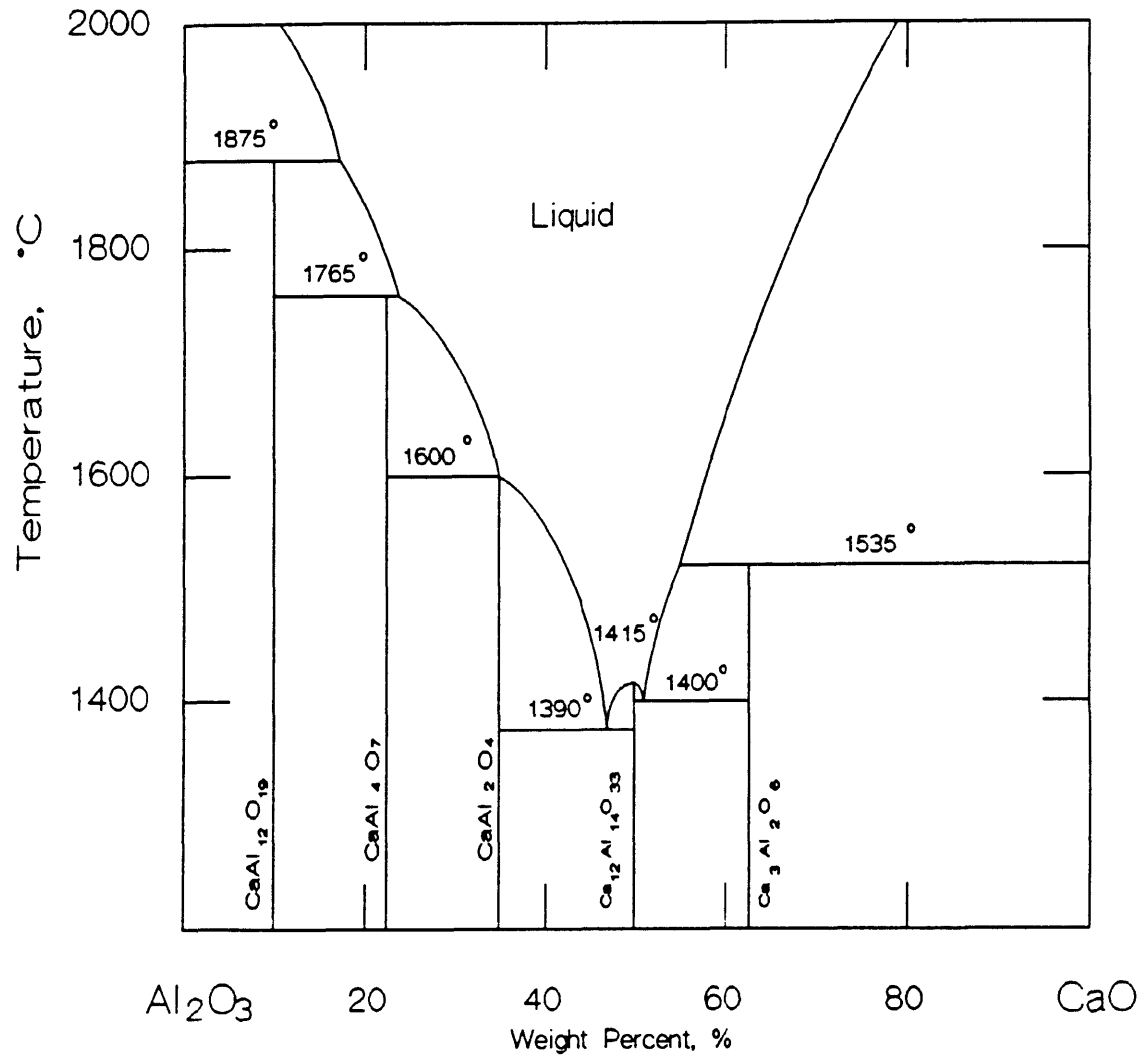


Figure 2.7: CaO-Al₂O₃ phase diagram [Levin, 1975].

CHAPTER 3

THERMODYNAMIC CALCULATIONS

This section of the thesis details the thermodynamic calculations used to predict the chemical reactions between the molten salt and plutonium mixture with the ceramic crucible materials. Solgasmix computer modeling software [Eriksson, 1975] was used to estimate the minimum free energies at a given temperature and pressure for the mixture of materials.

3.1 Solgasmix Computer Modeling

The Solgasmix software predicts the thermodynamic equilibrium reaction between a mixture of materials at selected temperatures and pressures. The software is useful when immiscible melts and non-stoichiometric solids are present or when the composition varies as a function of the pressure or temperature. Solgasmix was chosen as it was the most available software program at the time and has proven to be effective in other studies [Bagaasen, 1990; Wittmer, 1991]. The program calculates and minimizes the system free energy based on the following equation [Eriksson, 1975]:

$$(G/RT) = \sum n_i [(g^\circ/RT)_i + \ln a_i] \quad (3.1)$$

where G = total free energy of the system (J/mole),

R = gas constant (J/mole·K),
T = absolute temperature of system (K),
 n_i = amount of the i^{th} substance (moles),
 g° = standard chemical potential (J/mole), and
 a_i = activity of the i^{th} substance.

Iterations are performed during the computations until successive iterations converge on a final answer or conclude if the solution is undeterminable.

The Solgasmix software was loaded onto an IBM PS/2 Model 70 computer for all data calculations. The program calculates the possible combinations of reactants from the input information of materials, elemental quantities, temperature, and pressure. The calculations are based on the Gibbs free energy (ΔG°_f) as a function of temperature for each species being considered. The free energy-temperature relationship was calculated from the following equation [Lewis, 1961]:

$$\Delta G^\circ = a/T + b + cT + dT^2 + eT^3 + fT \ln T, \quad (3.2)$$

where a through f are calculated coefficients.

For this study, all six terms were considered. A value of zero was entered when the coefficient was unnecessary. Unknown coefficients were calculated by plotting the Gibbs free energy (ΔG°_f) [Oetting, 1967; Robie, 1978; Pankratz, 1982; Pankratz, 1984a,b; and Chase, 1986] versus temperature and determining the third order polynomial fit of the curve.

This data fit generated values for b, c, d, and e. Slide Write Plus™, a computer software package, was used to perform this data fit. In all cases where this method was utilized, the correlation coefficient (R-value) exceeded 0.999.

One limitation of the Solgasmix software version used in this model is chemical reactants considered from the reduction reaction. The user makes the decision of what materials may form in the DOR process. Actual reaction products, therefore, may inadvertently be overlooked. Other versions of the Solgasmix software contain databases for numerous compounds; reactant products are computer generated. This software version, however, was not available at the time of this study.

Solgasmix generates a table of the reactants and amounts for the output. This table is separated into five vertical columns and four horizontal sections. These sections are briefly summarized below.

The vertical sections are labeled as follows: SPECIES, X*/MOL, Y/MOL, P/ATM (MOLE FRACTION), and ACTIVITY. The 'SPECIES' column lists the chemical formulas of the individual gases, salts, and solids being considered in the reaction. These reactants are broken into three divisions that will be discussed shortly. The 'X*/MOL' column lists the starting amounts of the elemental species. Elemental quantities are input into the program; the computer calculates the

equilibrium reactant species present, 'Y/MOL'. The columns 'P/ATM' and 'MOLE FRACTION' specify the partial gas pressure and salt mole fractions respectively. The column 'ACTIVITY' designates the calculated activity values for the gases and salts.

The horizontal sections are separated into four segments. The first segment contains a list of usually three to five species present in the gas phase. The second section contains the entries 'CaCl₂' and 'CaO', the species mixed in the liquid salt phase. The third section includes all elemental species and solid compounds (typically seven to ten) that may be formed at equilibrium. The fourth section is a software generated statement of which reactants would be in the equilibrium solution given a specific free energy of formation.

3.2 Ceramic Materials

For this study, the ceramic materials discussed in Chapter 2 were modeled for predicted reactions in a molten calcium chloride (CaCl₂) salt containing plutonium oxide (PuO₂). The ceramic materials modeled are magnesium oxide (MgO), aluminum oxide (Al₂O₃), zirconium oxide (ZrO₂), silicon carbide (SiC), silicon nitride (Si₃N₄), and aluminum nitride (AlN). Thermodynamic data on these materials, materials present in the molten salt, and possible reactants were input

into the computer for each calculation. This data is included in Appendix A. Plutonium compounds considered in all calculations were Pu, PuO₂, PuOCl, and Pu₂O₃. Additional compounds (e.g., PuN and PuC) were considered for the non-oxide ceramic crucibles. Reduction of the crucibles to the constituent elemental species was also considered. Assumptions for the model were: 1) the crucible weight was 1000 moles; 2) the pressure was 1 atmosphere of argon; and 3) the system temperature was 1148 K.

3.2.1 Magnesium Oxide

The current DOR process uses magnesium oxide (MgO) as the crucible material due to magnesium oxide's stability in the molten salt and inertness to the plutonium metal. In the case for MgO, the model predicts complete reduction of 3.075 moles of PuO₂ to Pu metal and 0.3 moles of MgO reduced to Mg metal (refer to Table 3.1). The crucible, however, is not reduced under actual processing conditions. No other Pu-compounds (Pu₂O₃ and PuOCl) are predicted to form.

The results from this modeling study illustrate another limitation of the Solgasmix software. Even though the thermodynamics are favorable for magnesium oxide reduction, the reaction kinetics are significantly slow so that MgO reduction is negligible.

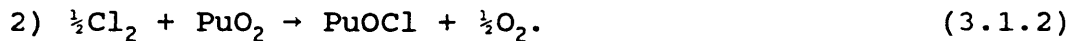
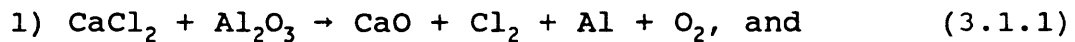
TABLE 3.1
Thermodynamic Modeling of DOR Process in MgO Crucible

SPECIES	X*/MOL	Y/MOL	P/ATM	ACTIVITY
Ar	.10000E+02	.10000E+02	.10000E+01	.10000E+01
Cl2	.45050E+02	.85228D-25	.85228D-26	.85228D-26
O2	.50308E+03	.11125D-41	.11125D-42	.11125D-42
			MOLE FRACTION	
CaCl2	.00000E+00	.45050E+02	.87476E+00	.87476E+00
CaO	.00000E+00	.64500E+01	.12524E+00	.12524E+00
Pu	.30750E+01	.30750E+01		
Ca	.51500E+02	.00000E+00		
Mg	.10000E+04	.30000E+00		
Pu2O3	.00000E+00	.00000E+00		
PuOCl	.00000E+00	.00000E+00		
MgO	.00000E+00	.99970E+03		
PuO2	.00000E+00	.00000E+00		

SPECIES NUMBER 10 (PuOCl) WOULD BE CONSIDERED IN THE EQUILIBRIUM SET OF PHASES IF ITS FREE ENERGY OF FORMATION WAS .14092E+05 J/MOLE MORE NEGATIVE.

3.2.2 Aluminum Oxide

As was stated in Chapter 2, an aluminum oxide (Al_2O_3) crucible is predicted to be unstable in the DOR processing environment (refer to Table 3.2). Alumina is predicted to reduce by 1.6375 moles in the molten chloride salt producing 3.275 moles of Al metal. The presence of Al in the salt increases the likelihood of plutonium contamination after chemical equilibrium is achieved. Table 3.2 shows an increase in the amount of CaO calculated to be present in the salt than was formed in the MgO modeling (8 moles vs. 6.5 moles). The excess CaO results from the formation of PuOCl as CaCl_2 reacts with Al_2O_3 and PuO_2 as shown in Equations 3.1.1 and 3.1.2.



3.075 moles of PuOCl are generated from the starting PuO_2 ; no Pu metal is expected to form under the proposed DOR processing conditions.

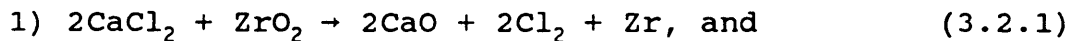
TABLE 3.2
Thermodynamic Modeling of DOR Process in Al₂O₃ Crucible

SPECIES	X*/MOL	Y/MOL	P/ATM	ACTIVITY
Ar	.10000E+02	.10000E+02	.10000E+01	.10000E+01
Cl ₂	.45050E+02	.24660D-23	.24660D-24	.24660D-24
O ₂	.15031E+04	.15311D-38	.15311D-39	.15311D-39
			MOLE FRACTION	
CaCl ₂	.00000E+00	.43513E+02	.84490E+00	.84490E+00
CaO	.00000E+00	.79875E+01	.15510E+00	.15510E+00
Pu	.30750E+01	.00000E+00		
Ca	.51500E+02	.00000E+00		
Al	.20000E+04	.32750E+01		
Pu ₂ O ₃	.00000E+00	.00000E+00		
PuOCl	.00000E+00	.30750E+01		
PuO ₂	.00000E+00	.00000E+00		
Al ₂ O ₃	.00000E+00	.99836E+03		

SPECIES NUMBER 9 (Pu₂O₃) WOULD BE CONSIDERED IN THE EQUILIBRIUM SET OF PHASES IF ITS FREE ENERGY OF FORMATION WAS .95487E+04 J/MOLE MORE NEGATIVE.

3.2.3 Zirconium Oxide

A zirconium dioxide (ZrO_2) crucible is also not predicted to be stable in the molten chloride salt (refer to Table 3.3). As shown in Table 3.3, zirconia is estimated to be reduced by 2.45 moles resulting in 2.45 moles of Zr metal present in the salt after chemical equilibrium is achieved. Excess calcium metal (0.3 moles) is calculated to be present in this example than was formed in the MgO modeling. The quantity of CaO formed at equilibrium is again greater than was present in the MgO model (7.8 moles versus 6.45 moles). The increased CaO quantity results from the formation of 2.8 moles of PuOCl and 0.15 moles Pu_2O_3 as the salt reacts with ZrO_2 and chlorine reacts with PuO_2 as shown in Equations 3.2.1 and 3.2.2.



Plutonium metal is not calculated to form at chemical equilibrium under the proposed DOR processing conditions.

TABLE 3.3
Thermodynamic Modeling of DOR Process in ZrO₂ Crucible

SPECIES	X*/MOL	Y/MOL	P/ATM	ACTIVITY
Ar	.10000E+02	.10000E+02	.10000E+01	.10000E+01
Cl2	.45050E+02	.18198D-23	.18198D-24	.18198D-24
O2	.10031E+04	.79819D-39	.79819D-40	.79819D-40
			MOLE FRACTION	
CaCl2	.00000E+00	.43658E+02	.84774E+00	.84774E+00
CaO	.00000E+00	.78415E+01	.15226E+00	.15226E+00
Pu	.30750E+01	.00000E+00		
Ca	.51500E+02	.00000E+00		
Zr	.10000E+04	.24563E+01		
Pu2O3	.00000E+00	.14598E+00		
PuOCl	.00000E+00	.27830E+01		
ZrO2	.00000E+00	.99754E+03		
PuO2	.00000E+00	.00000E+00		

SPECIES NUMBER 6 (Pu) WOULD BE CONSIDERED IN THE EQUILIBRIUM SET OF PHASES IF ITS FREE ENERGY OF FORMATION WAS .31899E+05 J/MOLE MORE NEGATIVE.

3.2.4 Silicon Carbide

Solgasmix modeling of the DOR process in a silicon carbide (SiC) crucible (refer to Table 3.4) predicts complete reduction of 3.075 moles of PuO₂ to Pu metal. SiC is also predicted to be reduced by 0.011 moles resulting in an equal amount of Si metal in the salt. Formation of various plutonium carbide compounds (PuC, PuC₂, and Pu₂C₃) and the formation of SiO₂ (cristobalite) were considered in this modeling. These phases, however, are not predicted to form at the chemical equilibrium under the proposed DOR conditions.

Based on the thermodynamic modeling results, silicon carbide merits further study as a candidate crucible material in the DOR process. The amount of Si, however, in the salt may contaminate the resultant plutonium ingot; the impurity level of Si in the resultant Pu ingot may be too excessive for successful removal by a subsequent electrorefining (ER) processing operation.

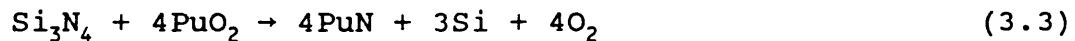
TABLE 3.4
Thermodynamic Modeling of DOR Process in SiC Crucible

SPECIES	X*/MOL	Y/MOL	P/ATM	ACTIVITY
Ar	.10000E+02	.10000E+02	.99888E+00	.99888E+00
Cl2	.45050E+02	.10394D-27	.10383D-28	.10383D-28
O2	.30750E+01	.15028D-47	.15011D-48	.15011D-48
C	.10000E+04	.11218D-01	.11206D-02	.11206D-02
			MOLE FRACTION	
CaCl2	.00000E+00	.45050E+02	.87988E+00	.87988E+00
CaO	.00000E+00	.61500E+01	.12012E+00	.12012E+00
Pu	.30750E+01	.30750E+01		
Ca	.51500E+02	.30000E+00		
Si	.10000E+04	.11218D-01		
Pu2O3	.00000E+00	.00000E+00		
PuOC1	.00000E+00	.00000E+00		
SiC	.00000E+00	.99999E+03		
PuO2	.00000E+00	.00000E+00		
PuC	.00000E+00	.00000E+00		
PuC2	.00000E+00	.00000E+00		
Pu2C3	.00000E+00	.00000E+00		
SiO2(C)	.00000E+00	.00000E+00		

SPECIES NUMBER 14 (PuC) WOULD BE CONSIDERED IN THE EQUILIBRIUM SET OF PHASES IF ITS FREE ENERGY OF FORMATION WAS .37600E+05 J/MOLE MORE NEGATIVE.

3.2.5 Silicon Nitride

Silicon nitride (Si_3N_4) is not predicted to be stable under the proposed DOR conditions (refer to Table 3.5). Silicon nitride is speculated to react with PuO_2 to form 3.075 moles of PuN as shown in Table 3.5. Free energy data (refer to Figure 3.1) show Si_3N_4 to be more stable than PuN on a molar basis. PuN, however, is more stable per mole of nitrogen (N) as the PuN free energy is lowered by a factor of four. PuN formation occurs due to the molar quantities (4 moles each) of PuO_2 and PuN dominating the system free energy as shown in the cell reduction reaction below.



Using data from Figure 3.1, the reaction free energy is approximately -475 kJ/mole. 2.31 moles of free Si metal and 0.3 moles excess Ca metal are calculated to be present in the salt, as shown in Table 3.5. The reaction for the formation for SiO_2 (cristobalite) was again considered but not predicted to occur. A second modeling study on Si_3N_4 with updated free energy data for PuN [Pankratz, 1984a] yielded identical results as 3.075 moles of PuN were again predicted to form.

TABLE 3.5
Thermodynamic Modeling of DOR Process in Si₃N₄ Crucible

SPECIES	X*/MOL	Y/MOL	P/ATM	ACTIVITY
Ar	.10000E+02	.10000E+02	.10000E+01	.10000E+01
Cl ₂	.45050E+02	.10383D-27	.10383D-28	.10383D-28
O ₂	.30750E+01	.15011D-47	.15011D-48	.15011D-48
N ₂	.20000E+04	.44213D-07	.44213D-08	.44213D-08
			MOLE FRACTION	
CaCl ₂	.00000E+00	.45050E+02	.87988E+00	.87988E+00
CaO	.00000E+00	.61500E+01	.12012E+00	.12012E+00
Pu	.30750E+01	.00000E+00		
Ca	.51500E+02	.30000E+00		
Si	.30000E+04	.23063E+01		
Pu ₂ O ₃	.00000E+00	.00000E+00		
PuOCl	.00000E+00	.00000E+00		
Si ₃ N ₄	.00000E+00	.99923E+03		
PuO ₂	.00000E+00	.00000E+00		
PuN	.00000E+00	.30750E+01		
SiO ₂ (C)	.00000E+00	.00000E+00		

SPECIES NUMBER 7 (Pu) WOULD BE CONSIDERED IN THE EQUILIBRIUM SET OF PHASES IF ITS FREE ENERGY OF FORMATION WAS .98825E+05 J/MOLE MORE NEGATIVE.

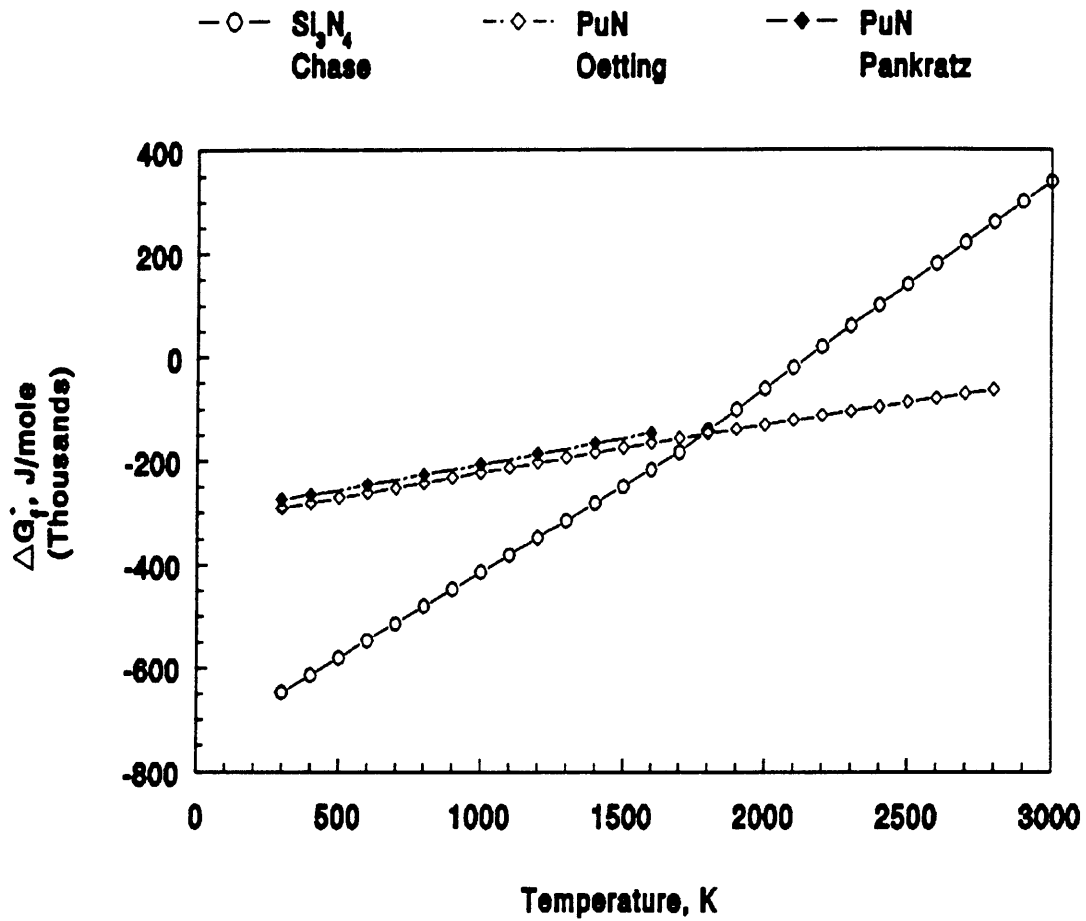


Figure 3.1: Gibbs Free Energy vs. Temperature of Si_3N_4 and PuN [Chase, 1985; Oetting, 1967; and Pankratz, 1984a].

3.2.6 Aluminum Nitride

Aluminum nitride stability in the DOR environment is uncertain. Modeling was again performed using older and newer free energy data for PuN. Aluminum nitride, like silicon nitride, is predicted to be reduced when using older free energy data for PuN. The chemical reaction with PuO₂ to form PuN is shown below.



From Table 3.6, 3.075 moles of AlN are reduced to Al metal and form 3.075 moles of PuN from the available nitrogen. Excess Ca metal (0.3 moles) is calculated to be present in the salt. PuO₂ reduction to Pu metal is not expected.

A second model utilized newer data for PuN [Pankratz, 1984a]. These data closely match the free energy of formation data for AlN, especially in the temperature region of interest for the DOR processing (refer to Figure 3.2). This model, however, did not reach chemical equilibrium. Aluminum nitride stability in the DOR environment is an unequivocal possibility. Data from Figure 3.2 shows AlN to be the more stable species at the modeling temperature (1148 K) when compared to more recent data for PuN.

TABLE 3.6
Thermodynamic Modeling of DOR Process in AlN Crucible

SPECIES	X*/MOL	Y/MOL	P/ATM	ACTIVITY
Ar	.10000E+02	.10000E+02	.10000E+01	.10000E+01
Cl2	.45050E+02	.10383D-27	.10383D-28	.10383D-28
O2	.30750E+01	.15011D-47	.15011D-48	.15011D-48
N2	.50000E+03	.19809D-16	.19809D-17	.19809D-17
			MOLE FRACTION	
CaCl2	.00000E+00	.45050E+02	.87988E+00	.87988E+00
CaO	.00000E+00	.61500E+01	.12012E+00	.12012E+00
Pu	.30750E+01	.00000E+00		
Ca	.51500E+02	.30000E+00		
Al	.10000E+04	.30750E+01		
Pu2O3	.00000E+00	.00000E+00		
PuOCl	.00000E+00	.00000E+00		
AlN	.00000E+00	.99693E+03		
PuO2	.00000E+00	.00000E+00		
PuN	.00000E+00	.30750E+01		
Al2O3	.00000E+00	.00000E+00		

SPECIES NUMBER 7 (Pu) WOULD BE CONSIDERED IN THE EQUILIBRIUM SET OF PHASES IF ITS FREE ENERGY OF FORMATION WAS .12564E+05 J/MOLE MORE NEGATIVE.

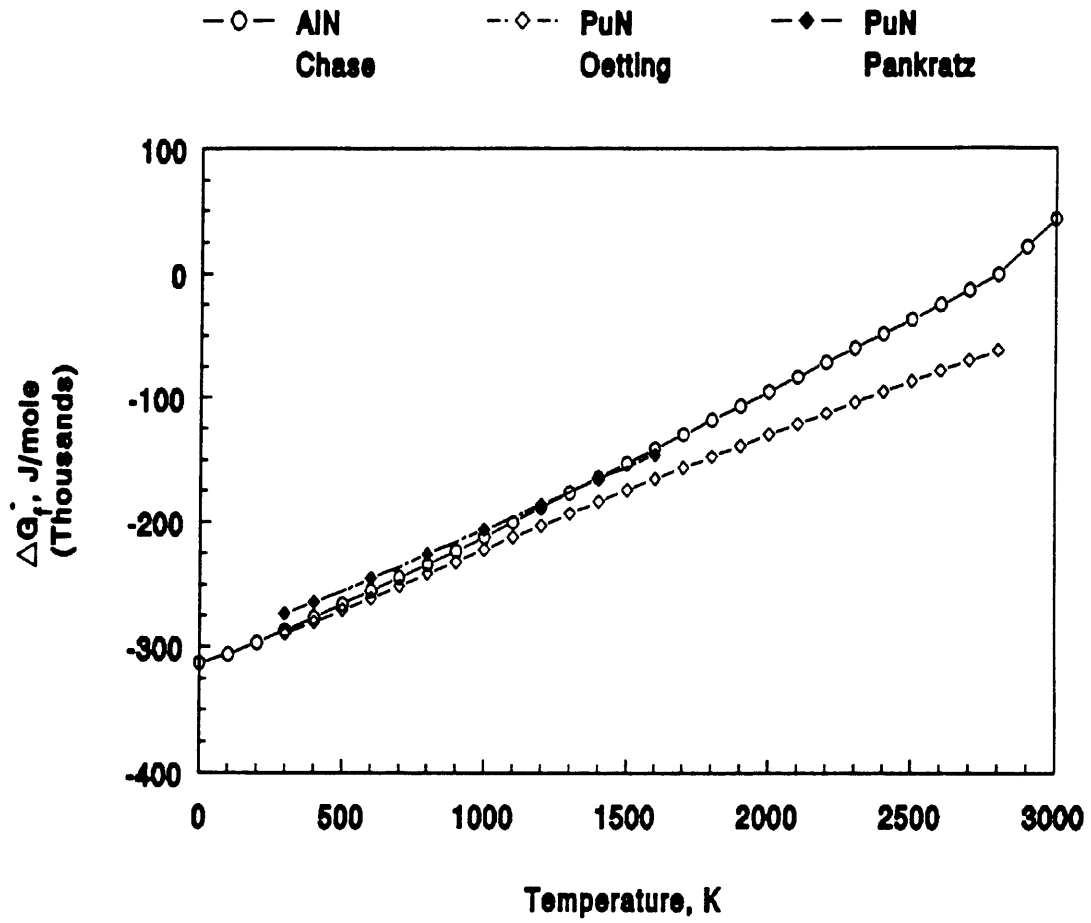


Figure 3.2: Gibbs Free Energy vs. Temperature of AlN and PuN [Chase, 1985; Oetting, 1967; and Pankratz, 1984a].

Aluminum nitride was also evaluated as a candidate material in the electrorefining (ER) of plutonium metal. Electrorefining is typically conducted in a sodium-potassium chloride (NaCl-KCl) salt or sodium-potassium-magnesium (NaCl-KCl-MgCl₂) salt with the sodium chloride and potassium chloride at equal molar ratios [Cleveland, 1970]. Calcium metal is not used in this processing scheme, and the formation of the oxide compounds can be ignored. Calculations from each salt mixture need only consider the formation of the respective gases, salts, metals, and nitride compounds (AlN and PuN) involved in the reaction.

The first calculation involved plutonium ER in a sodium-potassium chloride salt at 1148 K. Older [Oetting, 1967] and newer data [Pankratz, 1984a] for the formation of PuN were again considered. The first calculation was performed using older PuN data (refer to Table 3.7). These data estimate formation of 3.075 moles PuN from Pu. Aluminum nitride is again predicted to be reduced by 3.075 moles, as shown in Table 3.7; Al metal contamination (3.075 moles) is present in the salt. Calculations using more recent data for PuN were indeterminate.

The second calculation involved ER in a sodium-potassium-magnesium chloride salt mixture. Amounts for the individual salts were arbitrarily selected while maintaining equimolar

TABLE 3.7
Thermodynamic Modeling of ER Process in AlN Crucible

SPECIES	X*/MOL	Y/MOL	P/ATM	ACTIVITY
Ar	.10000E+02	.10000E+02	.10000E+01	.10000E+01
Cl ₂	.45050E+02	.18067D-05	.18067D-06	.18067D-06
N ₂	.50000E+03	.19807D-16	.19807D-17	.19807D-17
			MOLE FRACTION	
NaCl	.00000E+00	.45050E+02	.50000E+00	.50000E+00
KCl	.00000E+00	.45050E+02	.50000E+00	.50000E+00
Pu	.30750E+01	.00000E+00		
Na	.45050E+02	.00000E+00		
K	.45050E+02	.36134D-05		
Al	.10000E+04	.30750E+01		
AlN	.00000E+00	.99693E+03		
PuN	.00000E+00	.30750E+01		

SPECIES NUMBER 6 (Pu) WOULD BE CONSIDERED IN THE EQUILIBRIUM SET OF PHASES IF ITS FREE ENERGY OF FORMATION WAS .13389E+05 J/MOLE MORE NEGATIVE.

ratios of sodium chloride to potassium chloride. Older and newer free energy of formation data for PuN were again used. The results from this calculation (refer to Table 3.8) are nearly identical to those from the NaCl-KCl as 3.075 moles of Pu are calculated to form PuN; aluminum nitride is reduced by the same amount. Calculations using the more recent data for PuN were indeterminate.

TABLE 3.8
Thermodynamic Modeling of ER Process in AlN Crucible

SPECIES	X*/MOL	Y/MOL	P/ATM	ACTIVITY
Ar	.10000E+02	.10000E+02	.10000E+01	.10000E+01
Cl2	.45050E+02	.15985D-05	.15985D-06	.15985D-06
N2	.50000E+03	.19807D-16	.19807D-17	.19807D-17
			MOLE FRACTION	
NaCl	.00000E+00	.40000E+02	.47031E+00	.47031E+00
KCl	.00000E+00	.40000E+02	.47031E+00	.47031E+00
MgCl2	.00000E+00	.50500E+01	.59377D-01	.59377D-01
Pu	.30750E+01	.00000E+00		
Na	.40000E+02	.00000E+00		
K	.40000E+02	.31970D-05		
Mg	.50500E+01	.00000E+00		
Al	.10000E+04	.30750E+01		
AlN	.00000E+00	.99693E+03		
PuN	.00000E+00	.30750E+01		

MIXTURE NUMBER 3 WOULD BE CONSIDERED IN THE EQUILIBRIUM SET OF PHASES IF ITS FREE ENERGY OF FORMATION WAS .00000E+00 J/MOLE MORE NEGATIVE.

SPECIES NUMBER 7 (Pu) WOULD BE CONSIDERED IN THE EQUILIBRIUM SET OF PHASES IF ITS FREE ENERGY OF FORMATION WAS .13389E+05 J/MOLE MORE NEGATIVE.

CHAPTER 4
EXPERIMENTAL PROCEDURES

This section of the thesis contains a discussion of the experimental procedures used during this research. Topics discussed include raw materials, forming techniques, sintering work, salt release studies, and corrosion analysis. Efforts in X-ray diffraction (XRD) and scanning electron microscopy (SEM) are also detailed.

4.1 Raw Materials

Dow Chemical Company's spray dried aluminum nitride powder with calcium carbonate and added binders was evaluated. This powder formulation is detailed in Table 4.1. Dow Chemical has implemented a process for producing and spray

TABLE 4.1
Dow Chemical Company Aluminum Nitride Spray Dried Powder
(Weight percentage based on total solids content)

	<u>Material</u>	<u>Percentage</u>
Charge 1-	Experimental Ceramic Binder	2.3
	Polyethylene Glycol 3350	4.2
	<u>Ethanol</u>	<u>72.8 (Binders)</u>
Charge 2-	Aluminum Nitride	95.0
	Calcium Carbonate	5.0
	Fish Oil	0.5
	<u>Ethanol</u>	<u>72.8 (Ceramic)</u>

[Enloe, 1991; Khoury, 1991].

drying large quantities of aluminum nitride powder. The powder used in this research was donated by W.R. Grace & Company, Columbia, Maryland, and Coors Ceramics Company, Golden, Colorado. Acquisition of this powder enabled crucibles to be fabricated via an isostatic pressing operation on the ready-to-use powder.

4.2 Isostatic Pressing

Crucible shapes were isostatically pressed at the Coors Ceramics Company. Pressing was done under the supervision of Rob Lucernoni and Earl Lyon. The crucibles were formed at a pressure of 27,000 psi, or approximately 190 MPa, to ensure adequate green strength for handling and transportation. This forming technique was selected because a near-final green shape could be pressed with minimal machining required. A diagram of the green crucible shape is shown in Figure 4.1. A number of slugs were dry pressed at a similar pressure so that an appropriate sintering cycle could be determined for this material.

The crucible size was limited by the chamber size of the furnaces used in the salt compatibility testing. The chamber dimensions of the furnaces used in this research were approximately 2 inches in diameter by 3 inches to 5 inches in height for the hot zone. The volume limitation required

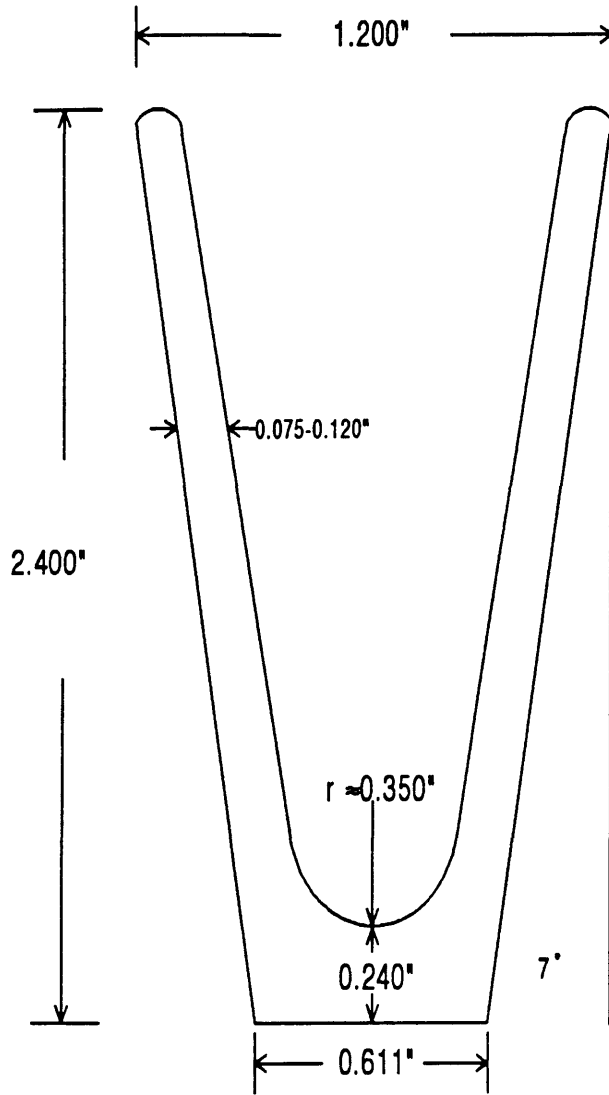


Figure 4.1: Green dimensions of aluminum nitride crucible.

crucible of lesser size; sintered crucible dimensions selected were 1 inch diameter by 2 in inches height. Dimensions of the green crucible were calculated assuming a 20% shrinkage during sintering. A rounded bottom and 7 degree taper were also designed and pressed to permit easier salt release than would be expected from a cylindrical crucible. The tapered walls provide an increasing diameter to allow the cooled salt to release; the rounded bottom provides no sharp or well-defined edge for the salt to adhere on cooling.

4.3 Sintering

Aluminum nitride crucibles and slugs were sintered at the Dow Chemical Company, Midland, Michigan, with the assistance of Dr. Arne Knudsen. The author worked extensively with Dr. Knudsen in determining suitable binder burnout and sintering cycles for yttrium oxide sinter-aided aluminum nitride in dry pressed and cast tape forms. This work was conducted during the author's employment with Coors Ceramics Company.

Binder burnout cycles were performed in a Lindberg retort furnace, and sintering was performed in a Thermal Technology/BREW graphite furnace located in the Advanced Ceramics Laboratory (Building 1776) at Dow Chemical Company. Sintering efforts are discussed in more detail below.

4.3.1 Binder Burnout

The spray dried aluminum nitride powder produced by Dow Chemical Company utilizes a Dow experimental binder, polyethylene glycol as a plasticizer, and fish oil as a pressing lubricant. These organic materials decompose at temperatures of 400°C to 600°C with the decomposition dependent on a number of variables including furnace atmosphere. Dow has conducted extensive work in determining appropriate binder burnout cycles for this powder in both air and nitrogen atmospheres. Air was the atmosphere of choice for this experiment. The burnout temperature was 550°C with a one hour soak at this temperature. The burnout temperature was based on thermal gravimetric analytical (TGA) results provided by Dow on this powder (refer to Figure 4.2) and personal discussions with Dr. Knudsen [Knudsen, 1991].

The binder burnout temperature should be selected so that not all the binder is removed. This gives the product, called a bisqued product, sufficient strength to allow handling prior to the sintering operation. Excess or free carbon present in the product also serves to reduce any oxygen present in the material; this is similar to work conducted with calcium carbide [Kurokawa, 1986]. Acceptable levels of free carbon are 0.1 to 0.2 percent. The presence of carbon yields a product with higher thermal conductivity; oxygen reacts with

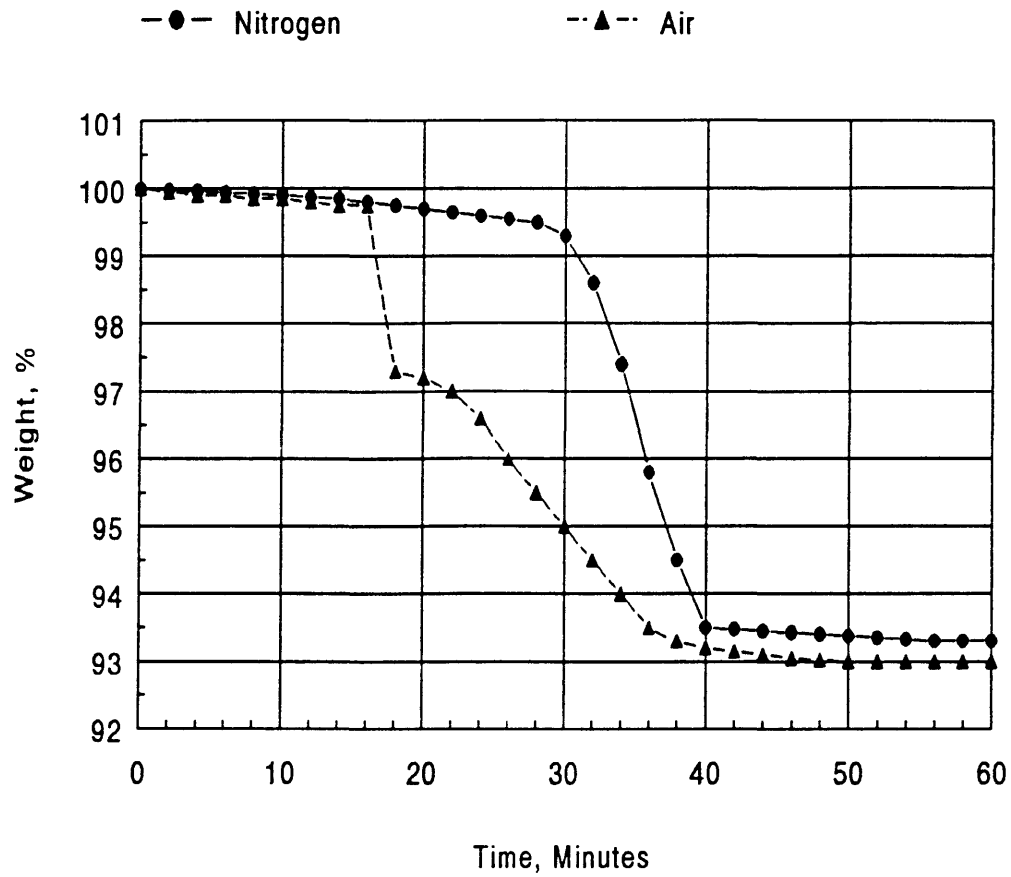


Figure 4.2: TGA on spray dried aluminum nitride powder [Knudsen, 1991]. Burnout temperature was 600°C at a 10°C/minute heat-up rate.

carbon to form carbon dioxide. If the product contains excess carbon (greater than 0.3 percent), however, sintering may be incomplete resulting in residual porosity in the fired sample [Khoury, 1991].

4.3.2 Sintering

Slugs and crucibles were placed in a boron nitride (BN) crucible and subsequently sintered in a BREW/Thermal Technology graphite furnace. This furnace is capable of achieving temperatures in excess of 2000°C in nitrogen, argon, or vacuum and provides a reducing atmosphere due to the presence of the graphite elements [Andersen, 1991]. The BN crucible provides a localized atmosphere around the samples and protects the samples from being excessively reduced in the graphite furnace [Knudsen, 1991].

The sintering cycle consisted of a soak temperature of 1850°C and a soak time of five hours. The high soak temperature was determined to be necessary to achieve the theoretical density of 3.26 gm/cc for aluminum nitride. The structure can be purified by removal calcium aluminate from the grain boundaries at the high temperature. A more pure crystal structure results [Knudsen, 1991].

Two sintering runs were performed for this research. The first run entailed sintering one crucible and two slugs in a

boron nitride crucible to confirm adequate sintering conditions. The sintering atmosphere was flowing nitrogen. The second sintering operation involved sintering the four remaining crucibles and slugs in a boron nitride crucible under similar sintering conditions. These sintering runs resulted in three good crucibles and two cracked crucibles. The cracking was possibly due to handling.

The slugs from these sintering runs were measured for fired bulk density (FBD) to confirm the degree of sintering. The average FBD of the six slugs was 3.24 gm/cc (as measured by the Archimedes method), or approximately 99.4 percent of the theoretical density of 3.26 gm/cc. The decreased FBD may be due to closed porosity in the structure and/or a lower density secondary phase ($\text{Ca}_x\text{Al}_y\text{O}_z$).

4.4 Analytical Techniques

In this study, two analytical techniques were employed in the characterization of as-fired and salt exposed samples. These techniques are X-ray diffraction (XRD) and scanning electron microscopy (SEM). The details of each are briefly discussed in this section.

4.4.1 X-ray Diffraction

X-ray characterization measurements were performed on the Rigaku X-ray diffraction unit located in the CSM Physics building. The diffractometer is supplemented by a DMAX computer program for data collection and analysis. The "loose powder method" sample preparation was chosen for the samples. A glass slide was cut to the appropriate size for the X-ray unit (approximately two inches by one inch), and double stick tape was applied to the slide in a location that corresponded to the approximate location for the X-ray focal spot. Single sided tape was applied to the opposite end of the slide to maintain a near equal height across the slide. Powder was placed on double stick tape and the excess powder was removed. The X-ray scan was performed from 10 degrees to 70 degrees (2θ) using the copper wavelength of radiation ($K_{\alpha 1} = 1.540598 \text{ \AA}$). The background radiation was not eliminated for any of the sample runs. The scan was run in 0.05 degree increments with a one second stop ($\Delta t = 1 \text{ second}$) at each angle increment.

Preliminary X-ray characterizations were performed on individual samples of aluminum nitride and calcium carbonate powder to form a basis for subsequent measurements. These data were compared with theoretical values for 2θ and the d-spacing as calculated from Bragg's law, which is as follows

[Cullity, 1978]:

$$n\lambda = 2d\sin\theta \quad (4.1)$$

where n = order of reflection ($n = 1$),
 λ = X-ray wavelength (1.5406 Å),
 d = crystal d-spacing (Å⁻¹), and
 θ = angle of incidence of the diffraction beam
on the sample (°).

Comparison between theoretical and experimental XRD data was used to determine the purity of the starting powders and the primary phases present in the sintered and exposed samples. These data are included in Appendices B and C.

Subsequent X-ray characterizations were performed on sintered aluminum nitride and molten chloride salt samples. This XRD characterization was performed to determine final species present in the samples. Secondary phases present in sufficient quantities could also be identified.

4.4.2 Scanning Electron Microscopy

The JEOL JXA-840 scanning electron microscopy unit located in Hill Hall at the Colorado School of Mines was used for microstructural analysis. The work was performed under the direction of Robert McGrew. Samples were analyzed at magnifications of 33X, 500X, 2000X, 5000X, and 10,000X; these magnifications provided details regarding the grain size,

crystal structure, and grain boundary appearance.

In this analysis, as-fired surfaces and molten salt exposed samples were examined. This analysis was performed to ascertain the effects of the molten salt on the grain shape and boundaries. All samples were carbon coated to permit analysis by SEM. The results from this analysis are discussed in greater detail in Chapter 5.

4.5 Molten Salt Exposure

Aluminum nitride crucibles were exposed to direct oxide reduction (DOR) and electrorefining (ER) salts for corrosion analysis. The exposure entailed performing a high temperature melting of DOR salts (CaCl_2 salt/Ca metal) and ER salt (NaCl-KCl) in aluminum nitride crucibles. Melting was conducted in an inert atmosphere (argon). The salt release from the crucible was examined on cooling. Any attack of the salt on the crucible could be assessed with SEM by comparing the as-fired surface with the exposed surface.

4.5.1 DOR Salt Exposure

The DOR molten salt exposure entailed exposing the AlN crucible to the molten chloride salt/metal mixture at 800°C to 850°C for an extended period of time. A soak time of 3 hours and a 2 hour heat-up time were arbitrarily chosen for the

first study conducted at the Colorado School of Mines, Golden, Colorado. A soak time of 1½ hours and maximum furnace heating rate were chosen for the second study conducted at the Los Alamos National Laboratory, Los Alamos, New Mexico. Both test methods are detailed below.

In the first test, calcium chloride and calcium metal were weighed in a ratio that approximated the mole amounts used in the Solgasmix calculations in Chapter 3. Salt charges used were 1.6460 grams of CaCl_2 and 0.0851 grams of Ca metal. These charges corresponded to 95.084 weight percent and 4.916 weight percent for the CaCl_2 and Ca metal, respectively. A technical grade CaCl_2 salt used in Rocky Flats production and a 99 percent pure Ca metal available at CSM were used for testing. These materials were selected to simulate actual exposure conditions encountered in a typical reduction operation for producing Pu metal.

Heat treatments were conducted under flowing argon gas in a Coors Biomedical Cerestore™ furnace. These furnaces are designed for lower temperature firing profiles (typically less than 1300°C) and result in a highly precise uniform temperature due to the small chamber volume (approximately 2 inches diameter by 3 inches height). Argon gas (99.998 percent pure) was flowed through the chamber at a rate of approximately 1 liter per minute (a flow rate equivalent to

flushing the chamber $2\frac{1}{2}$ times per minute) to minimize the oxidation potential during the thermal heat treatment.

To evaluate the corrosion resistance of the crucible in the molten salt, five firing cycles were planned; the number of cycles was narrowed to one after the results of the first firing showed significant wetting by the salt/metal mixture on the crucible. There was no apparent salt release. A sample of the salt/metal mixture was used for subsequent XRD and the remainder of the salt mixture was removed under flowing water to permit further crucible testing at Los Alamos.

The second DOR salt exposure entailed exposing one aluminum nitride crucible to calcium chloride salt (4.56 grams) followed by exposing a second crucible to a mixture of calcium chloride salt (3.87 grams) and calcium metal (0.20 grams). The ratio of the salt to metal again approximated that used in the Solgasmix calculations. The salt had been stored in a dry box at a temperature of 110°C to minimize salt degradation by hydration. Calcium metal had been stored under argon gas to minimize oxidation. A salt sample was sealed in a glass ampule for subsequent XRD analysis.

Heat treatments were conducted under flowing argon gas in a Sybron Thermolyne MiniMelt™ furnace (refer to Figure 4.3). This furnace is designed for low temperature firing profiles (typically less than 1000°C) with the temperature measured by

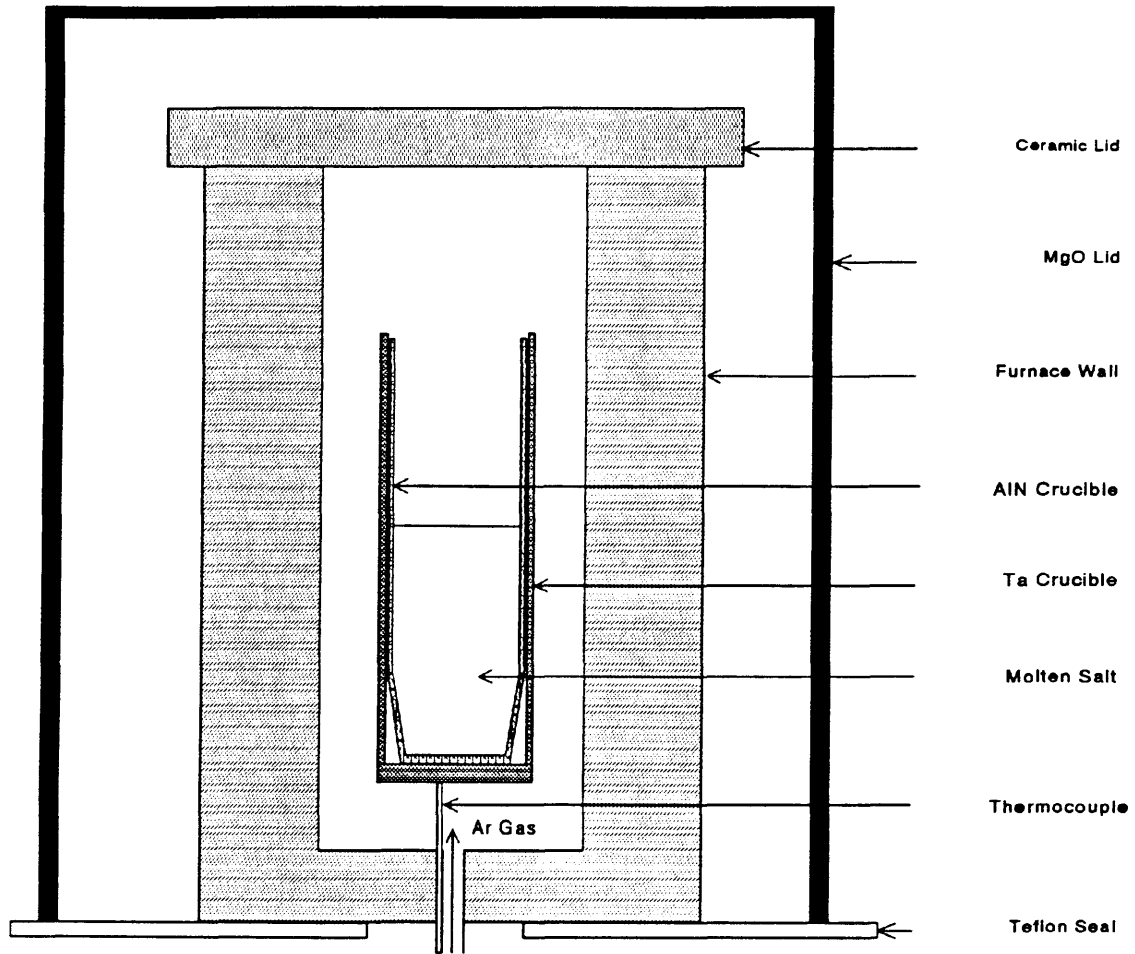


Figure 4.3: Sybron Thermolyne MiniMelt™ furnace setup for DOR salt exposure.

a Type K thermocouple. Argon gas was flowed through the furnace at a rate of approximately 5 liters per minute during the initial heat-up rate and 1 liter per minute at temperature to minimize the oxidation potential during the thermal heat treatment. The aluminum nitride crucible and salt were placed in a tantalum crucible which was subsequently placed in the furnace. The furnace was allowed to heat at the maximum heating rate possible. The rapid heat-up was due to the furnace lacking a controllable programmer at the time of testing. Heat-up was noted to take 1½ hours for the furnace to reach a maximum of 830°C to 835°C, and the soak time at temperature was 1½ hours. The furnace was allowed to free cool under flowing argon gas. After exposure, the crucibles with salt cakes intact were sealed in glass ampules to minimize salt degradation by hydration during transport from Los Alamos.

A scanning electron microscope was utilized to ascertain corrosion of the crucible from exposure to the molten salt. The analysis was performed after the crucible had been sectioned using a Buehler Isomet™ wafering saw in an oil bath (to minimize moisture attack of the salt from an aqueous lubricant). For this analysis, one crucible surface had been exposed to a molten salt/metal (testing at CSM) and subsequently exposed to a molten salt (testing at Los Alamos).

The second crucible had been exposed to a molten salt/metal. The oil was removed by a solvent rinse. Solvents used were methanol, ethanol, and acetone. The crucibles were placed under vacuum for 48 hours to further dry the samples. Corrosion could be analyzed by comparing grain shapes and boundaries of exposed samples to grains from an as-fired surface. Energy dispersive X-ray analysis, or EDX, also aided in the corrosion determination. Aluminum, chlorine, and calcium concentrations were measured at three locations on the crucible/salt samples. Chlorine and calcium migration could be monitored in this fashion. Finally, X-ray diffraction was utilized to determine changes in the salt by comparing results from the cooled salt cakes with virgin samples.

4.5.2 ER Salt Exposure

Because of the lack of release by the DOR salts, a decision was made to evaluate electrorefining (ER) salt release from the remaining aluminum nitride crucible. The ER process typically uses a mixture of sodium chloride (NaCl), potassium chloride (KCl), and magnesium chloride (MgCl₂) salts in an environment that is less harsh than the DOR processing environment as no reducing agent (calcium metal) is present. ER salts also have a greater tendency to shrink on cooling allowing for easier salt removal from the crucible.

The ER salt compatibility testing was conducted in an Applied Test Systems Model 3210™ furnace at Los Alamos. A Honeywell programmer controlled the heating rate and soak temperatures for this testing. A picture of the furnace is shown in Figure 4.4. Cold testing, or non-radioactive testing, used a 50/50 mole ratio mixture of sodium chloride (NaCl) and potassium chloride (KCl).

In this experiment, a 1:1 molar ratio of sodium chloride and potassium chloride salt was placed in the aluminum nitride crucible. The salt mass was not recorded. The crucible and contents were vacuum sealed in a Pyrex™ tube before heating (Pyrex™ was inadvertently used in place of quartz). The vacuum seal prevented oxygen contamination of the molten salt during the cycle. The sealed contents were heated to 850°C in 3½ hours and soaked at temperature for 2 hours. These parameters mirror actual ER processing conditions. Heat-up and soak were in air; argon gas was not required due to the crucible being sealed.

A scanning electron microscope was utilized to monitor corrosion of the crucible from exposure to the molten salt. This crucible was also sectioned using a Buehler Isomet™ wafering saw in an oil bath to examine the ceramic/salt interface (the salt was removed before the crucible was cut). The oil was removed by an acetone rinse. The corrosion could

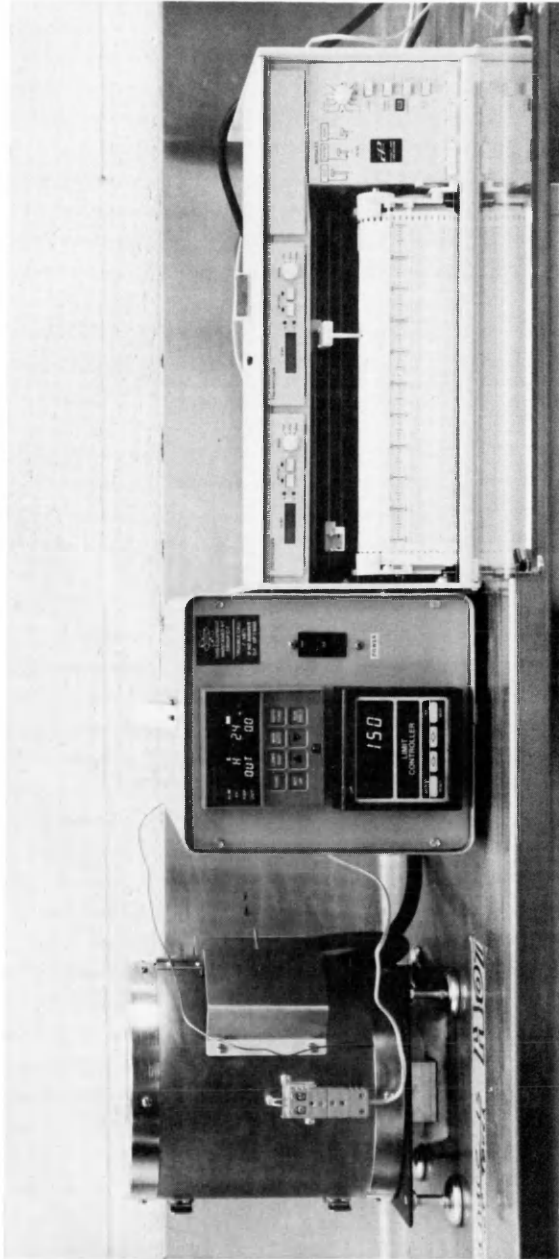


Figure 4.4: Photograph of Applied Test Systems furnace.

be studied against the as-fired surface and DOR salt exposed samples. Grain boundaries and grain shapes of the relative samples could be evaluated for corrosion analysis. The use of energy dispersive X-ray analysis, or EDX, again aided in the corrosion determination; chlorine, sodium, and potassium in the ceramic interior structure could be identified. These elements are not present in the as-fired structure in measurable quantities.

CHAPTER 5

DISCUSSION OF RESULTS

The experimental results obtained during the course of this research are discussed in this chapter of the thesis. Topics discussed include the results of the fabrication techniques, direct oxide reduction (DOR) salt exposure results, and electrorefining (ER) salt exposure results. Photographs, X-ray diffraction (XRD) data, and scanning electron microscopy (SEM) results from the sintered and exposed aluminum nitride samples are also presented.

5.1 Fabrication Techniques

The isostatic pressing and sintering techniques utilized in this research proved to be quite successful in the fabrication of aluminum nitride crucibles. Crucibles were produced with desired dimensional and shape characteristics, satisfactory fired bulk density, and minimal amounts of secondary phases in the grain boundaries. These characteristics were verified by fired bulk density (FBD) measurements, XRD analysis of powder and sintered samples, and SEM/EDX analysis of sintered samples.

5.1.1 Isostatic Pressing

Isostatic pressing enabled aluminum nitride crucibles to be fabricated at a high green density and near-final shape. This pressing technique resulted in a green compact with sufficient green strength to allow transportation for sintering. Isostatic pressing also resulted in the desired crucible characteristics (rounded crucible bottom, smooth transition from crucible to walls, and tapered sides) without the need for green machining, an operation that would increase the likelihood of introducing flaws into the ceramic.

5.1.2 Sintering

Aluminum nitride crucibles were sintered at 1850°C for a 5 hour soak. A picture of a sintered crucible is shown in Figure 5.1. The sintering operation produced a ceramic with a fired density of 3.24 gm/cc, or 99.4 percent the theoretical density of 3.26 gm/cc, as measured on comparative slugs. The crucibles were assumed to have a similar fired density to that of the slugs as the processing conditions (forming pressure and sintering) for each were similar. Shrinkage data collected on slugs ranged between 22.8 percent to 23.8 percent.

X-ray diffraction data of aluminum nitride powder samples confirm the sintering operation to be successful in producing

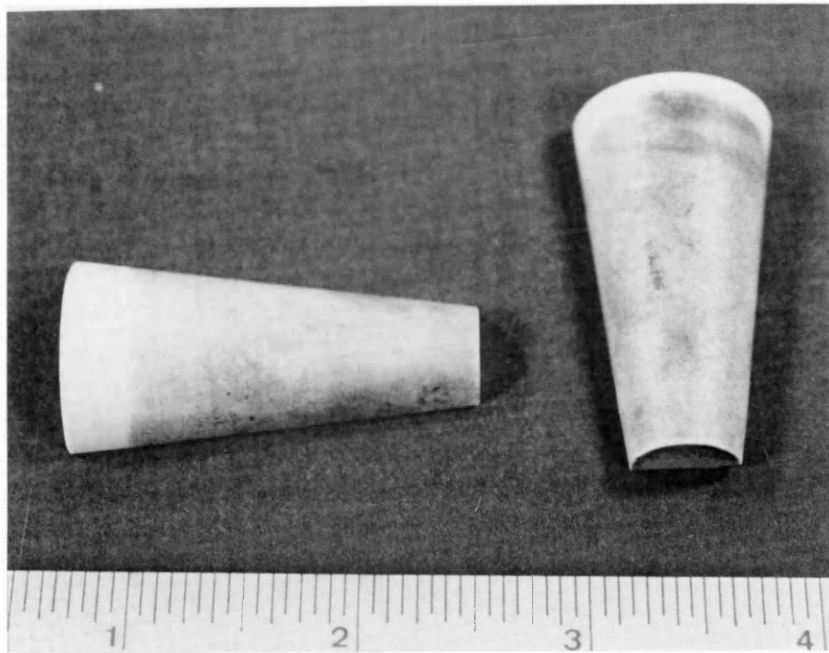


Figure 5.1: Photograph of sintered AlN crucible.

a sintered piece with minimal secondary phases present. Samples analyzed include aluminum nitride powder (refer to Figure 5.2), spray dried powder with binders and calcium carbonate (refer to Figure 5.3) and sintered aluminum nitride powder (refer to Figure 5.4). Figure 5.2 shows the seven characteristic peaks (peak near $70^\circ 2\theta$ is partially hidden) associated with aluminum nitride (refer to Appendix B, PD-PDS Card # 25-1133). Impurity species in the powder are below the background radiation level. Figure 5.3 also shows these seven peaks with additional peaks observed at 29.5° and 23.5° . These peaks are characteristic for calcium carbonate (refer to Appendix B, JC-PDS Card # 24-27) present as the sintering additive. Figure 5.4 again shows the seven aluminum nitride peaks with additional peaks being observed near 25° and 35° . These peaks are attributed to CaAl_2O_4 , $\text{Ca}_2\text{Al}_2\text{O}_5$, and CaAl_4O_7 (refer to Appendix B, JC-PDS Card #'s 23-1036, 33-252, and 23-1037) produced from the chemical reaction between CaO and Al_2O_3 during the sintering process. The formation of this phase was described in Chapter 2. As expected, calcium carbonate is not present in the sintered material; the primary peak associated with calcium carbonate (29.5°) is not observed. Other impurity species are at or below the background radiation level.

The microstructure of the as-fired surface on sintered

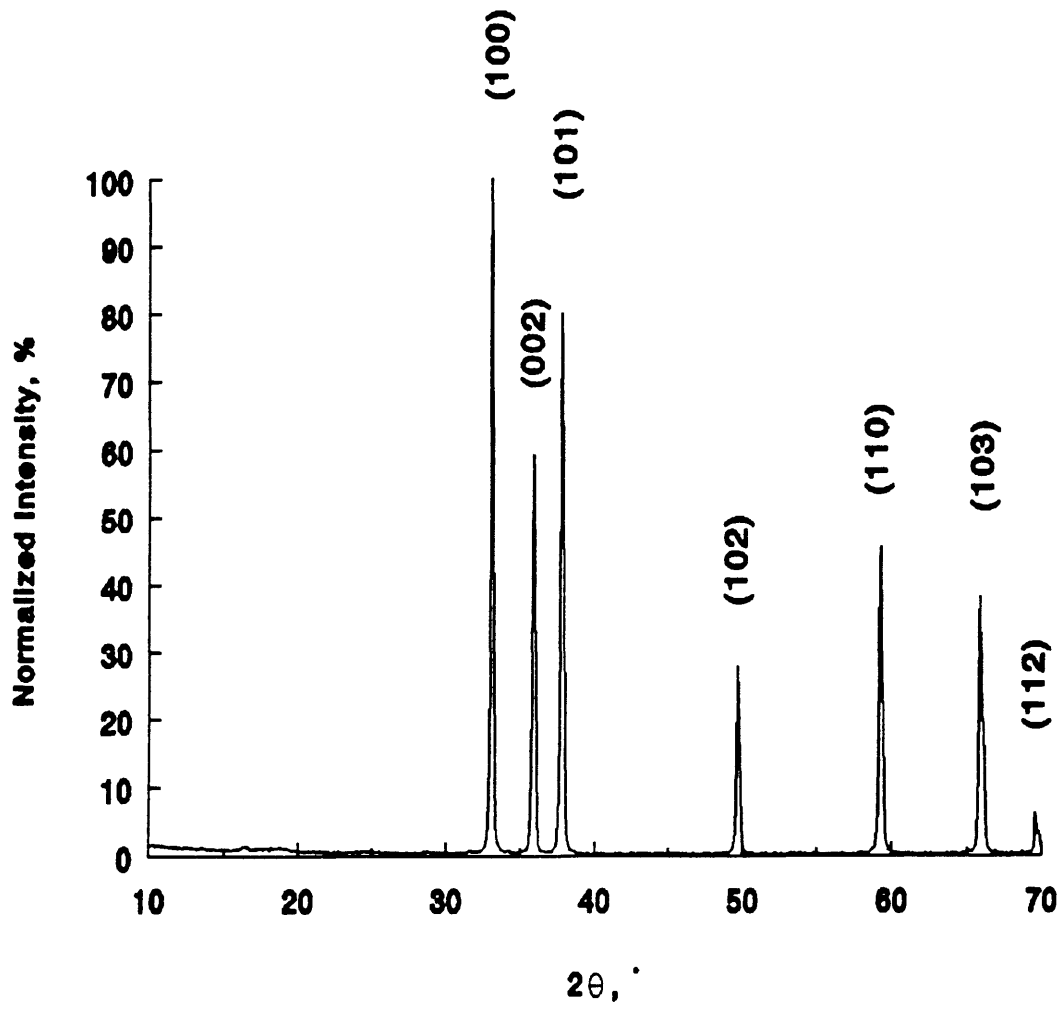


Figure 5.2: XRD pattern of AlN powder.

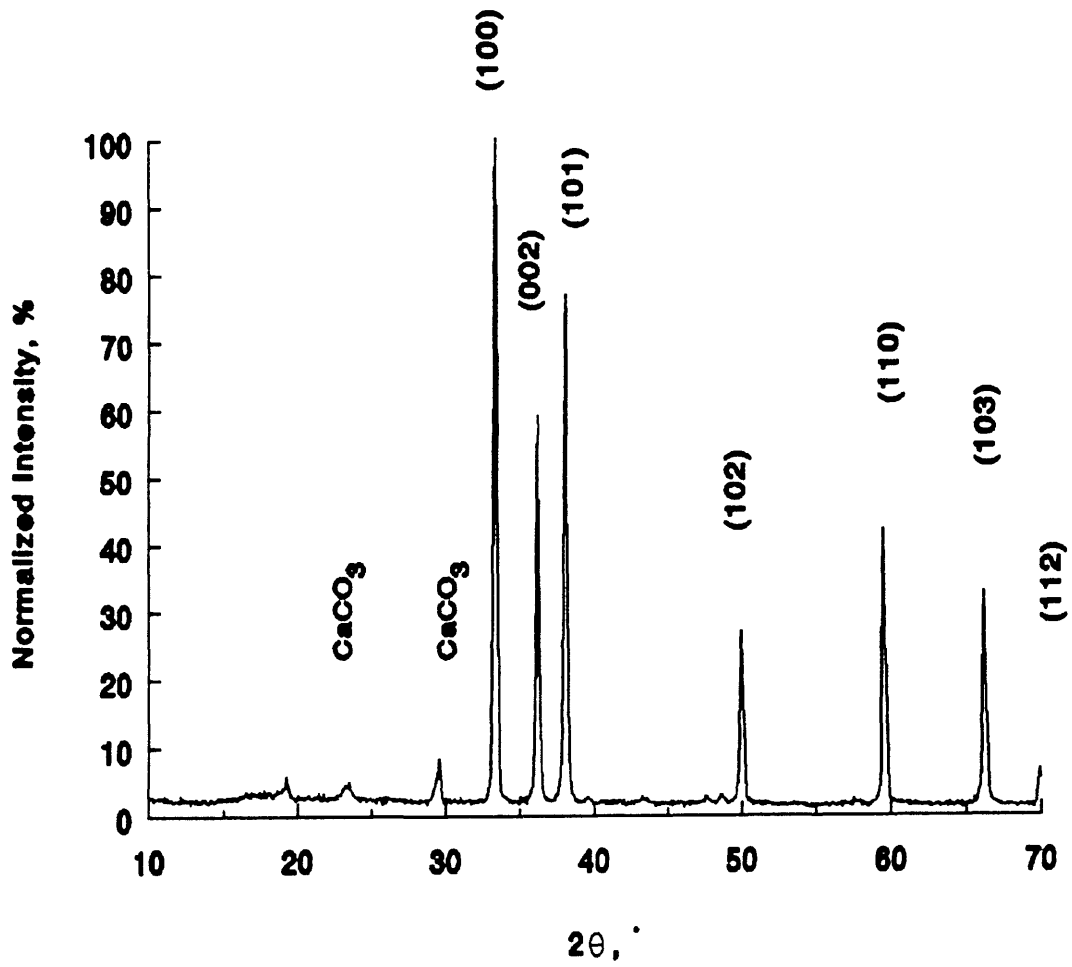


Figure 5.3: XRD pattern of spray dried AlN powder.

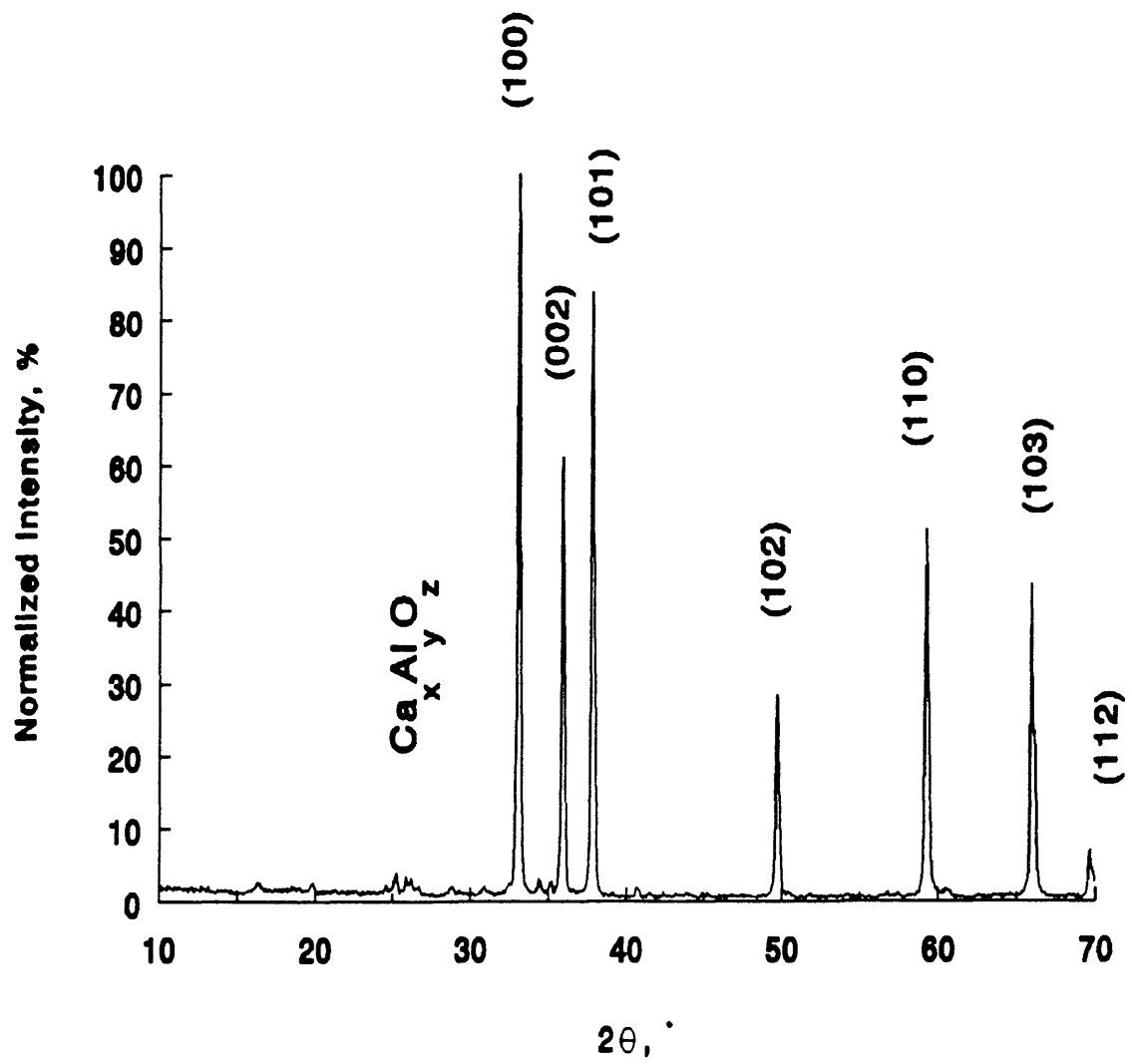


Figure 5.4: XRD pattern from sintered AlN.

slugs confirms the high degree of sintering. Sintering is confirmed by low levels of secondary phases in the grain boundaries and few open pores visible (refer to Figures 5.5 and 5.6). The secondary phase observed in the grain boundaries was identified as CaAl_2O_4 , $\text{Ca}_2\text{Al}_2\text{O}_5$, and CaAl_4O_7 by XRD analysis. EDX analysis on this material shows the aluminum and calcium atomic concentrations to be 99.22 percent and 0.78 percent, respectively as averaged from data collected at five sites. The lack of pores and uniform grain size in the sintered compact also give an indication of good powder processing and pressing characteristics. The average grain size can be ascertained to be six to seven microns. The particle size range is two to 10 microns.

5.2 DOR Salt Exposure

The aluminum nitride crucible was evaluated for salt release and corrosive attack in a DOR salt environment. The salt release test was subjective. The crucible was flipped and observed to see if the cooled salt cake would release or not. The corrosive attack evaluation was more detailed, and involved X-ray diffraction (XRD) and scanning electron microscopy/energy dispersive X-ray (SEM/EDX) analyses of the exposed samples (crucible and salt). The results of these tests are discussed in greater detail below.

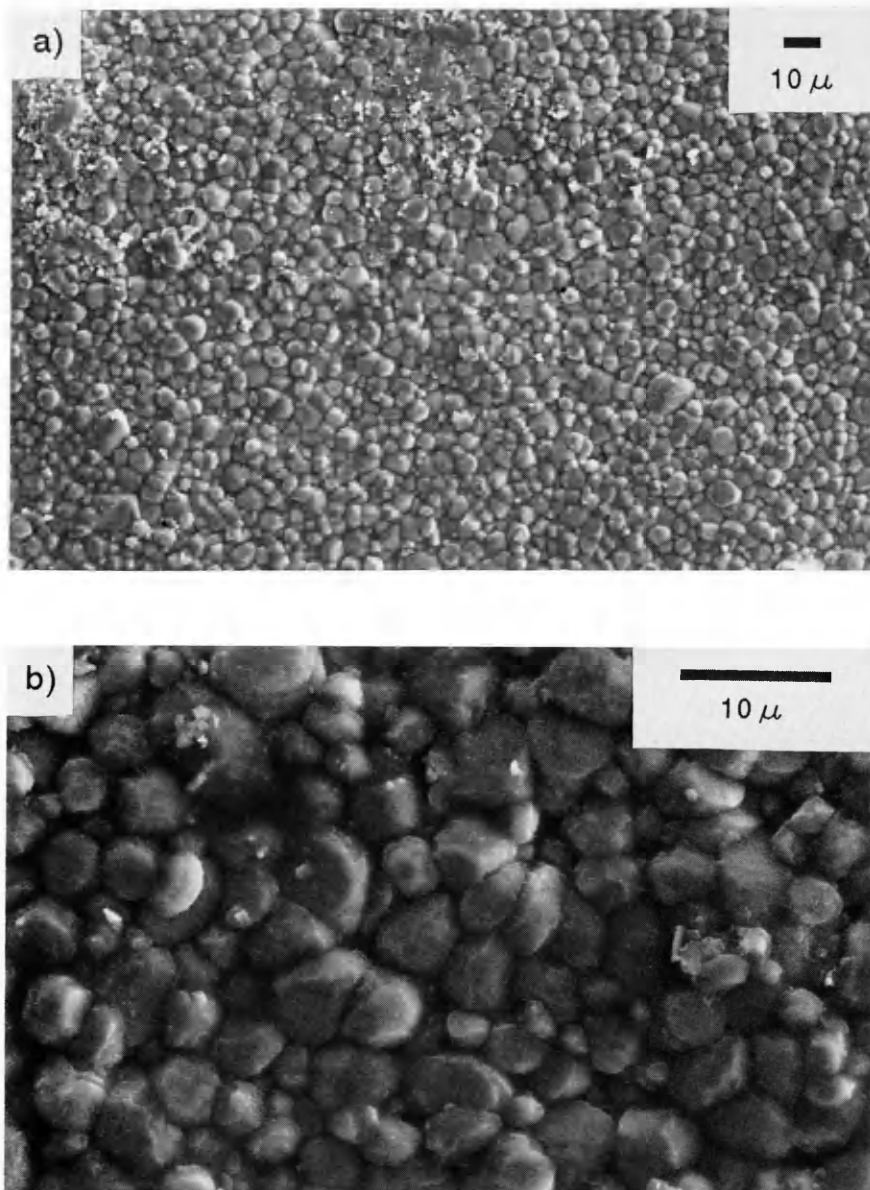


Figure 5.5: SEM micrographs of sintered AlN at a) 500X and b) 2,000X.

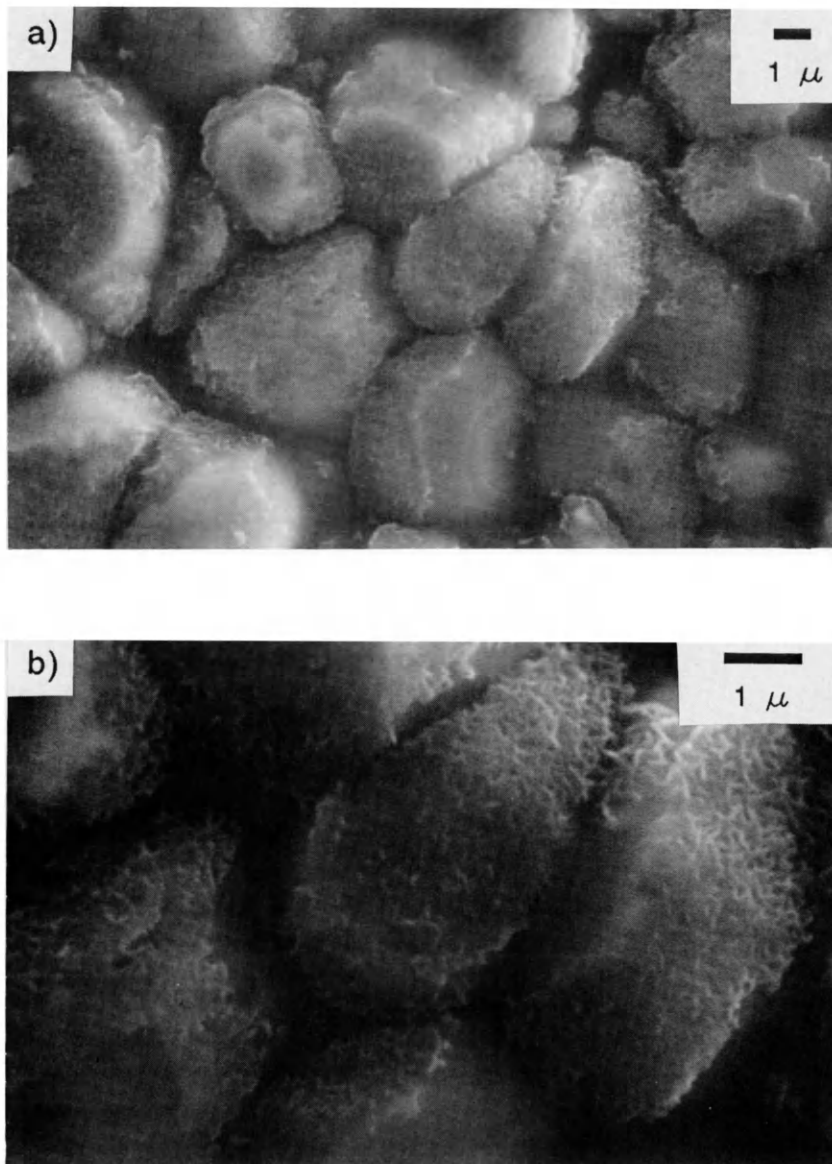


Figure 5.6: SEM micrographs of sintered AlN at a) 5,000X and b) 10,000X.

5.2.1 Calcium Chloride Salt

The heat treatment of the calcium chloride salt in the aluminum nitride crucible resulted in significant salt wetting on the aluminum nitride crucible. A picture of this wetting phenomenon is shown in Figure 5.7. This crucible had earlier been evaluated for release by a technical grade calcium chloride salt/calcium metal. That test produced similar wetting results. Wetting is attributed to the ceramic-molten salt surface energy being lower than the ceramic-argon (vapor) surface energy ($\gamma_{sv} > \gamma_{sl}$). The spreading coefficient, therefore, was positive; a liquid will wet a solid when the spreading coefficient is positive [Hiemenz, 1986; Kingery, 1976]. Wetting also resulted in strong adhesion between the salt and the crucible.

Melting of the calcium chloride salt in the aluminum nitride crucible resulted in strong salt adherence to the crucible. Adherence can be explained by several factors: crucible wetting, poor crucible design, salt mass, and corrosive attack of the crucible by the salt. SEM/EDX analysis of a cross section of the crucible show significant calcium and chlorine migration from the ceramic/salt interface through the ceramic matrix. These photomicrographs are shown in Figures 5.8 and 5.9. EDX results of the representative areas are provided in Table 5.1.

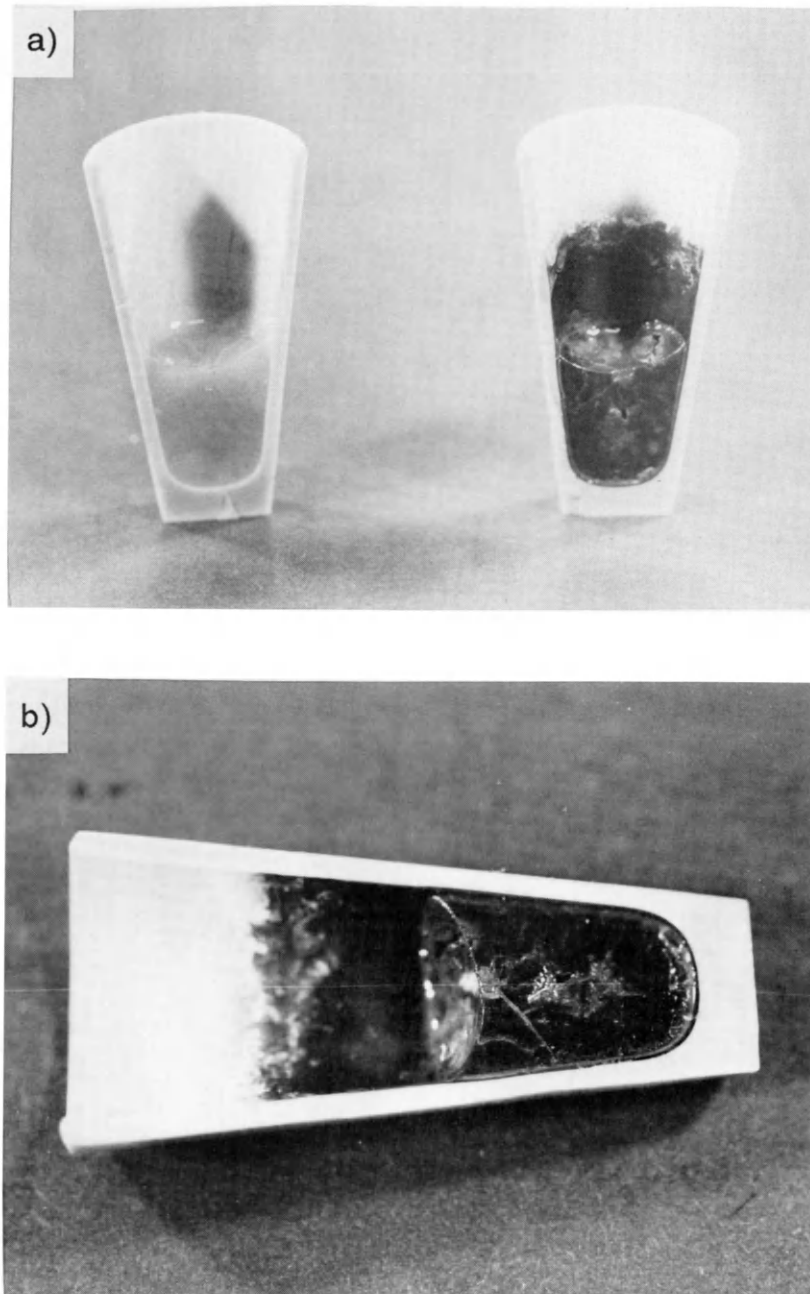


Figure 5.7: Photographs of wetting phenomenon on AlN crucible cross sections by a) CaCl_2 salt (left) and Ca/CaCl_2 salt (right), and b) Ca/CaCl_2 salt.

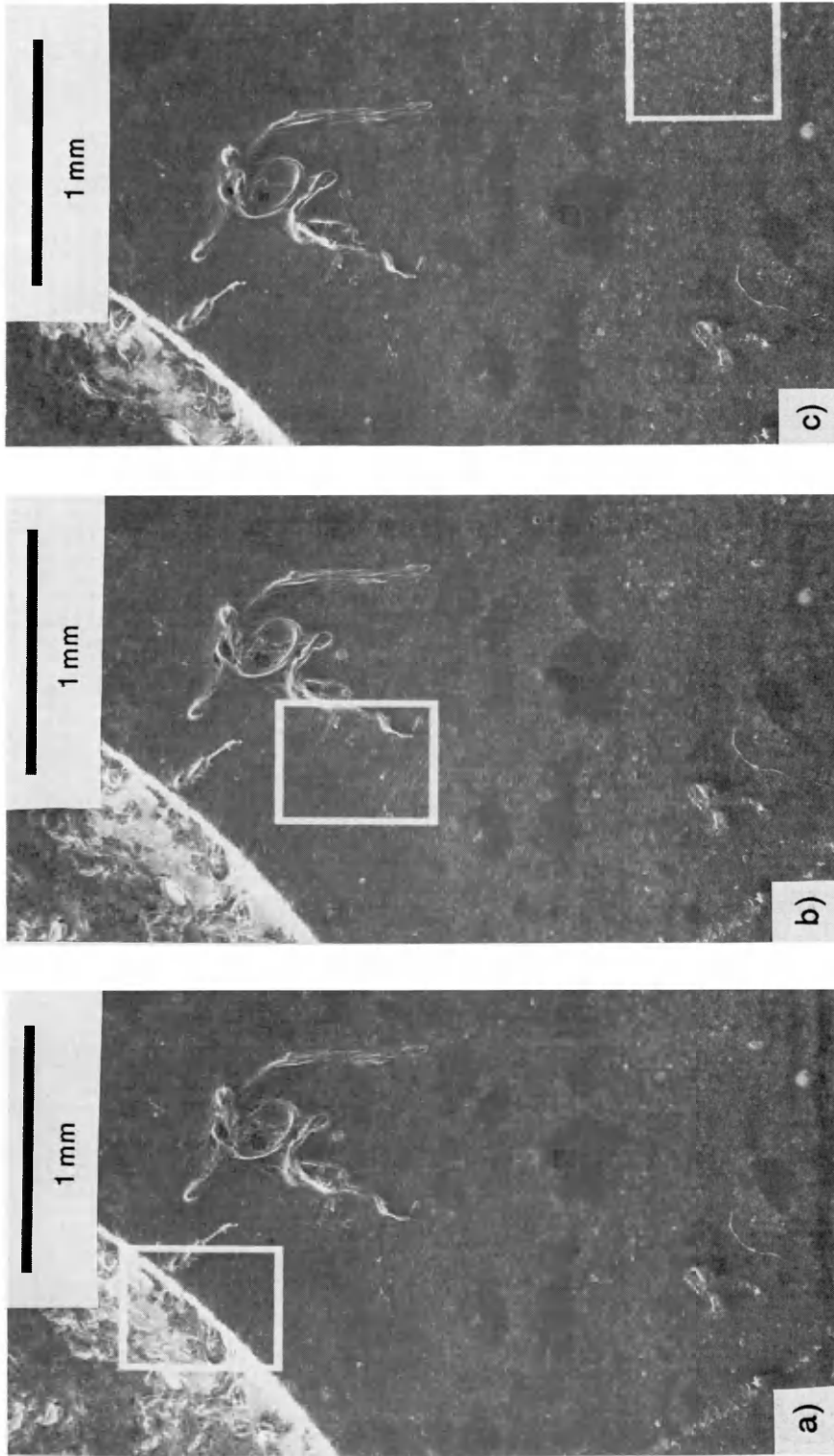


Figure 5.8: SEM micrographs of CaCl_2 exposed AlN crucible at 33X of a) ceramic/salt interface, b) mid-range, and c) ceramic interior.

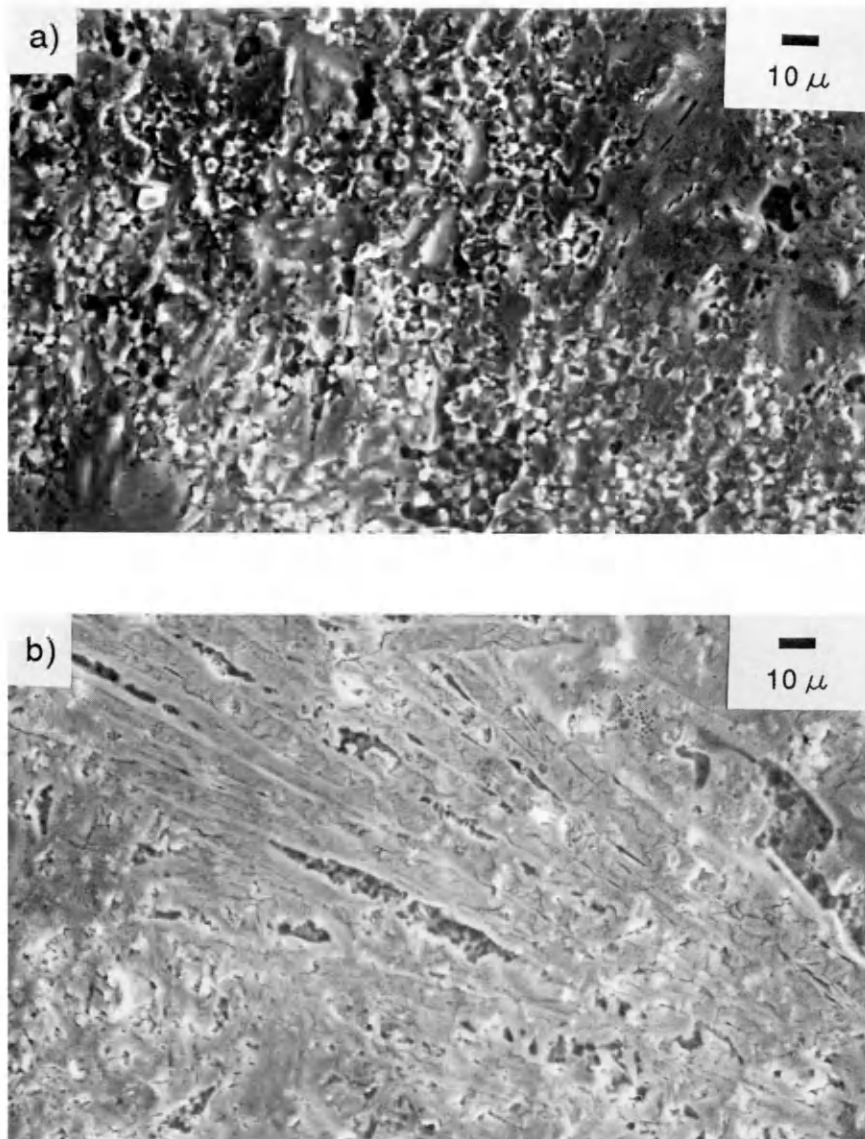


Figure 5.9: SEM Micrographs of CaCl_2 exposed AlN crucible at 500X of a) ceramic matrix, and b) near ceramic/salt interface.

Higher magnifications of the ceramic matrix and ceramic/salt interface (refer to Figure 5.9) provide a comparison between the two regions (extremes in calcium and chlorine concentrations). The photomicrograph of the ceramic interior (refer to Figure 5.9a) shows a number of voids. The voids may be due to closed porosity, pullout during the cutting operation, or corrosive attack by the molten salt. The photomicrograph of the interface region (refer to Figure 5.9b), however, shows the grain structure to be more closed with fewer pores visible. The open structure of the ceramic interior appears to result from corrosive attack by the molten salt. Attack is evidenced by the more closed structure composed almost entirely of calcium and chlorine at the ceramic/salt interface (refer to Table 5.1). The open structure of the ceramic interior is more apparent in the calcium metal/calcium chloride salt system.

The corrosive attack of the crucible by the salt is most likely occurring at the aluminum nitride grain boundaries.

TABLE 5.1
EDX Results of CaCl_2 Salt Exposed AlN

<u>Figure</u>	<u>Al (At. %)</u>	<u>Ca (At. %)</u>	<u>Cl (At. %)</u>
5.8a	0.31	40.88	58.81
5.8b	55.55	18.39	26.05
5.8c	96.34	1.85	1.81

Secondary phases of calcium aluminate at the grain boundaries are attacked by the molten salt or species in the salt (Ca , Cl_2 , Ca^{2+} , Cl^-) allowing for calcium and chlorine migration throughout the structure. Possible attack mechanisms are discussed later in the chapter. Attack is evidenced by EDX results from the respective regions and the change in grain structure and shape from that of the as-fired surface. This attack was not observed in studies on hot pressed aluminum nitride utilizing yttrium oxide as a sintering additive [Marra, 1991]. The lack of attack on the $\text{AlN-Y}_2\text{O}_3$ ceramic may be due to the sintering aid and resulting secondary phases and/or the processing technique (hot pressing).

X-ray diffraction patterns of the virgin and molten calcium chloride salts (refer to Figures 5.10 and 5.11) indicate a change in the salt composition from melting. The virgin salt charge shows the characteristic peaks for calcium chloride at 2θ values of 29.8° and 20.3° (refer to Appendix B, JC-PDS Card # 24-223). Additional peaks are attributed to hydrated salt. Degradation is due to the hygroscopic nature of calcium chloride. Differences between experimental and theoretical values of the d-spacing are suspected to result from sample preparation. Data from the molten salt cake shows a shift in peak position with the maximum intensity occurring at a 2θ value of 20.2° and secondary peaks observed at 29.6°

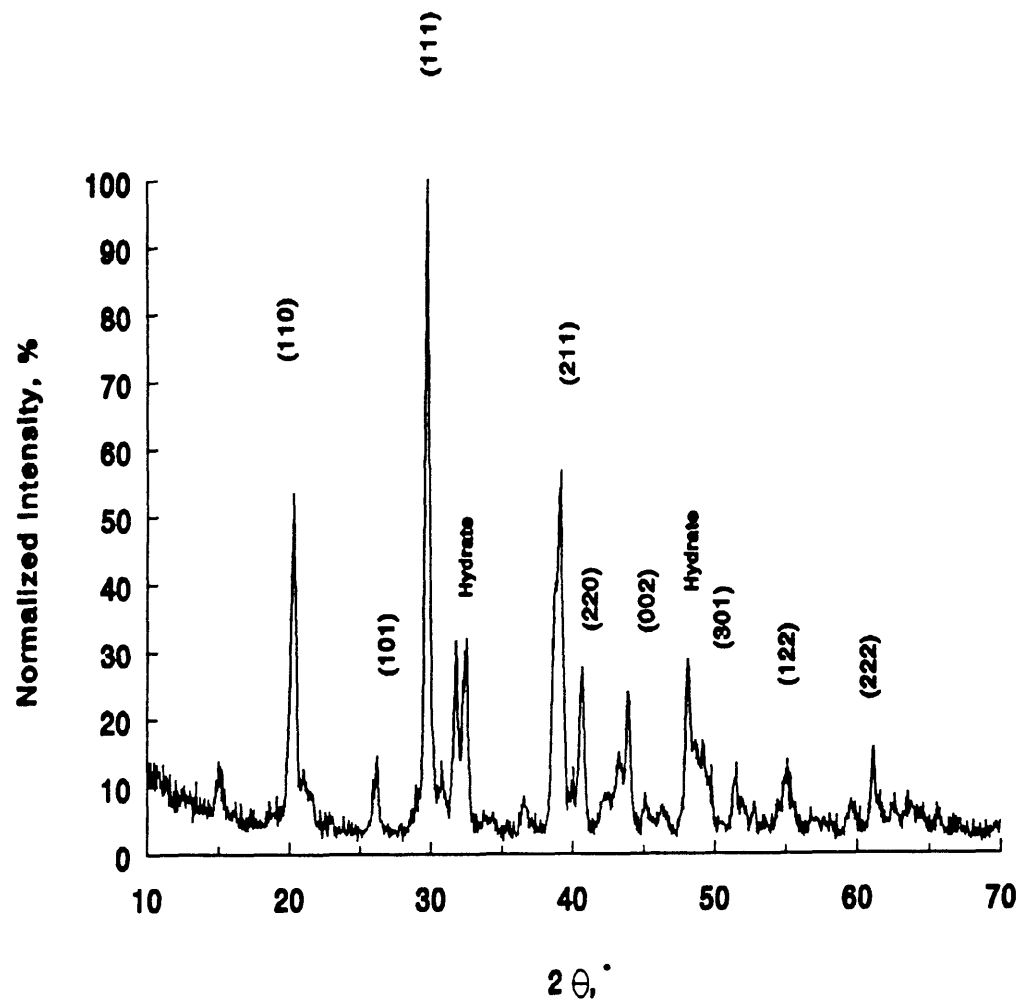


Figure 5.10: XRD pattern of virgin CaCl_2 salt.

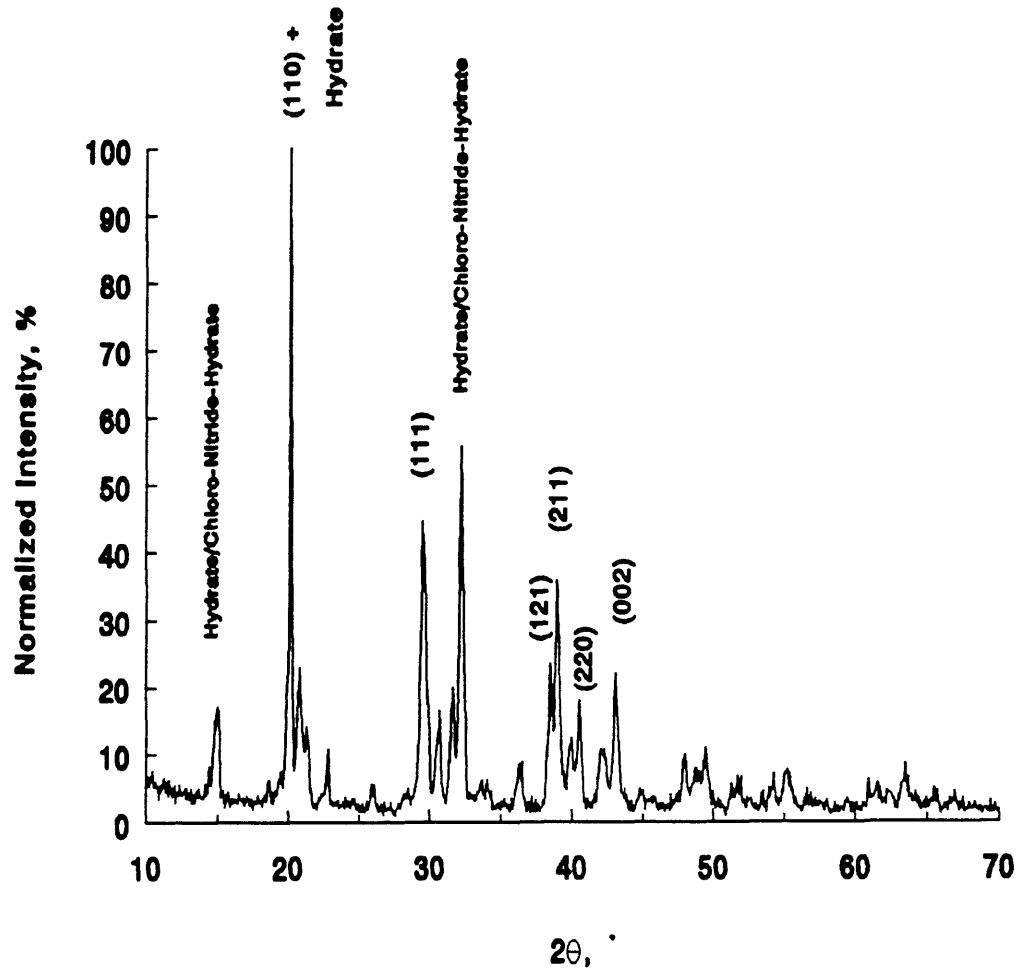


Figure 5.11: XRD pattern of molten CaCl_2 salt.

32.2°. The shift in the peak position, again, is attributed to salt degradation from environmental attack; calcium chloride reacts with moisture to form a hydrated salt, $\text{CaCl}_2 \cdot 2\text{H}_2\text{O}$ (refer to Appendix B, JC-PDS Card # 1-989). Other species that may be present in the salt, as characterized by XRD, include calcium nitride, $\gamma\text{-Ca}_3\text{N}_2$ (JC-PDS Card # 21-153), and calcium chloryl nitride hydrate, $\text{CaNClO}_2 \cdot x\text{H}_2\text{O}$ (JC-PDS Card # 21-836). These species, if indeed present, represent further evidence of crucible breakdown from corrosive attack by the salt.

5.2.2 Calcium Metal/Calcium Chloride Salt

Melting of the calcium metal/calcium chloride salt mixture also produced significant salt wetting on the aluminum nitride crucible (refer to Figure 5.7). The cooled salt/metal cake was much darker than that of the calcium chloride salt (brown opposed to clear/white coloration) with discoloration noted above the salt cake and along the crucible interior wall. The salt again did not show any tendency to release from the crucible. Salt adherence is due to wetting and corrosive attack on the crucible. The XRD pattern from this salt (refer to Figure 5.12) again deviated from the virgin salt. The shift in peak position is due to calcium metal in the salt and hydration. The high calcium peak is noted at 32°; a large chunk of unreacted calcium was ground with the

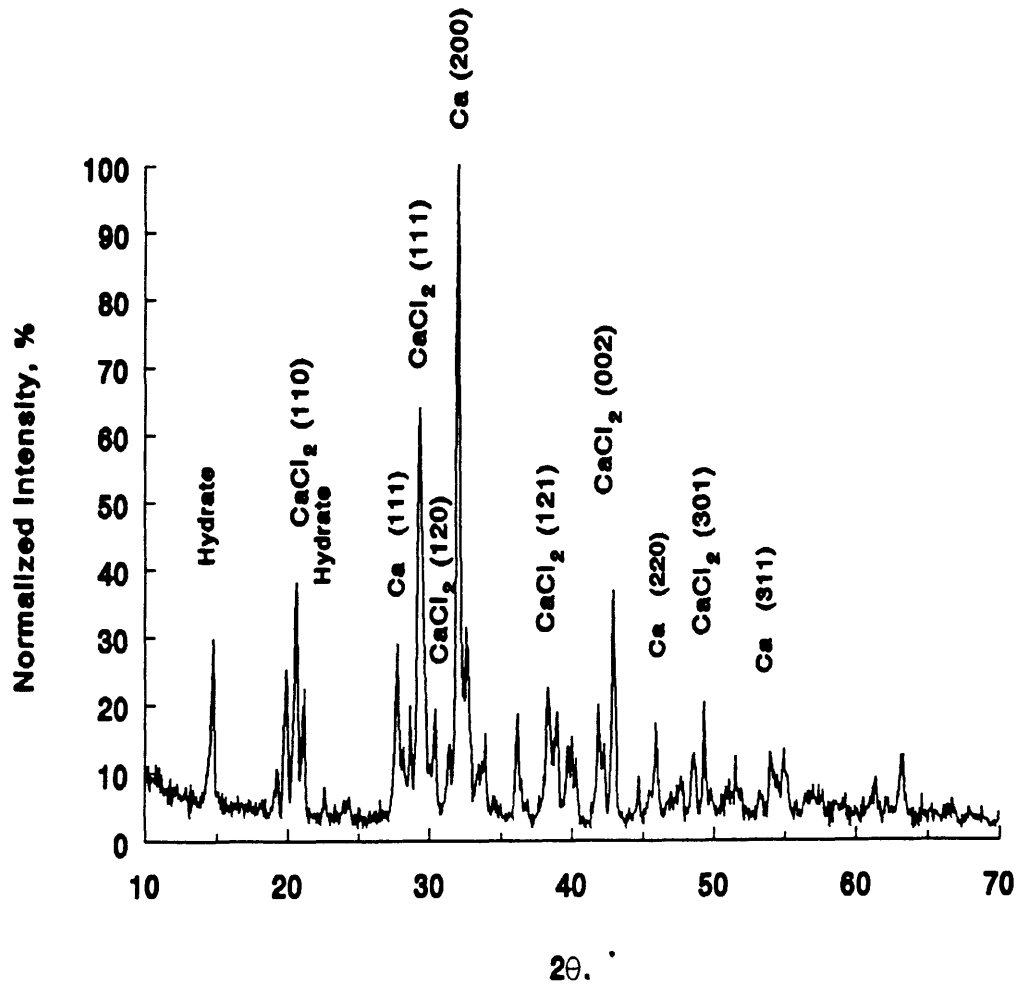


Figure 5.12: XRD pattern of molten Ca/CaCl₂ salt.

salt causing the shift in peak position. The XRD pattern, therefore, is not indicative of the actual salt composition. SEM/EDX analysis of a cross section of the crucible again shows significant calcium and chlorine migration of the salt from the ceramic/salt interface through the ceramic matrix. These photomicrographs are shown in Figures 5.13, 5.14, and 5.15 with the EDX results of the representative areas provided in Table 5.2.

Higher magnifications of these regions (refer to Figures 5.14 and 5.15) exhibit a broad difference in the microstructure between the ceramic/salt interface to the ceramic interior. The ceramic interior (refer to Figure 5.14a) displays a number of voids in the structure. Higher magnification (Figure 5.14b) of this region shows rounded off grains indicating corrosive attack of the structure. A number of smaller particles are also observed and presumed to be a secondary phase and/or salt. The interface region (refer to

TABLE 5.2
EDX Results of Ca/CaCl₂ Salt Exposed AlN

<u>Figure</u>	<u>Al (At. %)</u>	<u>Ca (At. %)</u>	<u>Cl (At. %)</u>
5.13a	0.91	39.59	59.50
5.13b	71.78	11.90	16.32
5.13c	98.42	0.50	1.08

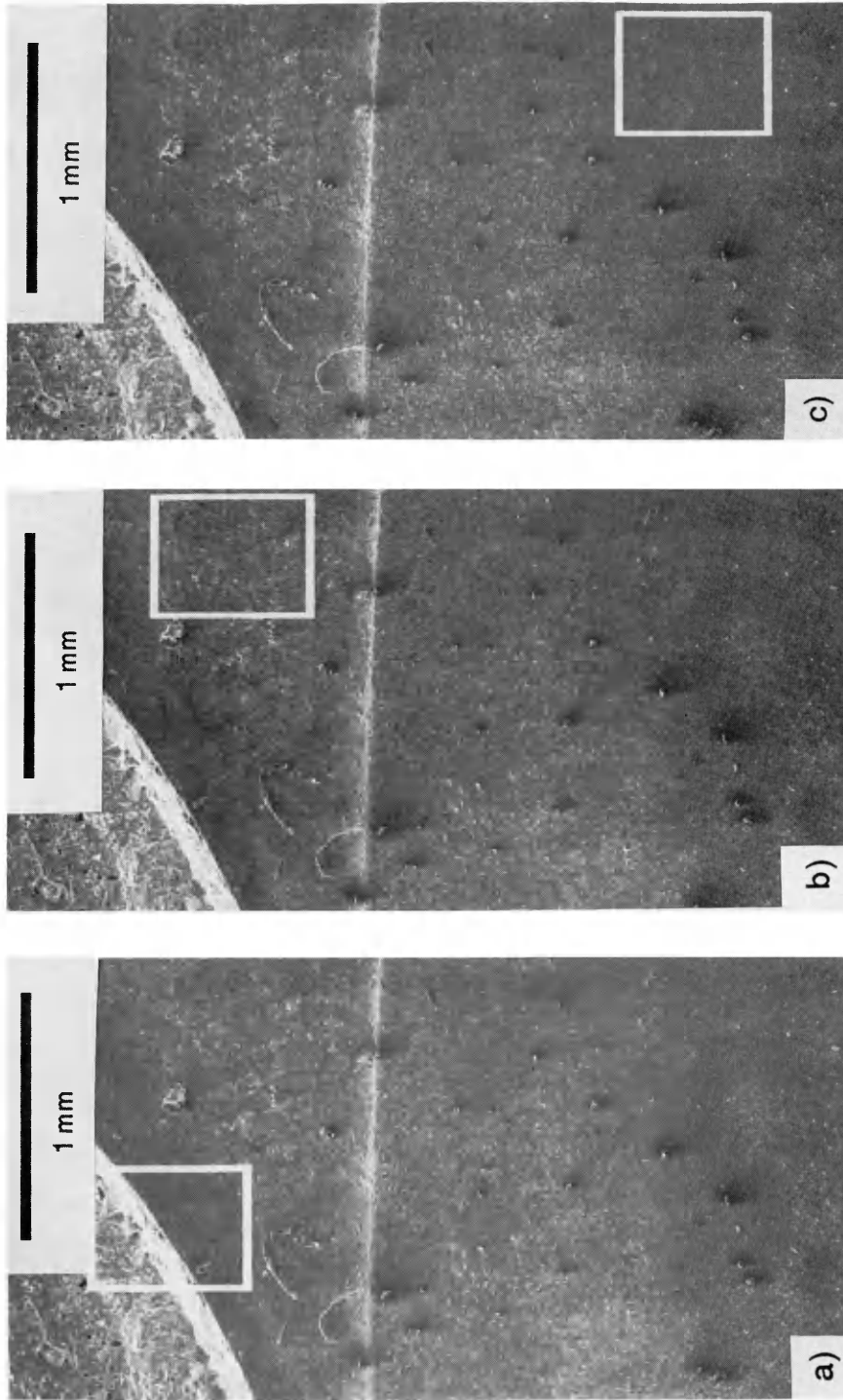


Figure 5.13: SEM micrographs of Ca/CaCl₂ exposed AlN crucible at 33X of a) ceramic/salt interface, b) mid-range, and c) ceramic interior.

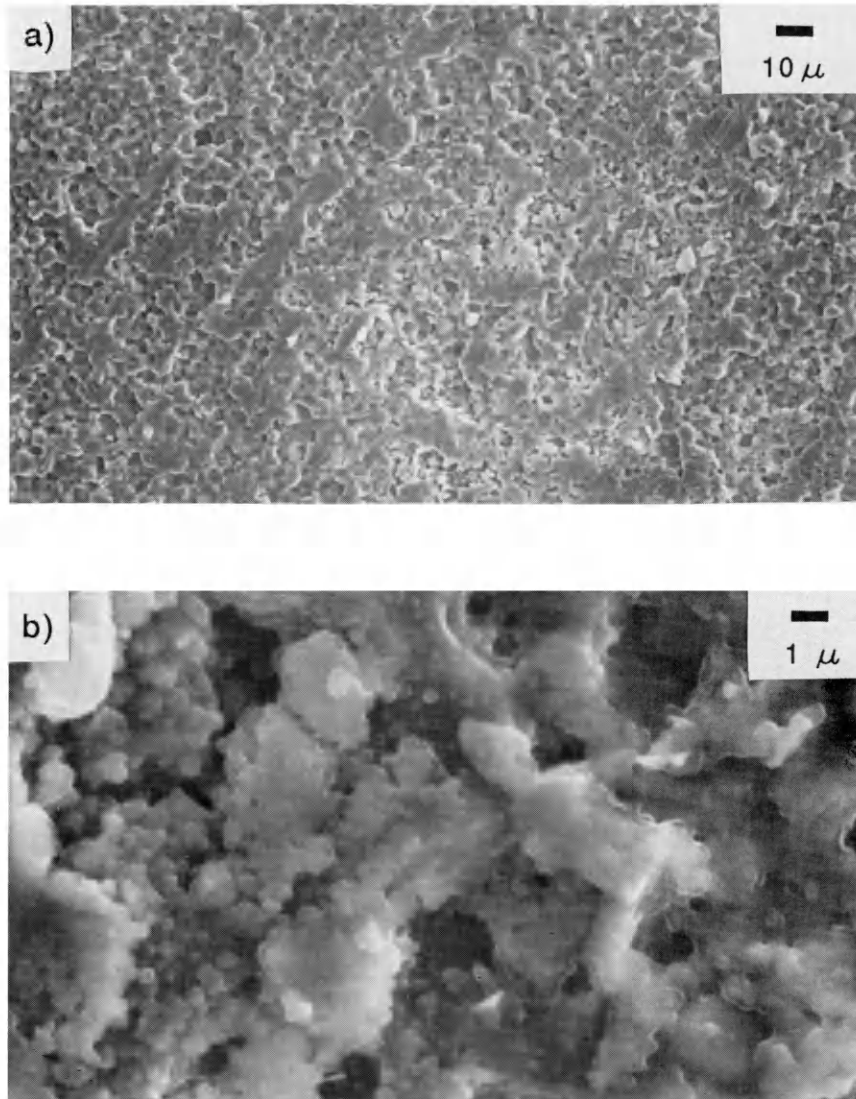


Figure 5.14: SEM Micrographs of Ca/CaCl₂ exposed AlN crucible of ceramic interior grain structure at a) 500X and b) 5,000X.

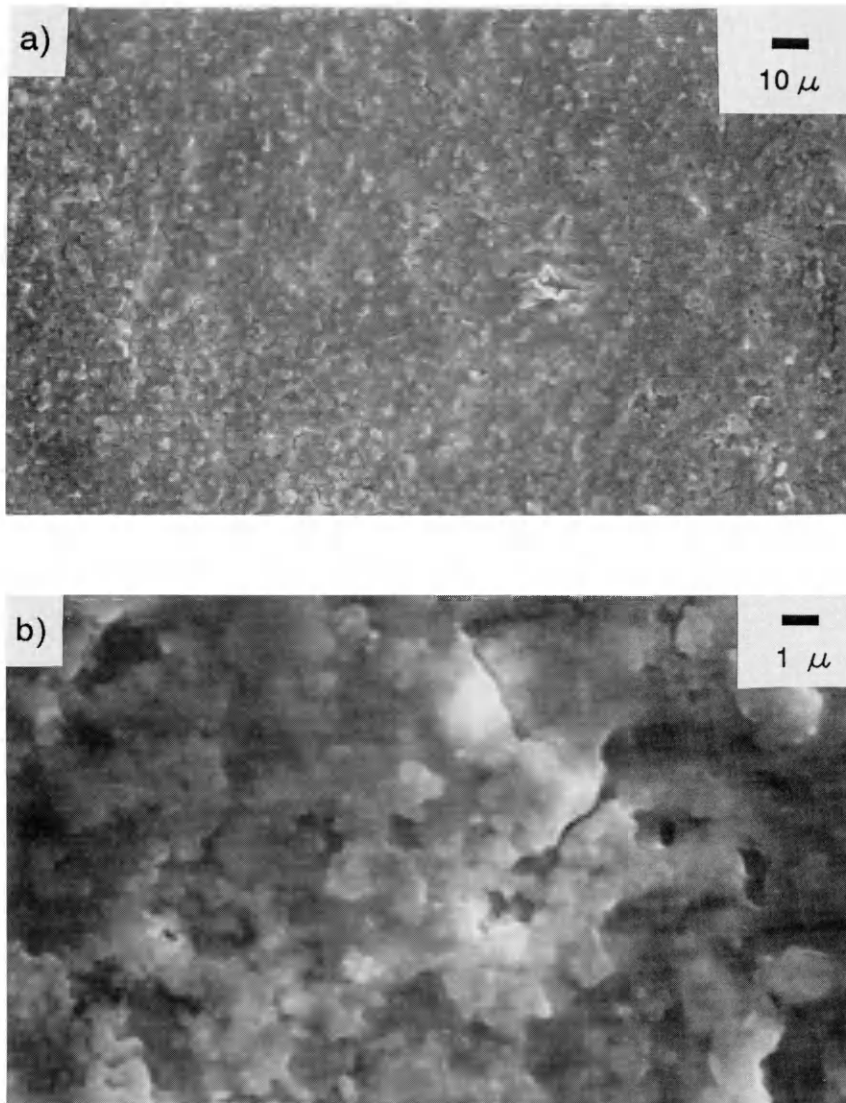


Figure 5.15: SEM Micrographs of Ca/CaCl₂ exposed AlN crucible of ceramic/salt interface grain structure at a) 500X and b) 5,000X.

Figure 5.15a) shows fewer voids in the structure than are present in the ceramic interior region. Rounded off grains are prevalent throughout the matrix.

5.2.3 Evaluation of Corrosion

The calcium chloride salts used in the DOR processing scheme caused extensive corrosion of the aluminum nitride crystal structure. Attack can be attributed to one of several mechanisms. These mechanisms include gaseous chlorine attack, attack by a reactive salt ion or ions (Ca^{2+} and Cl^-), enhanced mass diffusion between the crucible and the salt, and crucible decomposition in the molten salt. The EDX results from the calcium metal/calcium chloride salt (refer to Table 5.2) will only be considered in this analysis. The crucible used in the calcium chloride salt compatibility had previously been exposed to a calcium metal/calcium chloride salt; the atomic percentages in Table 5.1, therefore, are skewed.

The SEM/EDX results taken at the 3 positions (interface, interior #1, and interior #2) show calcium and chlorine migration through the ceramic matrix. The atomic percentages of calcium and chlorine at the interface are 39.6% and 59.5% respectively, as shown in Table 5.2. These levels are 11.9% and 16.3% at interior point #1 (Figure 5.13b) and 0.5% and 1.1% at interior point #2 (Figure 5.13c). The calcium

concentrations at these points may be somewhat skewed because of the presence of calcium containing secondary phases in the aluminum nitride grain boundaries. One can conclude from these results that the ratio of chlorine concentration to calcium concentration increases from the interface to the ceramic interior. The increasing chlorine to calcium ratio indicates that the main attack mechanism is chlorine migration through the crystal structure.

Four chlorine attack mechanisms are proposed. These mechanisms are: 1) mass diffusion from the crucible to the salt and vice versa; 2) solubility of the secondary phases in the molten salt; 3) gaseous chlorine attack; and 4) attack by a reactive chlorine ion. Mass diffusion involves transport of aluminum and nitrogen ions from the ceramic to the salt. Chlorine and calcium ions diffuse from the salt to the ceramic. This explanation accounts for the voids observed in the microstructure; aluminum and nitrogen are depleted from the ceramic through the diffusion process. The quantity of aluminum at the interface or in the salt (present as AlCl_3 , Al-Ca-O , etc.), however, is not sufficient for characterization and measurement by XRD. Nitrogen, however, may be present in the salt as calcium nitride or calcium chloryl nitride hydrate. Solubility of the secondary phases in the salt is occurring to some degree as characterized by

XRD (refer to Figures 5.16 and 5.17). The peak at 25° on the sintered aluminum nitride sample (refer to Figure 5.4) is not observed on exposed aluminum nitride. The chlorine gradient, however, from the interface to the ceramic interior appears to be more dominant than secondary phase solubility.

Gaseous chlorine attack occurs when the partial pressure of chlorine gas (p_{Cl_2}) exceeds an equilibrium partial pressure value. Chlorine attack results from a chlorine pressure/concentration gradient across the sample (higher chlorine levels at the interface and lower chlorine levels in the ceramic crystal structure). Chlorine, present as an atomic or molecular species, migrates from regions of higher chlorine concentrations to regions of lower concentrations along the grain boundaries to reach a pressure equilibrium [Werdecker, 1984; Kofstad, 1988]. From Kofstad's results, chlorine gas may be generated by one of the reactions shown below.



The presence of oxygen in the furnace is plausible. Oxygen could enter the furnace from a poor seal at the gas/thermocouple port. Chlorine gas could be generated from the chemical reaction between the salt and oxygen, as shown in equation 5.1.1. Similarly, chlorine gas could be generated from a chemical reaction between the salt, oxygen, and water

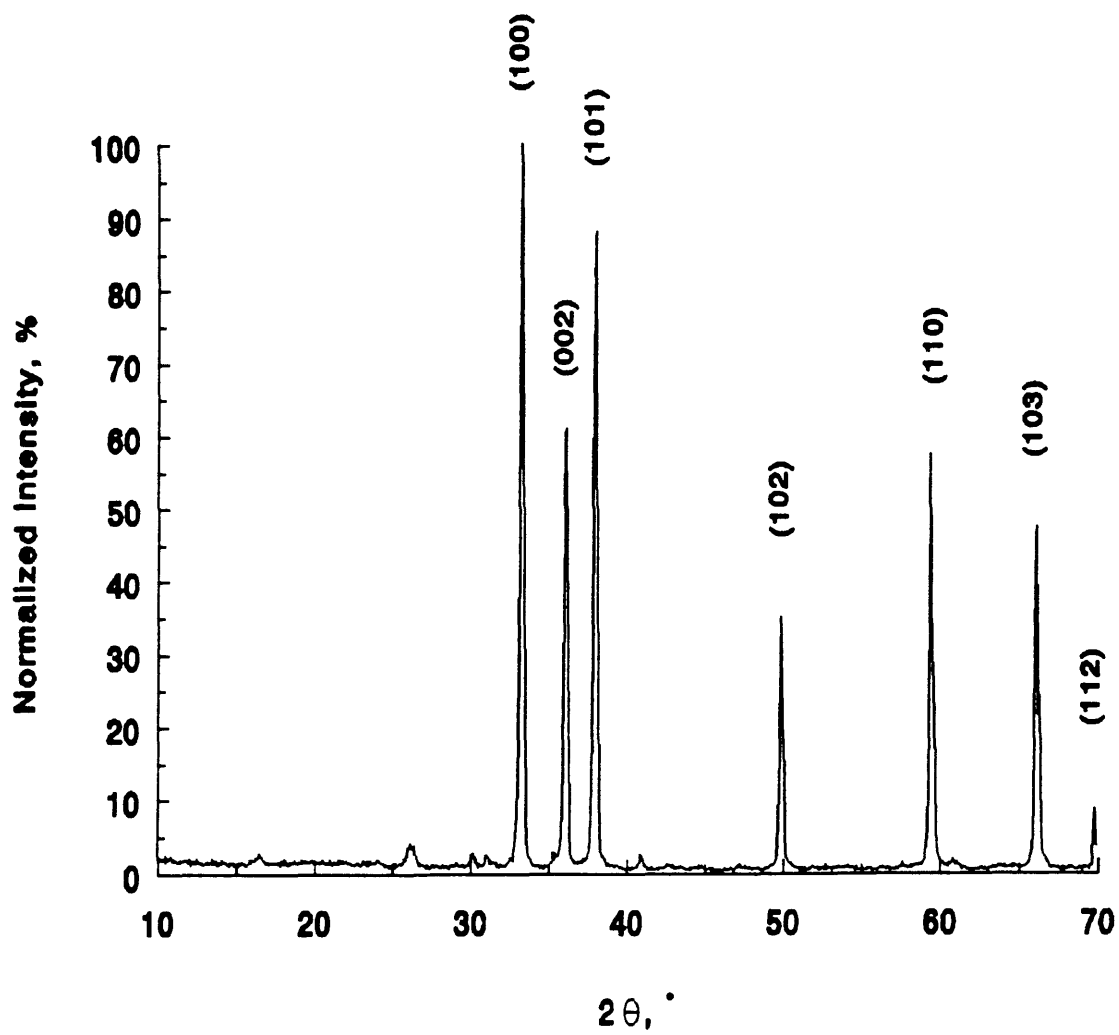


Figure 5.16: XRD pattern of CaCl_2 salt exposed AlN.

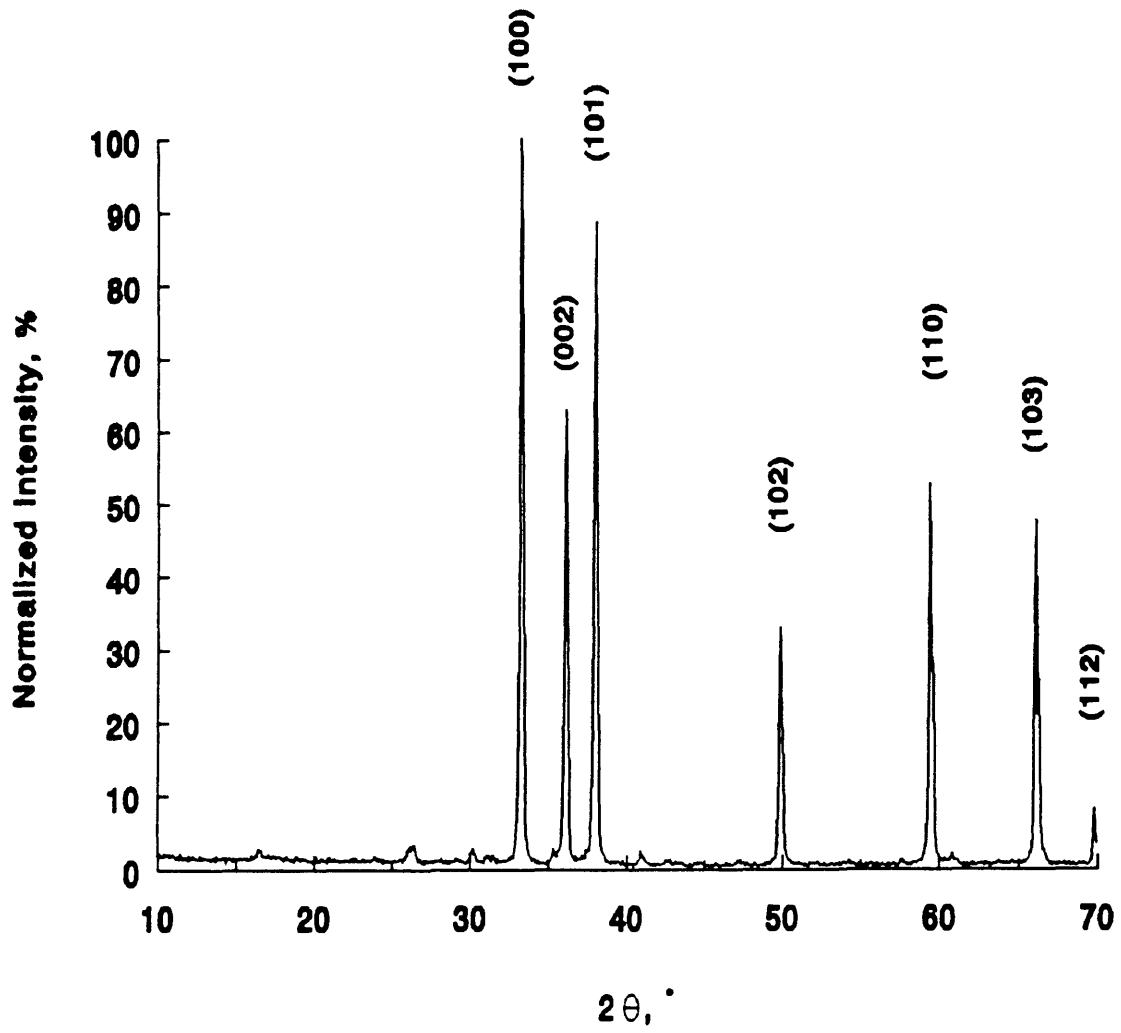


Figure 5.17: XRD pattern of Ca/CaCl₂ salt exposed AlN.

vapor as detailed in equation 5.2.2. Crucible attack occurs as chlorine gas is released from the salt oxidation/hydration. Chlorine diffusion at equilibrium is calculated by the following equation [Shewmon, 1963; Kingery, 1976]:

$$Dt/L^2 = 1 \quad (5.2)$$

where D = diffusion coefficient (cm^2/sec),

t = reaction time (sec), and

L = migration distance (cm).

In the example of the aluminum nitride crucible exposed to Ca/CaCl₂ at 835°C, the reaction time was 1½ hours, or 5400 seconds, and the chlorine migration distance was approximately 0.2 centimeters. These values correspond to a chlorine diffusion coefficient (D_{Cl}) of $7.4 \times 10^{-6} \text{ cm}^2/\text{sec}$. In comparison, diffusion coefficients for other ceramic materials at 1150 K are as follows: Al₂O₃ surface diffusion coefficient is $1.2 \times 10^{-15} \text{ cm}^2/\text{sec}$ [Gaddipati, 1986]; grain boundary diffusion coefficients for Co and Ni in MgO are $3.4 \times 10^{-14} \text{ cm}^2/\text{sec}$ and $1.7 \times 10^{-13} \text{ cm}^2/\text{sec}$, respectively [Bunch, 1985]; oxygen diffusion in Al₂O₃ is $1.2 \times 10^{-30} \text{ cm}^2/\text{sec}$ [Reed, 1980]; deuterium and tritium diffusion in MgO and SiC are $7.0 \times 10^{-7} \text{ cm}^2/\text{sec}$ [González, 1987] and 10^{-9} to $10^{-13} \text{ cm}^2/\text{sec}$ [Causey, 1978], respectively; and Cl diffusion in Cr₂O₃ is approximately $1.1 \times 10^{-13} \text{ cm}^2/\text{sec}$ [Quick, 1991]. The higher diffusion coefficient observed for chlorine in aluminum nitride is

due to a short-circuit diffusion process (i.e., grain boundary diffusion, defect diffusion). Chlorine migrates through the aluminum nitride as an atomic or molecular species [Kofstad, 1988] and attacks the aluminum nitride matrix allowing for increased diffusion due to the opened structure. The structure is infiltrated by molten calcium chloride salt as the salt fills the newly created voids. This infiltration is evidenced by SEM/EDX results of the microstructure. Calcium oxide and calcium hydroxide, if present in the salt, are not at sufficient levels to detect with XRD.

Ionic chlorine attack occurs as the molten calcium chloride salt dissociates into the individual species of Ca^{2+} and Cl^- ions. These ionic species may be extremely reactive at the temperatures involved (800°C to 850°C) as the ionic mobility is increased. Again, concentration gradients are present through the structure with higher calcium and chlorine concentrations at the interface than in the ceramic structure. The calcium gradient, however, would be somewhat lessened due to the presence of the calcium containing secondary phases in the aluminum nitride grain boundaries. Attack occurs as the ions traverse along the grain boundaries opening the structure. The newly created voids in the structure are thus filled as the molten salt infiltrates the structure.

5.3 ER Salt Exposure

The remaining aluminum nitride crucible was evaluated for salt release and corrosive attack in an ER salt environment. The salt release test was again subjective. The crucible was flipped and observed to see if the cooled salt cake would release or not. The corrosive attack evaluation involved SEM/EDX analysis of the exposed crucible. The results of these tests are discussed in greater detail below.

5.3.1 Sodium-Potassium Chloride Salt

The heat treatment of the equimolar sodium chloride-potassium chloride salt in the aluminum nitride crucible resulted in no apparent salt wetting on the aluminum nitride crucible. The lack of wetting is attributed to the ceramic-molten salt surface energy being higher than the ceramic-vacuum (vapor) surface energy ($\gamma_{SV} < \gamma_{SL}$). The spreading coefficient, therefore, was negative; a solid will not be wetted by a liquid when the spreading coefficient is negative [Hiemenz, 1986; Kingery, 1976]. Non-wetting also resulted in good salt release from the crucible due to the poor adhesion between the two.

SEM/EDX analysis of the ceramic microstructure (refer to Figures 5.18 and 5.19) show an open structure at the lower magnification photomicrographs (Figures 5.18a and 5.19a).

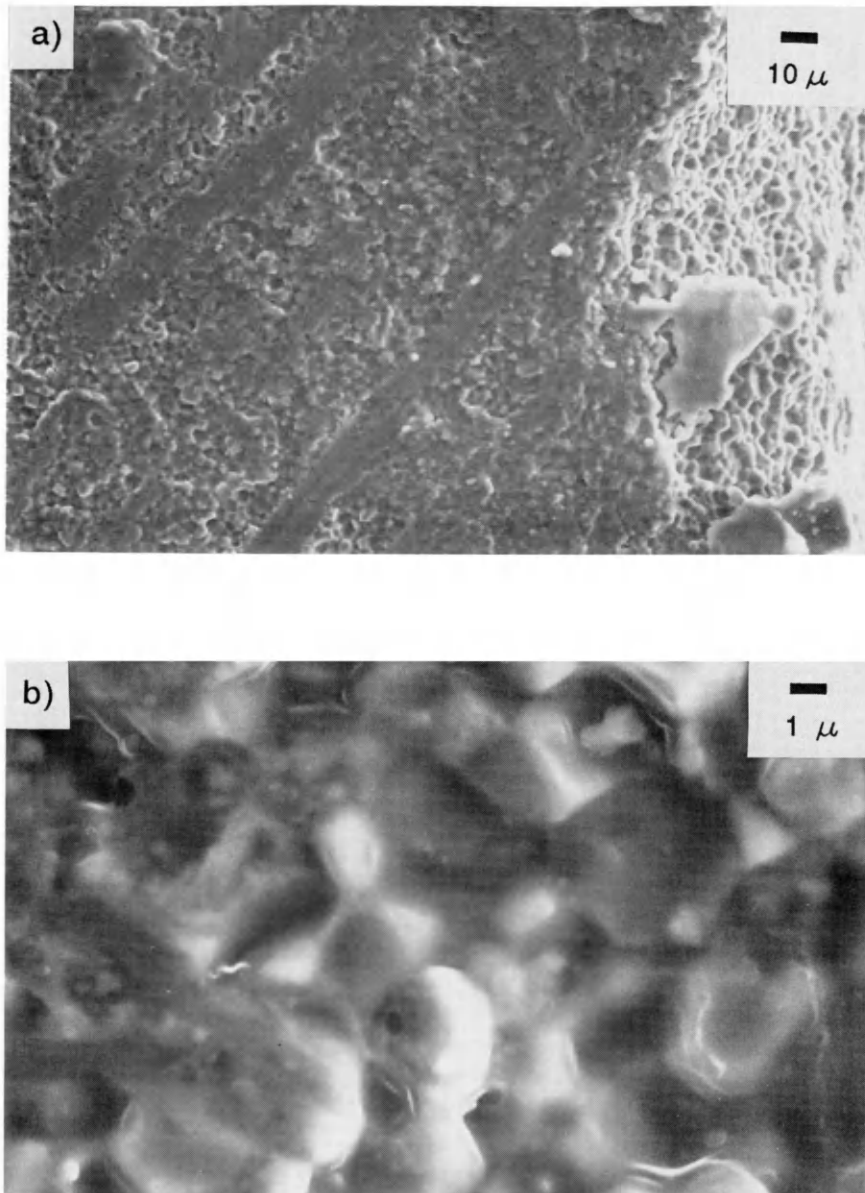


Figure 5.18: SEM Micrographs of NaCl-KCl exposed AlN crucible of ceramic grain structure near salt interface at a) 500X and b) 5,000X.

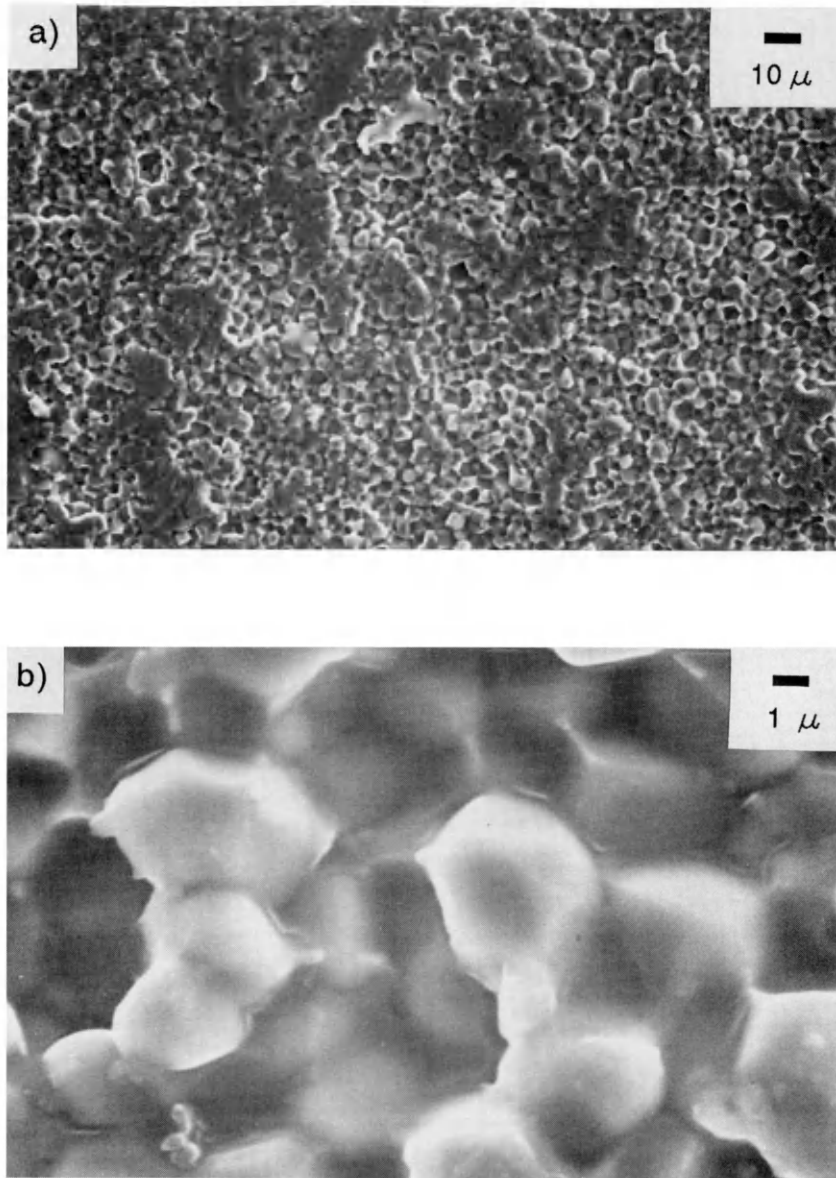


Figure 5.19: SEM Micrographs of NaCl-KCl exposed AlN crucible of ceramic grain structure in ceramic interior at a) 500X and b) 5,000X.

This open structure appears to be from pullout during the cutting operation as a dull blade was used to cut the crucible. Higher magnifications of these regions, however, show some subtle differences between the two regions. The photomicrograph of the ceramic/salt interface (refer to Figure 5.18b) shows the presence of a glassy phase in the grain boundaries. This phase is presumed to be a secondary phase or phases from the sintering operation. The shape of the grains in this region exhibits some round grains to be present; the rounded grains indicate possible corrosion of the ceramic. The glassy phase is also present in the photomicrograph of the ceramic interior (refer to Figure 5.19b). The grain shape in this region, however, is more sharp and distinct; few round grain shapes are present in the microstructure indicating no apparent corrosion of the ceramic. This region is more indicative of the as-fired ceramic.

EDX measurements were taken at three sites to ascertain salt migration through the ceramic structure. The sites examined are as follows: 1) approximately $10\mu\text{m}$ from the interface; 2) approximately $20\mu\text{m}$ from the interface (Figure 5.18); and approximately 1 mm from the interface (Figure 5.19). In the analysis, elements searched for were aluminum (Al), calcium (Ca), sodium (Na), potassium (K), and chlorine (Cl). Migration of the elements in the salt (Na, K, and Cl),

therefore, could be monitored and compared with the microstructure in the respective regions. The results from this EDX analysis are shown in Table 5.3 with elemental levels listed in atomic percentage.

The EDX results show migration of potassium and chlorine from the salt to the ceramic. Chlorine is more mobile, however, as noted by chlorine detection in the ceramic approximately 1 mm from the ceramic/salt interface. Potassium is present at the 10 μ m and 20 μ m sites but is not detected at the 1 mm site. Sodium was not detected in any of the samples.

5.3.2 Evaluation of Corrosion

The ER salt used in the compatibility testing did not produce the extensive corrosion on the aluminum nitride crucible that the DOR salt produced. The ER salt, however, appears to have resulted in limited corrosion near the ceramic/salt interface as noted by a few rounded off grains in the interface region. Corrosion is due to chlorine migration through the structure as measured by EDX of the respective

TABLE 5.3
EDX Results of NaCl-KCl Salt Exposed AlN

<u>Site</u>	<u>Al (At%)</u>	<u>Ca (At%)</u>	<u>Cl (At%)</u>	<u>Na (At%)</u>	<u>K (At%)</u>
10 μ m	95.18	2.60	1.55	0.00	0.67
20 μ m	97.16	1.68	0.83	0.00	0.33
1 mm	97.66	2.09	0.25	0.00	0.00

regions. Mechanisms for chlorine attack again are: 1) from a pressure gradient across a sample; or 2) from a reactive Cl^- ion. These mechanisms have been previously discussed.

The discrepancy in corrosion between the DOR salts and the ER salt can be attributed to chlorine gas generation. Chlorine gas could be generated in the DOR salt compatibility evaluation from a high temperature reaction between the salt and oxygen in the furnace. The ER salt compatibility evaluation, however, was conducted under a vacuum seal. Reaction between the salt and oxygen, therefore, in the ER salt evaluation is negligible. The crucible corrosion can be considered negligible under the limited salt exposure time and under non-oxidizing conditions.

CHAPTER 6

CONCLUSION

The objective of this research project was to fabricate an aluminum nitride crucible for molten salt and plutonium compatibility studies. The steps in the project are as follows:

- 1) procure spray dried aluminum nitride powder;
- 2) characterize powder samples by X-ray diffraction;
- 3) crucible forming and fabrication;
- 4) sintering;
- 5) DOR salt compatibility testing; and
- 6) ER salt compatibility.

This chapter of the thesis contains conclusions drawn from the work described. Recommendations for further study in this area of work and related areas of study have also been provided.

6.1 Enumerated Conclusions

The conclusions drawn from this study are as follows:

- a. Isostatic pressing proved successful in fabricating aluminum nitride crucibles. Proper tooling design permitted the pressing of a green shape that required minimal machining to achieve the designed tolerances.

b. Sintering conditions selected for this study (1850°C soak temperature, 5 hour soak time) proved successful in producing a near-fully dense aluminum nitride ceramic. The high degree of sintering is confirmed by X-ray diffraction of powder samples, fired bulk density measurement on sintered slugs, and scanning electron microscopy on the as-fired surface. Aluminum nitride samples were sintered to a 3.24 gm/cc fired bulk density, or 99.4% the theoretical density, at a 1850°C sintering temperature with minimal secondary phases present in the grain boundaries.

c. Solgasmix software predicts complete reduction of PuO_2 to Pu metal in a MgO crucible. MgO is also calculated to reduce to Mg metal; this reduction does not occur under actual processing condition.

d. An Al_2O_3 crucible is predicted by Solgasmix to be unstable in a DOR processing environment. PuOCl is estimated to form from the PuO_2 precursor.

e. A ZrO_2 crucible is also predicted by Solgasmix to be unstable in the DOR processing environment; Pu_2O_3 and PuOCl are calculated to be present at chemical equilibrium.

f. A SiC crucible is estimated by Solgasmix to undergo slight reduction in the DOR processing environment. Complete reduction of PuO_2 to Pu metal is also predicted.

g. A Si_3N_4 crucible is calculated by Solgasmix to be

unstable in the DOR processing environment. PuO_2 is predicted to react with the crucible to form PuN.

h. Aluminum nitride compatibility with plutonium, as determined using the Solgasmix computer program, is questionable. Calculations using older free energy data for PuN predict that PuN formation is more favorable than AlN stability. Calculations using newer free energy data for PuN, however, did not reach chemical equilibrium.

i. Aluminum nitride sintered with additions of calcium carbonate deteriorates in a molten calcium chloride salt and calcium metal/calcium chloride salt. The degradation of the ceramic is primarily due to chlorine attack along the grain boundaries allowing for salt infiltration into the ceramic structure. Rounded aluminum nitride grains are prevalent in the microstructure of salt exposed samples. Chlorine attack is believed to have resulted from a high temperature reaction between the salt and oxygen. Secondary phases resulting from the chemical reaction between the sintering additive and aluminum oxide are also soluble in the molten chloride salt.

j. Both calcium chloride salt and calcium metal/calcium chloride salt wet the aluminum nitride crucible. Wetting resulted in a strong adhesion between the salt and ceramic as salt release from the crucible was not observed. Adhesion was also due in part to the corrosive attack of the crucible by

the salt. Wetting characterization is essential for DOR crucible development.

k. An equimolar sodium chloride-potassium chloride salt did not wet the aluminum nitride crucible. The non-wetting resulted in good salt release from the crucible. The salt, however, did produce limited corrosion near the ceramic/salt interface. Corrosion is attributed to chlorine migration from the salt to the ceramic.

6.2 Recommendations for Further Study

a. Evaluate the corrosion resistance and wetting behavior of a pressureless sintered yttrium oxide sinter-aided aluminum nitride in a molten calcium chloride/calcium metal salt.

b. Conduct plutonium compatibility testing in aluminum nitride ceramic crucibles to determine whether aluminum nitride or plutonium nitride (PuN) formation is favorable.

c. Fabricate aluminum nitride with enhanced sintering techniques (higher temperature, longer soak time, pressure assisted) to reduce the secondary phases present in the grain boundaries. Evaluate this material for corrosion resistance in molten Ca/CaCl₂ salt and NaCl-KCl salt environments.

d. Continue crucible compatibility evaluations in DOR and ER salts using other crucible materials. Potential

ceramic materials include silicon carbide which was predicted to be stable in the DOR processing environment.

BIBLIOGRAPHY

- Abid, A. et al. (1986); "The thermal stability of AlN," J. of Matl. Sci., Vol. 21, pp. 1301-1304.
- Adamson, A.W. (1973); A Textbook of Physical Chemistry, Academic Press, NY, NY.
- American Ceramic Society (1991); Ceramic Source™ '91, Vol. 6, ed. by L.M. Shepard, Am. Cer. Soc., Westerville, OH.
- Andersen, F. (1991); Personal communications, Thermal Technology, Inc.
- Axler, K.M. (1990); "Solubility studies of the Ca-CaO-CaCl₂ system", M.S. Thesis, Colorado School of Mines, Golden, CO.
- Bagaasen, L.M. et al. (1990); "Investigation of coated refractory metals for plutonium processing," Trans. Am. Nuc. Soc., Vol. 62, pp. 240-241.
- Blakeley, K. (1990); Personal communications, Advanced Refractory Technology, Inc.
- Blum, J.B. and Anzai, K. (1989); "Aluminum nitride substrates for hybrid microelectronic applications," Hybrid Circuit Technology, Vol. 6, No. 8.
- Borom, M.P. et al. (1972); "Thermal conductivity of commercial aluminum nitride," Am. Cer. Soc. Bull., Vol. 51, No. 11, pp. 852-856.
- Bowen, P. et al. (1990); "Degradation of aluminum nitride powder in an aqueous environment," J. Am. Cer. Soc., Vol. 73, No. 3, pp. 724-728.
- Bunch, R.M. et al. (1985); "Light scattering measurements of diffusional growth in nickel- and cobalt-doped MgO," J. Applied Physics, Vol. 58, No. 4, pp. 1474-1482.
- Burke, J.E. (1958); "Recrystallization and sintering in ceramics," in Ceramic Fabrication Processes, ed. by W.D. Kingery, John Wiley & Sons, NY, NY, pp. 120-131.

- Causey, R.A. et al. (1978); "Hydrogen diffusion and solubility in silicon carbide," J. Am. Cer. Soc., Vol. 61, No. 5, pp. 221-225.
- Chase, M.W. et al. (1986); JANAF Thermochemical Tables, American Institute for Physics (3rd edition) NY, NY.
- Cleveland, J.M. (1970); The Chemistry of Plutonium, Gordon and Breach Science Publishers, NY, NY.
- Cook, L.P. et al. (1989); "Model for molten salt corrosion of ceramics," in Ceramics Transactions-Volume 10 Corrosion and Corrosive Degradation of Ceramics, ed. by R.E. Tressler and M. McNallum, Am. Cer. Soc., Westerville, OH, pp. 251-275.
- Cormack, A.N. (1989); "Intrinsic disorder in aluminum nitride," J. Am. Cer. Soc., Vol. 72, No. 9, pp. 1730-1732.
- Coyle, R.T. et al. (1985); The Corrosion of Materials in Molten Alkali Carbonate Salt at 900°C, Solar Energy Research Institute, Golden, CO.
- Cullity, B.D. (1978); Elements of X-ray Diffraction, Addison-Wesley Publishing (2nd edition), Reading MA.
- Cusick, M.J. (1989); "Plasma-arc synthesis of ultra-fine aluminum-nitride powder for electronic applications," Ph.D. Dissertation, Colorado School of Mines, Golden, CO.
- Cutler, I.B. (1978); "Active powders," in Ceramic Processing Before Firing, ed. by G.Y. Onoda, Jr. and L.L. Hench, John Wiley & Sons, NY, NY, pp. 21-29.
- Dettmer, E.S. et al. (1989); "Steady state thermal conductivity measurements of AlN and SiC substrate materials," IEEE Trans. on CHMT, Vol. CHMT-12, No. 4, pp. 543-547.
- Dunworth, R.J. and Brodsky, M.B. (1961); "Plutonium," in Metals Handbook Volume 1, ed. by T. Lyman, Amer. Soc. for Metals (8th edition), Novelty, OH, pp. 1218-1219.
- Ellinger, F.H. et al. (1968); "Constitution of plutonium alloys," LA-3870, Los Alamos Scientific Laboratory of the University of CA, Los Alamos, NM.

- Enloe, J. (1991); Personal communications, W.R. Grace & Co.
- Eriksson, G. (1975); "Thermodynamic studies of high temperature equilibria," *Chemica Scripta*, Vol. 8, No. 3, pp. 100-103.
- Fox, D.S. et al. (1989); "Hot corrosion of silicon carbide and silicon nitride at 1000°C," in Ceramics Transactions-Volume 10 Corrosion and Corrosive Degradation of Ceramics, ed. by R.E. Tressler and M. McNallum, Am. Cer. Soc., Westerville, OH, pp 227-249.
- Gaddipati, A.R. and Scott, W.D. (1986); "Surface mass transport of alumina," *J. Mat. Sci.*, Vol. 21, No. 2, pp. 419-423.
- González, R. and Chen, Y. (1987); "Deuteron diffusion and photoluminescence in lithium-doped MgO crystals," *Physical Review B*, Vol. 35, No. 15, pp. 8202-8206.
- Hiemenz, P.C. (1986); "Surface tension and contact angle: Application to pure substances." Chap. 6 in Principles in Colloid and Surface Chemistry, ed. by J.J. Lagowski, Marcel Dekker, Inc., NY, NY.
- Henager, C.H., Jr. and Jones, R.H. (1989); "Molten salt corrosion of hot-pressed Si₃N₄/SiC-reinforced composites and effects of molten salt exposure on slow crack growth of hot-pressed Si₃N₄," in Ceramics Transactions-Volume 10 Corrosion and Corrosive Degradation of Ceramics, ed. by R.E. Tressler and M. McNallum, Am. Cer. Soc., Westerville, OH, pp 197-210.
- Horsfield, H.T. (1934); "Strength of asphalt mixtures," *Journal of the Society of Chem. Ind. Transactions*, Vol. 53, pp. 107-115.
- Interrante, L.V. et al. (1986); "Studies of organometallic precursors to aluminum nitride," in Better Ceramics Through Chemistry II Volume 73, ed. by C.J. Brinker et al., Materials Research Society, MRS, Pittsburgh, PA, pp. 359-366.
- Iwase, N. et al. (1984); "Development of a high thermal conductive AlN ceramic substrate technology," *International J. for Hybrid Microelectronics*, Vol. 7, No. 4, pp. 49-53.

- Janeway, P.A. (1990); "ART taps new source of high-performance materials," *Ceramic Industry*, Vol. 135, No. 4. pp. 28-31.
- Johnson, D.W., Jr. and Gallagher, P.K. (1978); "Reactive powders from solutions," in Ceramic Processing Before Firing, ed. by G.Y. Onoda, Jr. and L.L. Hench, John Wiley & Sons, NY, NY, pp. 125-139.
- Keramont Advanced Ceramics Products Group (1986); "Aluminum nitride," Keramont Technical Data Sheet, Tucson, AZ.
- Khoury, I. (1991); Personal communications, Dow Chemical Co.
- Kingery, W.D. (1958); "Sintering in the presence of a liquid phase," in Ceramic Fabrication Processes, ed. by W.D. Kingery, John Wiley & Sons, NY, NY, pp. 131-143.
- Kingery, W.D. et al. (1976); Introduction to Ceramics, John Wiley & Sons (2nd edition), NY, NY.
- Kittel, C. (1986); Introduction to Solid State Physics, John Wiley & Sons (6th edition), NY, NY.
- Knudsen, A. (1991); Personal communications, Dow Chemical Co.
- Kofstad, P. (1988); "Growth and protective properties of chromia (Cr_2O_3) and alumina (Al_2O_3) scales, protective coatings." Chap. 12 in High Temperature Corrosion, Elsevier Applied Science Publishers Ltd., London.
- Komeya, K. et al. (1982); "Effects of various additives on sintering of aluminum nitride," NASA TM-76650.
- Kuramoto, N. et al. (1986a); "Translucent AlN ceramic substrate," 3rd IEEE CHMT Symp., pp. 424-429.
- Kuramoto, N. and Taniguchi, H. (1986b); "Fine powder of aluminum nitride, composition and sintered body thereof and processes for their production," U.S. Patent # 4,618,592.
- Kuramoto, N. et al. (1988); "Development of translucent aluminum nitride ceramics," *Am. Cer. Soc. Bull.*, Vol. 68, No. 4, pp. 883-887.

- Kurokawa, Y. et al. (1985); "AlN substrates with high thermal conductivity," IEEE Trans. on CHMT, Vol. CHMT-8, No. 2, pp. 247-252.
- Kurokawa, Y. et al. (1986); "Development of highly thermal conductive AlN substrate by green sheet technology," Proc. 3rd IEEE CHMT Symp., pp. 412-418.
- Kurokawa, Y. et al. (1988); "Development and microstructural characterization of high thermal-conductivity aluminum nitride ceramics," J. Am. Cer. Soc., Vol. 71, No. 7, pp. 588-594.
- Kuczynski, G.C. (1949); "Self-diffusion in sintering of metallic particles," J. of Metals Transactions, Vol. 1, No. 2, pp. 169-178.
- Levin, E.M. and McMurdie, H.F. (1975); Phase Diagrams for Ceramists, 1975 Supplement, American Ceramic Society, Westerville, OH, p. 132.
- Lewis, G.N. and Randall, M. (1961); Thermodynamics, rev. by K.S. Pitzer and L. Brewer, McGraw-Hill(2nd edition), NY, NY.
- Lopez, P. (1991); Personal communications, Los Alamos National Laboratory.
- Marra, J.E. (1991); Personal communications, Westinghouse Savannah River Co.
- Maya, L (1986); "Synthetic approaches to aluminum nitride via pyrolysis of a precursor," Advanced Ceramic Materials, Vol. 1, No. 2, pp. 150-153.
- McNallum, M. et al. (1989); "The mechanism of high temperature corrosion of SiC in flue gases from aluminum remelting furnaces," in Ceramics Transactions-Volume 10 Corrosion and Corrosive Degradation of Ceramics, ed. by R.E. Tressler and M. McNallum, Am. Cer. Soc., Westerville, OH, pp 445-467.
- Niesz, D.E. and Bennett, R.B. (1978); "Structure and properties of agglomerates," in Ceramic Processing Before Firing, ed. by G.Y. Onoda, Jr. and L.L. Hench, John Wiley & Sons, NY, NY, pp. 61-73.

- Ochi, A. et al. (1988); "The synthesis of aluminum nitride from aluminum hydride," in Better Ceramics Through Chemistry III Volume 121, ed. by C.J. Brinker et al., Materials Research Society, MRS, Pittsburgh, PA, pp. 663-666.
- Oetting, F.L. (1967); "Chemical thermodynamic properties of plutonium compounds," Chemical Reviews, Vol. 67, pp. 261-297.
- Onoda, G.Y., Jr. and Hench, L.L. (1978); "Physical characterization terminology," in Ceramic Processing Before Firing, ed. by G.Y. Onoda, Jr. and L.L. Hench, John Wiley & Sons, NY, NY, pp. 35-37.
- Paine, R.T. et. al. (1988); "Synthesis of AlN and AlN/SiC ceramics from polymeric molecular precursors," in Better Ceramics Through Chemistry III Volume 121, ed. by C.J. Brinker et al., Materials Research Society, MRS, Pittsburgh, PA, pp. 461-464.
- Pankratz, L.B. (1982); Thermodynamic Properties of Elements and Oxides, U.S. Bureau of Mines, Bulletin No. 672, U.S. Government Printing Office, Washington, D.C.
- Pankratz, L.B. et. al. (1984a); Thermodynamic Data for Mineral Technology, U.S. Bureau of Mines, Bulletin No. 677, U.S. Government Printing Office, Washington, D.C.
- Pankratz, L.B. (1984b); Thermodynamic Properties of Halides, U.S. Bureau of Mines, Bulletin No. 674, U.S. Government Printing Office, Washington, D.C.
- Pask, J.A., et al. (1976); "Dependence of sintering characteristics on thermodynamics and geometric factors," in Ceramic Microstructure '76, ed. by R.M. Fulrath and J.A. Pask, University of California-Berkeley, Berkeley, CA, pp. 246-254.
- Pollock, D.D. (1985); Electrical Conduction in Solids: An Introduction, Am. Soc. Metals, Metals Park, OH.
- Price, J.R. and Van Roode, M. (1989); "Corrosion resistant coatings for silicon carbide," in Ceramics Transactions-Volume 10 Corrosion and Corrosive Degradation of Ceramics, ed. by R.E. Tressler and M. McNallum, American Ceramic Society, Westerville, OH, pp 469-493.

- Quick, N.R. (1991); Personal communications, EG&G Rocky Flats, Inc.
- Reed, D.J. and Wuensch, B.J. (1980); "Ion-probe measurement of oxygen self-diffusion in single crystal Al_2O_3 ," J. Am. Cer. Soc., Vol. 63, No. 1-2, pp. 88-92.
- Reed, J.S. (1988); Introduction to the Principles of Ceramic Processing, John Wiley & Sons, NY, NY.
- Rhines, F.N. (1978); "Dynamic particle stacking," in Ceramic Processing Before Firing, ed. by G.Y. Onoda, Jr. and L.L. Hench, John Wiley & Sons, NY, NY, pp. 321-341.
- Robie, R.A. et. al. (1978); Thermodynamic Properties of Minerals and Related Substances at 298.15K and 1 Bar (10^5 Pascals) Pressure and at Higher Temperatures, U.S. Geological Survey Bulletin No. 1452, U.S. Government Printing Office, Washington, D.C.
- Roth, R.S. et al. (1981); Phase Diagrams for Ceramists, Volume IV, American Ceramic Society, Columbus, OH, pp. 95, 101.
- Saito, S. and Sawaoka, A. (1976); "Microstructure and strength of nitride ceramics," in Ceramic Microstructure '76, ed. by R.M. Fulrath and J.A. Pask, University of California-Berkeley, Berkeley, CA, pp. 645-667.
- Seibold, M. and Rüssel, C. (1988); "A novel route to aluminum nitride ceramics using a polyaminoalane precursor," in Better Ceramics Through Chemistry III Volume 121, ed. by C.J. Brinker et al., Materials Research Society, MRS, Pittsburgh, PA, pp. 477-482.
- Seibold, M.M. and Rüssel, C. (1989); "Thermal conversion of preceramic polyiminoalane precursors to aluminum nitride: Characterization of pyrolysis products," J. Am. Cer. Soc., Vol. 72, No. 8, pp. 1505-1505.
- Selman, J.R. and Maru, H.C. (1981); "Physical chemistry of alkali carbonate melts," in Advances in Molten Salt Chemistry Volume 4, ed. by G. Mamantov and J. Braunstein, Plenum Press, NY, NY, pp. 159-190.
- Shewmon, P.G. (1963); Diffusion in Solids, McGraw-Hill, NY, NY.

- Shukla, V.N. and Hill, D.C. (1989); "Binder evolution from powder compacts: Thermal profile for injection molded articles," J. Am. Cer. Soc., Vol. 72, No. 10, pp. 1797-1803.
- Slack, G.A. (1973); "Nonmetallic crystals with high thermal conductivity," J. Phys. Chem., Vol. 34, pp. 321-335.
- Slack, G.A. et al. (1987); "The intrinsic thermal conductivity of AlN," J. Phys. Chem. Solids, Vol. 48, No. 7, pp. 641-647.
- Solymar, L. and Walsh, D. (1979); Lectures on the Electrical Properties of Materials, Oxford University Press (2nd edition), London.
- Swalin, R.A. (1972); Thermodynamics of Solids, John Wiley & Sons (2nd edition), NY, NY.
- Tokuyama Soda Co., Ltd. (1986); "Shapal technical bulletin," Tokuyama Soda Technical Data Sheet, Tokyo, Japan.
- Tokuyama Soda Co., Ltd. (1987); "Measurement of thermal conductivity of Shapal AlN substrate," Tokuyama Soda Technical Data Sheet, Tokyo, Japan.
- Tremper, R.T. and Gordon, R.S. (1978); "Agglomeration effects on the sintering of alumina powders prepared by autoclaving aluminum metal," in Ceramic Processing Before Firing, ed. by G.Y. Onoda, Jr. and L.L. Hench, John Wiley & Sons, NY, NY, pp. 153-176.
- Troczynski, T.B. and Nicholson, P.S. (1989); "Effect of additives on the pressureless sintering of aluminum nitride between 1500° and 1800°C," J. Am. Cer. Soc., Vol. 72, No. 8, pp. 1488-1491.
- Udagawa, E. et al. (1990); "Influence of firing-gas pressure on the microstructure and thermal conductivity of AlN ceramics," J. Matl. Sci. Letters, Vol. 9, No. 1, pp. 116-118.
- VanDamme, N.S. et al. (1989); "Liquid-phase sintering of aluminum nitride by europium oxide additives," J. Am. Cer. Soc., Vol. 72, No. 8, pp. 1409-1414.

- Virkar, A.V. et al. (1989); "Thermodynamic and kinetic effects of oxygen removal on the thermal conductivity of aluminum nitride," J. Am. Cer. Soc., Vol. 72, No. 11, pp. 2031-2042.
- Werdecker, W. and Aldinger, F. (1984); "Aluminum nitride-An alternative ceramic substrate for high power applications in microcircuits," IEEE Trans. on CHMT, Vol. CHMT-7, No. 4, pp. 399-404.
- Wittmer, D.E. and Temuri, M.Z. (1991); "Thermochemical studies in selected metal-carbon-oxygen systems," J. Am. Cer. Soc. , Vol. 74, No. 5, pp. 973-982.

APPENDICES

Appendix A: Solgasmix Thermodynamic Data

DOR Thermo Data at 1148K in MgO Crucible
0602070302

Ar	Cl	O	Pu	Ca	Mg	
Ar	1.0	0.0	0.0	0.0	0.0	0.0
Cl2	0.0	2.0	0.0	0.0	0.0	0.0
O2	0.0	0.0	2.0	0.0	0.0	0.0
CaCl2	0.0	2.0	0.0	0.0	1.0	0.0
CaO	0.0	0.0	1.0	0.0	1.0	0.0
Pu	0.0	0.0	0.0	1.0	0.0	0.0
Ca	0.0	0.0	0.0	0.0	1.0	0.0
Mg	0.0	0.0	0.0	0.0	0.0	1.0
Pu2O3	0.0	0.0	3.0	2.0	0.0	0.0
PuOCl	0.0	1.0	1.0	1.0	0.0	0.0
MgO	0.0	0.0	1.0	0.0	0.0	1.0
PuO2	0.0	0.0	2.0	1.0	0.0	0.0
1	2	3	6	7	8	
1						
6	1	2	3	4	5	6
0.0		0.0		0.0		0.0
0.0		0.0		0.0		0.0
0.0		0.0		0.0		0.0
0.0		-817553.6	471.118	0.0	0.0	-44.392
0.0		-630105.02	88.058	0.0046089	4.3955e-6	0.0
0.0		0.0	0.0	0.0	0.0	0.0
0.0		0.0	0.0	0.0	0.0	0.0
0.0		0.0	0.0	0.0	0.0	0.0
1198925.2	-1752142.3	482.44	0.00797	0.0		-24.59774
0.0		-938864.5	268.7	0.0	0.0	-14.094
0.0		-589905.35	47.509	0.055	-6.0374e-6	0.0
911693.6	-1071601.9	309.3859	-0.00188	0.0		-14.00385

Appendix A: Solgasmix Thermodynamic Data (continued)

DOR Thermo Data at 1148K in Al₂O₃ Crucible
0602070302

Ar	Cl	O	Pu	Ca	Al		
Ar	1.0	0.0	0.0	0.0	0.0	0.0	0.0
Cl ₂	0.0	2.0	0.0	0.0	0.0	0.0	0.0
O ₂	0.0	0.0	2.0	0.0	0.0	0.0	0.0
CaCl ₂	0.0	2.0	0.0	0.0	1.0	0.0	0.0
CaO	0.0	0.0	1.0	0.0	1.0	0.0	0.0
Pu	0.0	0.0	0.0	1.0	0.0	0.0	0.0
Ca	0.0	0.0	0.0	0.0	1.0	0.0	0.0
Al	0.0	0.0	0.0	0.0	0.0	0.0	1.0
Pu ₂ O ₃	0.0	0.0	3.0	2.0	0.0	0.0	0.0
PuOCl	0.0	1.0	1.0	1.0	0.0	0.0	0.0
PuO ₂	0.0	0.0	2.0	1.0	0.0	0.0	0.0
Al ₂ O ₃	0.0	0.0	3.0	0.0	0.0	0.0	2.0
1	2	3	6	7	8		
1							
6	1	2	3	4	5	6	
0.0		0.0		0.0		0.0	0.0
0.0		0.0		0.0		0.0	0.0
0.0		0.0		0.0		0.0	0.0
0.0		-817553.6	471.118	0.0		0.0	-44.392
0.0		-630105.02	88.058	0.004609		4.3955e-6	0.0
0.0		0.0	0.0	0.0		0.0	0.0
0.0		0.0	0.0	0.0		0.0	0.0
0.0		0.0	0.0	0.0		0.0	0.0
1198925.2		-1742142.3	482.244	0.00797		0.0	-24.59774
0.0		-938864.5	268.7	0.0		0.0	-14.094
911693.6		-1071601.9	309.3859	-0.00188		0.0	-14.00385
0.0		-1673622.1	315.775	-0.004209		2.7021e-6	0.0

Appendix A: Solgasmix Thermodynamic Data (continued)

 DOR Thermo Data at 1148K in ZrO₂ Crucible
 0602070302

Ar	Cl	O	Pu	Ca	Zr	
Ar	1.0	0.0	0.0	0.0	0.0	0.0
Cl ₂	0.0	2.0	0.0	0.0	0.0	0.0
O ₂	0.0	0.0	2.0	0.0	0.0	0.0
CaCl ₂	0.0	2.0	0.0	0.0	1.0	0.0
CaO	0.0	0.0	1.0	0.0	1.0	0.0
Pu	0.0	0.0	0.0	1.0	0.0	0.0
Ca	0.0	0.0	0.0	0.0	1.0	0.0
Zr	0.0	0.0	0.0	0.0	0.0	1.0
Pu ₂ O ₃	0.0	0.0	3.0	2.0	0.0	0.0
PuOCl	0.0	1.0	1.0	1.0	0.0	0.0
ZrO ₂	0.0	0.0	2.0	0.0	0.0	1.0
PuO ₂	0.0	0.0	2.0	1.0	0.0	0.0
1 2 3 6 7 8						
1						
6 1 2 3 4 5 6						
0.0		0.0	0.0	0.0	0.0	0.0
0.0		0.0	0.0	0.0	0.0	0.0
0.0		0.0	0.0	0.0	0.0	0.0
0.0	-817553.6	471.118	0.0	0.0	0.0	-44.392
0.0	-630105.02	88.058	0.0046089	4.3955e-6	0.0	0.0
0.0	0.0	0.0	0.0	0.0	0.0	0.0
0.0	0.0	0.0	0.0	0.0	0.0	0.0
0.0	0.0	0.0	0.0	0.0	0.0	0.0
1198925.2	-1752124.2	482.44	0.00797	0.0	0.0	-24.59774
0.0	-938864.5	268.7	0.0	0.0	0.0	-14.094
0.0	-1095860.3	194.756	-8.8567e-3	1.7766e-6	0.0	0.0
911693.6	-1071601.9	309.3859	-0.00188	0.0	0.0	-14.00385

Appendix A: Solgasmix Thermodynamic Data (continued)

DOR Thermo Data at 1148K in SiC Crucible
0702110402

Ar	Cl	O	C	Pu	Ca	Si	
Ar	1.0	0.0	0.0	0.0	0.0	0.0	0.0
Cl2	0.0	2.0	0.0	0.0	0.0	0.0	0.0
O2	0.0	0.0	2.0	0.0	0.0	0.0	0.0
C	0.0	0.0	0.0	1.0	0.0	0.0	0.0
CaCl2	0.0	2.0	0.0	0.0	0.0	1.0	0.0
CaO	0.0	0.0	1.0	0.0	0.0	1.0	0.0
Pu	0.0	0.0	0.0	0.0	1.0	0.0	0.0
Ca	0.0	0.0	0.0	0.0	0.0	1.0	0.0
Si	0.0	0.0	0.0	0.0	0.0	0.0	1.0
Pu2O3	0.0	0.0	3.0	0.0	2.0	0.0	0.0
PuOCl	0.0	1.0	1.0	0.0	1.0	0.0	0.0
SiC	0.0	0.0	0.0	1.0	0.0	0.0	1.0
PuO2	0.0	0.0	2.0	0.0	1.0	0.0	0.0
PuC	0.0	0.0	0.0	0.8	1.0	0.0	0.0
PuC2	0.0	0.0	0.0	2.0	1.0	0.0	0.0
Pu2C3	0.0	0.0	0.0	3.0	2.0	0.0	0.0
SiO2(C)	0.0	0.0	2.0	0.0	0.0	0.0	1.0
1	2	3	4	7	8	9	
1							
6	1	2	3	4	5	6	
0.0			0.0		0.0		0.0
0.0			0.0		0.0		0.0
0.0			0.0		0.0		0.0
0.0			0.0		0.0		0.0
0.0		-817553.6	471.118	0.0	0.0		-44.392
0.0		-630105.02	88.058	0.004609	4.3955e-6	0.0	
0.0		0.0	0.0	0.0	0.0		0.0
0.0		0.0	0.0	0.0	0.0		0.0
0.0		0.0	0.0	0.0	0.0		0.0
1198925.2		-1742142.3	482.244	0.00797	0.0		-24.59774
0.0		-938864.5	268.7	0.0	0.0		-14.094
0.0		-71331.751	1.148	2.2918e-3	1.4189e-6	0.0	
911693.6		-1071601.9	309.3859	-0.00188	0.0		-14.00385
0.0		-1119.0024	-28.1751	0.014013	-3.8109e-6	0.0	
0.0		-5040.063	-20.192	0.010011	-2.2703e-6	0.0	
0.0		-8171.03	-46.7771	0.023959	-5.4884e-6	0.0	
0.0		-902868.57	168.673	1.4340e-3	1.1211e-6	0.0	

Appendix A: Solgasmix Thermodynamic Data (continued)

DOR Thermo Data at 1148K in Si₃N₄ Crucible #1
0702090402

Ar	Cl	O	N	Pu	Ca	Si	
Ar	1.0	0.0	0.0	0.0	0.0	0.0	0.0
Cl2	0.0	2.0	0.0	0.0	0.0	0.0	0.0
O2	0.0	0.0	2.0	0.0	0.0	0.0	0.0
N2	0.0	0.0	0.0	2.0	0.0	0.0	0.0
CaCl2	0.0	2.0	0.0	0.0	0.0	1.0	0.0
CaO	0.0	0.0	1.0	0.0	0.0	1.0	0.0
Pu	0.0	0.0	0.0	0.0	1.0	0.0	0.0
Ca	0.0	0.0	0.0	0.0	0.0	1.0	0.0
Si	0.0	0.0	0.0	0.0	0.0	0.0	1.0
Pu2O3	0.0	0.0	3.0	0.0	2.0	0.0	0.0
PuOCl	0.0	1.0	1.0	0.0	1.0	0.0	0.0
Si3N4	0.0	0.0	0.0	4.0	0.0	0.0	3.0
PuO2	0.0	0.0	2.0	0.0	1.0	0.0	0.0
PuN	0.0	0.0	0.0	1.0	1.0	0.0	0.0
SiO2(C)	0.0	0.0	2.0	0.0	0.0	0.0	1.0
1 2 3 4 7 8 9							
1							
6 1 2 3 4 5 6							
0.0		0.0	0.0	0.0	0.0	0.0	0.0
0.0		0.0	0.0	0.0	0.0	0.0	0.0
0.0		0.0	0.0	0.0	0.0	0.0	0.0
0.0		0.0	0.0	0.0	0.0	0.0	0.0
0.0	-817553.6		471.118	0.0	0.0		-44.392
0.0	-630105.02		88.058	0.0046089	4.3955e-6		0.0
0.0	0.0		0.0	0.0	0.0		0.0
0.0	0.0		0.0	0.0	0.0		0.0
0.0	0.0		0.0	0.0	0.0		0.0
1198925.2	-1752142.3		482.44	0.00797	0.0		-24.59774
0.0	-938864.5		268.7	0.0	0.0		-14.094
0.0	-735038.44		300.268	0.016	1.3345e-6		0.0
911693.6	-1071601.9		309.3859	-0.00188	0.0		-14.00385
0.0	-319018.17		97.71109	9.5000e-5	-7.9775e-7		0.0
0.0	-902868.57		168.673	1.4400e-3	1.1211e-6		0.0

Appendix A: Solgasmix Thermodynamic Data (continued)

DOR Thermo Data at 1148K in Si₃N₄ Crucible #2
0702090402

Ar	Cl	O	N	Pu	Ca	Si	
Ar	1.0	0.0	0.0	0.0	0.0	0.0	0.0
Cl ₂	0.0	2.0	0.0	0.0	0.0	0.0	0.0
O ₂	0.0	0.0	2.0	0.0	0.0	0.0	0.0
N ₂	0.0	0.0	0.0	2.0	0.0	0.0	0.0
CaCl ₂	0.0	2.0	0.0	0.0	0.0	1.0	0.0
CaO	0.0	0.0	1.0	0.0	0.0	1.0	0.0
Pu	0.0	0.0	0.0	0.0	1.0	0.0	0.0
Ca	0.0	0.0	0.0	0.0	0.0	1.0	0.0
Si	0.0	0.0	0.0	0.0	0.0	0.0	1.0
Pu ₂ O ₃	0.0	0.0	3.0	0.0	2.0	0.0	0.0
PuOCl	0.0	1.0	1.0	0.0	1.0	0.0	0.0
Si ₃ N ₄	0.0	0.0	0.0	4.0	0.0	0.0	3.0
PuO ₂	0.0	0.0	2.0	0.0	1.0	0.0	0.0
PuN	0.0	0.0	0.0	1.0	1.0	0.0	0.0
SiO ₂ (C)	0.0	0.0	2.0	0.0	0.0	0.0	1.0
1 2 3 4 7 8 9							
1							
6 1 2 3 4 5 6							
0.0		0.0	0.0	0.0	0.0	0.0	0.0
0.0		0.0	0.0	0.0	0.0	0.0	0.0
0.0		0.0	0.0	0.0	0.0	0.0	0.0
0.0		0.0	0.0	0.0	0.0	0.0	0.0
0.0		-817553.6	471.118	0.0	0.0		-44.392
0.0		-630105.02	88.058	0.0046089	4.3955e-6	0.0	
0.0		0.0	0.0	0.0	0.0	0.0	0.0
0.0		0.0	0.0	0.0	0.0	0.0	0.0
0.0		0.0	0.0	0.0	0.0	0.0	0.0
1198925.2		-1752142.3	482.44	0.00797	0.0		-24.59774
0.0		-938864.5	268.7	0.0	0.0		-14.094
0.0		-735038.44	300.268	0.016	1.3345e-6	0.0	
911693.6		-1071601.9	309.3859	-0.00188	0.0		-14.00385
0.0		-298985.55	81.379613	0.016622	-4.9127e-6	0.0	
0.0		-902868.57	168.673	1.4400e-3	1.1211e-6	0.0	

Appendix A: Solgasmix Thermodynamic Data (continued)

DOR Thermo Data at 1148K in AlN Crucible #1

0702090402

Ar	Cl	O	N	Pu	Ca	Al	
Ar	1.0	0.0	0.0	0.0	0.0	0.0	0.0
Cl2	0.0	2.0	0.0	0.0	0.0	0.0	0.0
O2	0.0	0.0	2.0	0.0	0.0	0.0	0.0
N2	0.0	0.0	0.0	2.0	0.0	0.0	0.0
CaCl2	0.0	2.0	0.0	0.0	0.0	1.0	0.0
CaO	0.0	0.0	1.0	0.0	0.0	1.0	0.0
Pu	0.0	0.0	0.0	0.0	1.0	0.0	0.0
Ca	0.0	0.0	0.0	0.0	0.0	1.0	0.0
Al	0.0	0.0	0.0	0.0	0.0	0.0	1.0
Pu2O3	0.0	0.0	3.0	0.0	2.0	0.0	0.0
PuOCl	0.0	1.0	1.0	0.0	1.0	0.0	0.0
AlN	0.0	0.0	0.0	1.0	0.0	0.0	1.0
PuO2	0.0	0.0	2.0	0.0	1.0	0.0	0.0
PuN	0.0	0.0	0.0	1.0	1.0	0.0	0.0
Al2O3	0.0	0.0	3.0	0.0	0.0	0.0	2.0
1	2	3	4	7	8	9	
1							
6	1	2	3	4	5	6	
0.0			0.0		0.0		0.0
0.0		0.0		0.0		0.0	0.0
0.0		0.0		0.0		0.0	0.0
0.0		0.0		0.0		0.0	0.0
0.0		-817553.6	471.118	0.0	0.0		-44.392
0.0		-630105.02	88.058	0.004609	4.3955e-6	0.0	
0.0		0.0	0.0	0.0	0.0		0.0
0.0		0.0	0.0	0.0	0.0		0.0
0.0		0.0	0.0	0.0	0.0		0.0
1198925.2	-1742142.3	482.244	0.00797	0.0			-24.59774
0.0	-938864.5	268.7	0.0	0.0			-14.094
0.0	-317334.54	105.236	2.3000e-5	1.2919e-6	0.0		
911693.6	-1071601.9	309.3859	-0.00188	0.0			-14.00385
0.0	-319018.17	97.71109	9.5000e-5	-7.9775e-7	0.0		
0.0	-1673622.1	315.775	-0.004209	2.7021e-6	0.0		

Appendix A: Solgasmix Thermodynamic Data (continued)

DOR Thermo Data at 1148K in AlN Crucible #2

0702090402

Ar	Cl	O	N	Pu	Ca	Al	
Ar	1.0	0.0	0.0	0.0	0.0	0.0	0.0
Cl2	0.0	2.0	0.0	0.0	0.0	0.0	0.0
O2	0.0	0.0	2.0	0.0	0.0	0.0	0.0
N2	0.0	0.0	0.0	2.0	0.0	0.0	0.0
CaCl2	0.0	2.0	0.0	0.0	0.0	1.0	0.0
CaO	0.0	0.0	1.0	0.0	0.0	1.0	0.0
Pu	0.0	0.0	0.0	0.0	1.0	0.0	0.0
Ca	0.0	0.0	0.0	0.0	0.0	1.0	0.0
Al	0.0	0.0	0.0	0.0	0.0	0.0	1.0
Pu2O3	0.0	0.0	3.0	0.0	2.0	0.0	0.0
PuOCl	0.0	1.0	1.0	0.0	1.0	0.0	0.0
AlN	0.0	0.0	0.0	1.0	0.0	0.0	1.0
PuO2	0.0	0.0	2.0	0.0	1.0	0.0	0.0
PuN	0.0	0.0	0.0	1.0	1.0	0.0	0.0
Al2O3	0.0	0.0	3.0	0.0	0.0	0.0	2.0
1	2	3	4	7	8	9	
1							
6	1	2	3	4	5	6	
0.0		0.0	0.0	0.0	0.0	0.0	0.0
0.0		0.0	0.0	0.0	0.0	0.0	0.0
0.0		0.0	0.0	0.0	0.0	0.0	0.0
0.0		0.0	0.0	0.0	0.0	0.0	0.0
0.0		-817553.6	471.118	0.0	0.0	-44.392	
0.0		-630105.02	88.058	0.004609	4.3955e-6	0.0	
0.0		0.0	0.0	0.0	0.0	0.0	0.0
0.0		0.0	0.0	0.0	0.0	0.0	0.0
0.0		0.0	0.0	0.0	0.0	0.0	0.0
1198925.2		-1742142.3	482.244	0.00797	0.0	-24.59774	
0.0		-938864.5	268.7	0.0	0.0	-14.094	
0.0		-317334.54	105.236	2.3000e-5	1.2919e-6	0.0	
911693.6		-1071601.9	309.3859	-0.00188	0.0	-14.00385	
0.0		-298985.55	81.379613	0.016622	-4.9127e-6	0.0	
0.0		-1673622.1	315.775	-0.004209	2.7021e-6	0.0	

Appendix A: Solgasmix Thermodynamic Data (continued)

ER Thermo Data at 1148K in AlN Crucible #1
0702060302

Ar	Cl	N	Pu	Na	K	Al	
Ar	1.0	0.0	0.0	0.0	0.0	0.0	0.0
Cl ₂	0.0	2.0	0.0	0.0	0.0	0.0	0.0
N ₂	0.0	0.0	2.0	0.0	0.0	0.0	0.0
NaCl	0.0	1.0	0.0	0.0	1.0	0.0	0.0
KCl	0.0	1.0	0.0	0.0	0.0	1.0	0.0
Pu	0.0	0.0	0.0	1.0	0.0	0.0	0.0
Na	0.0	0.0	0.0	0.0	1.0	0.0	0.0
K	0.0	0.0	0.0	0.0	0.0	1.0	0.0
Al	0.0	0.0	0.0	0.0	0.0	0.0	1.0
AlN	0.0	0.0	1.0	0.0	0.0	0.0	1.0
PuN	0.0	0.0	1.0	1.0	0.0	0.0	0.0
1 2 3 6 7 8 9							
1							
6 1 2 3 4 5 6							
0.0	0.0	0.0	0.0	0.0	0.0	0.0	0.0
0.0	0.0	0.0	0.0	0.0	0.0	0.0	0.0
0.0	0.0	0.0	0.0	0.0	0.0	0.0	0.0
118721.	-400446.5	226.463	-2.008e-4	0.0		-20.677	
400513.4	-522953.98	427.37	6.945e-4	0.0		-4.50198	
0.0	0.0	0.0	0.0	0.0	0.0	0.0	0.0
0.0	0.0	0.0	0.0	0.0	0.0	0.0	0.0
0.0	0.0	0.0	0.0	0.0	0.0	0.0	0.0
0.0	0.0	0.0	0.0	0.0	0.0	0.0	0.0
0.0	-317334.54	105.236	2.3000e-5	1.2919e-6	0.0	0.0	0.0
0.0	-319018.17	97.71109	9.5000e-5	-7.9775e-7	0.0	0.0	0.0

Appendix A: Solgasmix Thermodynamic Data (continued)

ER Thermo Data at 1148K in AlN Crucible #2
0702060302

Ar	Cl	N	Pu	Na	K	Al	
Ar	1.0	0.0	0.0	0.0	0.0	0.0	0.0
Cl ₂	0.0	2.0	0.0	0.0	0.0	0.0	0.0
N ₂	0.0	0.0	2.0	0.0	0.0	0.0	0.0
NaCl	0.0	1.0	0.0	0.0	1.0	0.0	0.0
KCl	0.0	1.0	0.0	0.0	0.0	1.0	0.0
Pu	0.0	0.0	0.0	1.0	0.0	0.0	0.0
Na	0.0	0.0	0.0	0.0	1.0	0.0	0.0
K	0.0	0.0	0.0	0.0	0.0	1.0	0.0
Al	0.0	0.0	0.0	0.0	0.0	0.0	1.0
AlN	0.0	0.0	1.0	0.0	0.0	0.0	1.0
PuN	0.0	0.0	1.0	1.0	0.0	0.0	0.0
1 2 3 6 7 8 9							
1							
6 1 2 3 4 5 6							
0.0	0.0	0.0	0.0	0.0	0.0	0.0	0.0
0.0	0.0	0.0	0.0	0.0	0.0	0.0	0.0
0.0	0.0	0.0	0.0	0.0	0.0	0.0	0.0
118721.	-400446.5	226.463	-2.008e-4	0.0		-20.677	
400513.4	-522953.98	427.37	6.945e-4	0.0		-4.50198	
0.0	0.0	0.0	0.0	0.0	0.0	0.0	0.0
0.0	0.0	0.0	0.0	0.0	0.0	0.0	0.0
0.0	0.0	0.0	0.0	0.0	0.0	0.0	0.0
0.0	0.0	0.0	0.0	0.0	0.0	0.0	0.0
0.0	-317334.54	105.236	2.3000e-5	1.2919e-6	0.0	0.0	0.0
0.0	-298985.55	81.379613	0.016622	-4.9127e-6	0.0	0.0	0.0

Appendix A: Solgasmix Thermodynamic Data (continued)

ER Thermo Data at 1148K in AlN Crucible #3
0803070303

Ar	Cl	N	Pu	Na	K	Mg	Al
Ar	1.0	0.0	0.0	0.0	0.0	0.0	0.0
Cl2	0.0	2.0	0.0	0.0	0.0	0.0	0.0
N2	0.0	0.0	2.0	0.0	0.0	0.0	0.0
NaCl	0.0	1.0	0.0	0.0	1.0	0.0	0.0
KCl	0.0	1.0	0.0	0.0	0.0	1.0	0.0
MgCl2	0.0	2.0	0.0	0.0	0.0	0.0	1.0
Pu	0.0	0.0	0.0	1.0	0.0	0.0	0.0
Na	0.0	0.0	0.0	0.0	1.0	0.0	0.0
K	0.0	0.0	0.0	0.0	0.0	1.0	0.0
Mg	0.0	0.0	0.0	0.0	0.0	0.0	1.0
Al	0.0	0.0	0.0	0.0	0.0	0.0	0.0
AlN	0.0	0.0	1.0	0.0	0.0	0.0	0.0
PuN	0.0	0.0	1.0	1.0	0.0	0.0	0.0
1 2 3 7 8 9 10 11							
1							
6 1 2 3 4 5 6							
0.0	0.0	0.0	0.0	0.0	0.0	0.0	0.0
0.0	0.0	0.0	0.0	0.0	0.0	0.0	0.0
0.0	0.0	0.0	0.0	0.0	0.0	0.0	0.0
118721.	-400446.5	226.463	-2.008e-4	0.0	-20.677		
400513.4	-522953.98	427.37	6.945e-4	0.0	-4.50198		
-694334.8	-627378.25	349.979	0.004862	0.0	-30.7273		
0.0	0.0	0.0	0.0	0.0	0.0	0.0	0.0
0.0	0.0	0.0	0.0	0.0	0.0	0.0	0.0
0.0	0.0	0.0	0.0	0.0	0.0	0.0	0.0
0.0	0.0	0.0	0.0	0.0	0.0	0.0	0.0
0.0	0.0	0.0	0.0	0.0	0.0	0.0	0.0
0.0	-317334.54	105.236	2.3000e-5	1.2919e-6	0.0		
0.0	-319018.17	97.71109	9.5000e-5	-7.9775e-7	0.0		

Appendix A: Solgasmix Thermodynamic Data (continued)

ER Thermo Data at 1148K in AlN Crucible #4
0803070303

Ar	Cl	N	Pu	Na	K	Mg	Al
Ar	1.0	0.0	0.0	0.0	0.0	0.0	0.0
Cl ₂	0.0	2.0	0.0	0.0	0.0	0.0	0.0
N ₂	0.0	0.0	2.0	0.0	0.0	0.0	0.0
NaCl	0.0	1.0	0.0	0.0	1.0	0.0	0.0
KCl	0.0	1.0	0.0	0.0	0.0	1.0	0.0
MgCl ₂	0.0	2.0	0.0	0.0	0.0	0.0	1.0
Pu	0.0	0.0	0.0	1.0	0.0	0.0	0.0
Na	0.0	0.0	0.0	0.0	1.0	0.0	0.0
K	0.0	0.0	0.0	0.0	0.0	1.0	0.0
Mg	0.0	0.0	0.0	0.0	0.0	0.0	1.0
Al	0.0	0.0	0.0	0.0	0.0	0.0	1.0
AlN	0.0	0.0	1.0	0.0	0.0	0.0	1.0
PuN	0.0	0.0	1.0	1.0	0.0	0.0	0.0
1 2 3 7 8 9 10 11							
1							
6 1 2 3 4 5 6							
0.0	0.0	0.0	0.0	0.0	0.0	0.0	0.0
0.0	0.0	0.0	0.0	0.0	0.0	0.0	0.0
0.0	0.0	0.0	0.0	0.0	0.0	0.0	0.0
118721.	-400446.5	226.463	-2.008e-4	0.0	-20.677		
400513.4	-522953.98	427.37	6.945e-4	0.0	-4.50198		
-694334.8	-627378.25	349.979	0.004862	0.0	-30.7273		
0.0	0.0	0.0	0.0	0.0	0.0	0.0	0.0
0.0	0.0	0.0	0.0	0.0	0.0	0.0	0.0
0.0	0.0	0.0	0.0	0.0	0.0	0.0	0.0
0.0	0.0	0.0	0.0	0.0	0.0	0.0	0.0
0.0	0.0	0.0	0.0	0.0	0.0	0.0	0.0
0.0	-317334.54	105.236	2.3000e-5	1.2919e-6	0.0	0.0	0.0
0.0	-298985.55	81.379613	0.016622	-4.9127e-6	0.0	0.0	0.0

Appendix B: JC-PDS X-Ray Diffraction Cards

Aluminum Nitride
 JC-PDS Card #25-1133

3.1114		4.9792								N		X P	P1
										14E B-			2
P63mc	186	2		3.261								41.74	3
P63mc	186	2	3.17A	3.261				40.99				41.74	4
I A NBS CP FOR													5
Aluminum Nitride													P 6
Al N													7
													8
NBSMA6	12	5	1975										19
NBSMA6			Ibid.										UC 29
AMMIAY	41	355	1956 Kohn et al.										OP 39
hP	4.00												A
A=2.13, B=2.20, Sign=+													OP 1B
Very pale gray													CL 2B
Pattern at 25 C.													TM 3B
Sample from Cerac/Pure, Inc. Menomonee Falls, Wisconsin.													SM 4B
A small amount of metallic aluminum was sieved out.													5B
Major impurities: 0.01-0.1% each Fe, Mg, Si, 0.003-0.03% each Co,													C6B
Cr, Cu, Sr, Ti, 0.001-0.01% each Ca, Ni.													7B
Merck Index, 8th Ed., p. 45.													8B
To replace 8-262.													AD 9B
1.00:	1.00	0.00	0.00 / 0.00	1.00	0.00 / 0.00	0.00	1.00						C
	3.111	3.111	4.979	90.00	90.00	120.00	41.74				12		D
	3.111	3.111	4.979	90.00	90.00	120.00	1.6003						E
Cu	1.54056	E	M	DDN			W	I					F
D	1.60		SS		79.5	.0117	26	28	238.2	3.29	0		G

2.69500100	1	0	0C	2.49000	60	0	0	2C	2.37100	80	1	0	1C	01I
1.82900	25	1	0	2C	1.55590	40	1	1	0C	1.41330	30	1	0	3C 02I
1.34750	5	2	0	0C	1.31940	25	1	1	2C	1.30070	10	2	0	1C 03I
1.24500	1	0	0	4C	1.18500	4	2	0	2C	1.13010	1	1	0	4C 04I
1.04610	9	2	0	3C	1.01840	3	2	1	0C	.997800	7	2	1	1C 05I
.972000	2	1	1	4C	.942500	3	2	1	2C	.934000	6	1	0	5C 06I
.914200	1L	2	0	4C	.898200	4	3	0	0C	.868000	10	2	1	3C 07I
.844800	5	3	0	2C	.829800	1	0	0	6C	.800800	5	2	0	5C 08I
.793100	1	1	0	6C	.788200	1L	2	1	4C					09I

S	2.70/X	2.37/8	2.49/6	1.56/4	1.41/3	1.83/3	1.32/3	1.30/1	0.87/1	1.05/1+			
S	2.70/X	2.49/6	2.37/8	1.83/3	1.56/4	1.41/3	1.35/1	1.32/3	1.30/1	1.25/1*			
			EGS	86/	8/13	1	0	10	86/03/05	W-02828			K

Appendix B: JC-PDS X-Ray Diffraction Cards (continued)

Calcium Carbonate
 JC-PDS Card #24-27

4.990		17.002						N				P1			
								76E C				2			
R-3c	167		6		2.722					366.63		3			
R-3c	167		6	2.37A	2.720			100.09		366.63		4			
I M FOR			mCALsCAL									5			
Calcium Carbonate												P 16			
Calcite												M 26			
CaCO ₃												7			
												8			
00GRNT		1973	Smith et al.,	Penn State University,								C19			
			University Park,	Pennsylvania, USA.								29			
ACCRA9	18	689	1965	Chesin et al.								UC 39			
hR	10.00											A			
1.00:	1.00	0.00	0.00 / 0.00	1.00	0.00 / 0.00	0.00	1.00					C			
	4.990	4.990	6.358	66.89	66.89	60.00	122.21				9	D			
	4.990	4.990	17.002	90.00	90.00	120.00	3.4072					E			
CuKα1	1.54050			DDN		C						F			
C P			CC		265.2	.0022	22	38	524.8	0.00	0	G			
3.85200	29	0	1	2	3.03000	100	1	0	4	2.83400	2	0	0	6	01I
2.49500	7	1	1	0	2.28400	18	1	1	3	2.09400	27	2	0	2	02I
1.92610	4	0	2	4	1.90710	17	0	1	8	1.87260	34	1	1	6	03I
1.62590	2	2	1	1	1.60400	15	1	2	2	1.58210	2	1	0	10	04I
1.52470	3	2	1	4	1.50610	2	1	1	9	1.44050	5	3	0	0	05I
1.41680	3	0	0	12	1.33610	3	0	2	10	1.17790	3	2	1	10	06I
1.15360	3	1	3	4	1.14170	3	2	2	6	1.04710	2	4	0	4	07I
1.04400	2	3	1	8											08I
C	3.03/X	1.87/3	3.85/3	2.09/3	2.28/2	1.91/2	1.60/2	2.50/1	1.44/1	1.93/1+					
C	3.85/3	3.03/X	2.83/1	2.50/1	2.28/2	2.09/3	1.93/1	1.91/2	1.87/3	1.63/1*					
06/19/84			lc	86/	1/21	0	0	10	86/01/06						K

Appendix B: JC-PDS X-Ray Diffraction Cards (continued)

Calcium Oxide
 JC-PDS Card #28-775

				M	P	1
				56.08	0.00	4
I						5
Calcium Oxide					P	6
CaO						7
						8
RJICAQ 18 208 1973 Kovgan, Nakhodnova.						9
CuK α 1.5418	F Ni	DD				F
D	BB					G
3.68000 40	3.33000100	3.00000100				01I
2.52000 20	2.28000 60	2.09000 40				02I
1.91000 60	1.88000 60					03I
B 3.33/X 3.00/X 2.28/6 1.91/6 1.88/6 3.68/4 2.09/4 2.52/2 0.00/1 0.00/1+						
B 3.68/4 3.33/X 3.00/X 2.52/2 2.28/6 2.09/4 1.91/6 1.88/6 0.00/1 0.00/1*						
	EGS 86/ 4/23	0 0 10	86/03/05	W-02864		K

Appendix B: JC-PDS X-Ray Diffraction Cards (continued)

Calcium Oxide, Lime
JC-PDS Card #4-777

4.8105						N	X P	1
Fm3m	225	4		3.345			111.32	3
Fm3m	225	4	2.59A	3.346	56.08		111.32	4
I MA NBS FOR			mHALsPER					5
Calcium Oxide								P 16
Lime, syn								M 26
CaO								7
								8
NBSCAA	1	43	1953 Swanson, Tatge.					19
990005	2		Winchell.					OP 29
cF	8.00							A
Colorless								CL 1B
B=1.837								OP 2B
\Ca C O3\			obtained from J.T. Baker Chemical Company and heated at					PRC3B
			925 C in Pt crucible for 1 hour.					PR 4B
			CaO sample mixed with petrolatum.					SM 5B
			NBS analysis shows about 0.21% MgO, 0.1% Ba, and no other impurity					ANC6B
			over 0.04%.					AN 7B
			Pattern at 27 C.					TM 8B
			Merck Index, 8th Ed., p. 194.					9B
			To replace 1-1160.					AD 0B
			Deleted by 37-1497.					DB 1B
1.00:	1.00	0.00	0.00 / 0.00	1.00	0.00 / 0.00	0.00	1.00	C
	3.402	3.402	3.402	60.00	60.00	60.00	27.83	1 D
	4.811	4.811	4.811	90.00	90.00	90.00	4.8105	E
CuKα1	1.54056		F Ni	DDN50.0				F
D			SI	59.8	.0167	13	13 286.3 2.10 0	G
2.77800	34	1	1	1C	2.40500100	2	0 OC	1.70100 45 2 2 OC 01I
1.45100	10	3	1	1C	1.39000	5	2 2 2C	1.20300 4 4 0 OC 02I
1.10360	4	3	3	1C	1.07550	9	4 2 OC	.981900 9 4 2 2C 03I
.925800	3	5	1	1C	.850400	4	4 4 OC	.813100 5 5 3 1C 04I
.801800	6	6	0	OC				05I
I	2.41/X	1.70/5	2.78/3	1.45/1	1.08/1	0.98/1	0.80/1	1.39/1 0.81/1 1.20/1+
I	2.78/3	2.41/X	1.70/5	1.45/1	1.39/1	1.20/1	1.10/1	1.08/1 0.98/1 0.93/1*
				EGS 86/ 8/13	1	0 10	86/03/05	K

Appendix B: JC-PDS X-Ray Diffraction Cards (continued)

Calcium Aluminum Oxide
 JC-PDS Card #23-1036

8.698	8.092	15.208		90.14		N	X P	1	
P21/c	14A						1070.40	3	
P21/a	14B		3.12A	0.245G		158.04	1070.40	4	
I	CP							5	
Calcium Aluminum Oxide								P	6
CaAl ₂ O ₄									17
CaO • Al ₂ O ₃								S	27
									8
JACGAR 3 188 1970 Baldock et al.									9
Plus 28 lines to 1.449.								LN	1B
To replace 1-888.								AD	2B
1.00:	0.00	0.00	1.00 / 0.00	-1.00	0.00 / 1.00	0.00	0.00	C	
	8.092	8.698	15.208	90.14	90.00	90.00	1070.40	35 D	
	15.208	8.092	8.698	90.00	90.14	90.00	1.8794	1.0749 E	
CuK α	1.5418		F Ni	DDN				F	
D			IO	18.9	0.031	30	51	7.7 2.52 1* G	

7.58000	2	0	0	2C	7.17000	2	0	1	1C	5.93000	2	-1	1	0C	011
5.53000	6	-1	1	1C	4.67000	25	1	1	2C	4.38000	2	2	0	0C	021
4.35000	2	0	1	3	4.04000	10	0	2	0C	3.91000	2	0	2	1C	031
3.85000	2	1	1	3C	3.83000	2	2	1	0C	3.80000	2	0	0	4C	041
3.77000	2	2	0	2C	3.71000	16	2	1	1C	3.67000	2	-1	2	0C	051
3.57000	2	0	2	2C	3.44000	2	0	1	4C	3.42000	6	2	1	2C	061
3.30000	6	1	2	2C	3.20000	10	-1	1	4C	3.16000	6	0	2	3C	071
3.06000	6	-2	1	3C	2.97100	100	1	2	3C	2.96600	100	-2	2	0C	081
2.90800	6	-2	2	1C	2.87200	6	-2	0	4C	2.85900	2	2	0	4C	091
2.85100	10	0	1	5C	2.77400	2	0	2	4C	2.76100	6	-2	2	2C	101
2.73000	2	3	1	0C	2.70300	2	1	1	5C	2.68200	2	3	1	1C	111
2.66000	2	0	3	1C	2.64200	2	-1	2	4C	2.57600	2	1	3	0C	121
2.53400	25	1	3	1	2.51800	35	0	0	6C	2.51400	35				131
2.43900	6	1	3	2C	2.41800	16	0	1	6C	2.40400	6	-3	1	3C	141
2.39900	25	3	1	3C	2.38400	6	-2	1	5C	2.33900	6	-2	2	4C	151
2.32900	10	1	1	6C	2.29600	2	1	3	3C	2.29200	6	2	3	0C	161
2.26600	6	2	3	1C	2.24800	2	3	2	2C	2.21900	2	-3	1	4C	171
2.19900	6	0	3	4C	2.19400	10	2	3	2C	2.17400	2	4	0	0C	181
2.14600	2	0	2	6C	2.13300	10	-1	3	4C	2.11900	2	2	2	5C	191
2.10800	2	2	1	6C	2.10100	6	4	1	0C	2.09400	6	-4	0	2C	201
2.08800	6	2	3	3C	2.07800	6	4	1	1C	2.04100	2	-1	1	7C	211
2.02300	10	0	4	0C	2.00500	2	-3	2	4C	1.97300	2	-3	3	0C	221
1.96400	2	-2	3	4C	1.95800	6	3	3	1C	1.94100	6	-4	1	3C	231
1.92600	6	-2	2	6C	1.92300	16	2	2	6C	1.91400	10	0	2	7C	241
1.90100	2	0	0	8C	1.88700	2	2	1	7C	1.87000	2	-1	2	7C	251
1.85900	2	-3	1	6C	1.85400	2	3	1	6C	1.84800	2	0	3	6C	261
1.84100	2	-3	3	3C	1.83600	6	1	4	3C	1.82900	2	2	3	5C	271
1.80700	2	-1	3	6C	1.78500	2	0	4	4C	1.75300	2	-2	2	7C	281
1.74900	2	1	4	4C	1.73600	2	5	0	0C	1.72800	2	-3	2	6C	291
1.72400	2	3	2	6C	1.70100	2	-2	3	6C	1.69800	2	3	1	7C	301
1.69000	2	5	1	1C	1.68100	6	4	3	1C	1.65900	6	-3	4	0C	311

0 2.97/X 2.52/4 2.51/4 4.67/3 2.53/3 2.40/3 3.71/2 2.42/2 1.92/2 4.04/1+
 0 7.58/1 7.17/1 5.93/1 5.53/1 4.67/3 4.38/1 4.35/1 4.04/1 3.91/1 3.85/1*
 EGS 85/ 1/20 3 0 08 84/12/13 K

Appendix B: JC-PDS X-Ray Diffraction Cards (continued)

Calcium Aluminum Oxide
JC-PDS Card #23-1037

12.888	8.888	5.443		106.93		N	X P	1
C2/c	15A						596.47	3
I2/a	15C		3.08A	0.724G		260.00	596.47	4
I	CP							5
Calcium Aluminum Oxide								P 6
CaAl4O7								17
CaO • 2Al2O3								S 27
								8
JACGAR 3 188 1970 Baldock et al.								9
To replace 7-82.								AD B
1.00:	1.00	0.00	1.00 / 0.00	-1.00	0.00 / 0.00	0.00	-1.00	C
	5.443	7.828	7.828	69.18	76.13	76.13	298.23	20 D
	12.445	8.888	5.443	90.00	97.80	90.00	1.4002 0.6124	E
CuK α	1.5418		F Ni	DDN				F
D			SS	40.7	0.018	30	41 35.8 1.42 0	G

7.20000	2	-1	1	0C	6.16000	6	2	0	0C	4.61000	6	-1	1	1C	011
4.44000	55	0	2	0C	3.91000	2	1	1	1C	3.73000	2	3	1	0C	021
3.60000	20	-2	2	0C	3.50000	100	-3	1	1C	3.38000	2	0	2	1C	031
3.23000	6	-2	2	1C	3.08000	30	4	0	0C	2.88200	20	1	3	0C	041
2.75300	25	2	2	1C	2.71200	25	3	1	1C	2.59900	60	-1	3	1C	051
2.53400	15	-4	2	0C	2.46200	6	-3	1	2C	2.45200	6	1	3	1C	061
2.43600	16	-5	1	1C	2.40400	6	3	3	0C	2.35000	2	-4	0	2C	071
2.32500	10	1	1	2C	2.22200	2	0	4	0C	2.18100	6	2	0	2C	081
2.08900	2	4	2	1C	2.08300	2	-4	2	2C	2.05400	16	3	3	1C	091
2.04400	6	0	4	1C	2.00800	2	-2	4	1C	2.00000	6	-1	3	2C	101
1.96300	6	5	1	1C	1.95900	6	2	2	2C	1.93800	6	-3	3	2C	111
1.92500	2	-6	2	1C	1.90500	6	-6	0	2C	1.89600	6	5	3	0C	121
1.86800	6	1	3	2C	1.80100	10	-7	1	1C	1.76200	10	-3	1	3C	131
1.75000	2	-6	2	2C	1.72800	2	7	1	0C	1.71400	2L	-2	4	2C	141
1.68800	6	-1	5	1C	1.67800	2L	-7	1	2C	1.66400	2L	5	3	1C	151
1.64600	2L	1	5	1C	1.63700	2	-5	1	3C	1.63000	4	4	2	2C	161
1.62400	6B	-4	2	3C	1.62000	6	4	4	1C	1.61100	2	-3	5	1C	171
1.56200	2B	-7	3	1C	1.55700	4	2	4	2C	1.55200	6	5	1	2C	181
1.54000	6	-6	4	1C	1.53600	12	-3	3	3C	1.53300	10	-1	3	3C	191
1.51400	4	7	3	0C	1.50900	2	-6	4	0C	1.48000	4	-7	3	2C	201
1.46900	2	2	2	3C	1.46000	2	-3	5	2C	1.45600	2	8	2	0C	211
1.45200	2	-5	3	3C	1.44400	2L	1	3	3C	1.44000	2	2	6	0C	221
1.43000	2	1	5	2C	1.42400	2	6	0	2C	1.41300	2L	-2	6	1C	231
1.40500	2	-2	4	3C	1.37200	10B	-4	4	3C	1.36400	2	-5	5	2C	241
1.35600	2	-2	0	4C	1.35300	2	9	1	0C	1.34700	2L	-4	0	4C	251
1.33500	6	4	6	0C											261

S 3.50/X 2.60/6 4.44/6 3.08/3 2.75/3 2.71/3 3.60/2 2.88/2 2.44/2 2.05/2+
S 7.20/1 6.16/1 4.61/1 4.44/6 3.91/1 3.73/1 3.60/2 3.50/X 3.38/1 3.23/1*
EGS 84/12/19 0 0 08 84/12/13 K

Appendix B: JC-PDS X-Ray Diffraction Cards (continued)

Calcium Aluminum Oxide
JC-PDS Card #25-121

5.564		21.892			N	P	1
P63/mmc	194	2	3.840	3.779		586.94	3
P63/mmc	194	2	3.05A	3.779	667.85	586.94	4
I M		mHOG					5
Calcium Aluminum Oxide							P 16
Hibonite-5H							M 26
CaAl12O19							7
							8
ZVMOAG	90	458	1961	Ykovlevskay.			19
NJMIAK	109	192	1968	Kato, Saalfeld.			UC 29
COREAF	242	2845	1956	Curien et al.			OP 39
hP	64.00						A
A=1.79, B=1.807, Sign=-							OP 1B
Brown-black							CL 2B
O assigned because indexing unsatisfactory, pattern not similar to that for \Ca Al12 O19\.							OOC3B
(Ed.)							OO 4B
Composition may include other elements, (Ca,Ln) \ (Al , Fe , Ti , Si , Mg)12 O19\ is given by Hey, "Chemical Index of Minerals", (Appendix 1963).							C5B
							C6B
							7B
Specimen from Gornaya Shoriya, USSR.							SM 8B
Analysis (wt%): \Si O2\ 1.50, \Al2 O3\ 74.00, \Ti O2\ 8.50, \Fe2 O3\ 0.45, FeO 2.30, \Re2 O3\ 3.50, CaO 6.50, MgO 5.20.							ANC9B
Deleted by 38-469.							AN 0B
							DB 1B
1.00: 1.00 0.00 0.00 / 0.00 1.00 0.00 / 0.00 0.00 1.00							C
5.564 5.564 21.892 90.00 90.00 120.00 586.94						12	D
5.564 5.564 21.892 90.00 90.00 120.00 3.9346							E
							F
							G
V		EO	2.3	0.175	30	74	2.7 0.92 4#
4.19000 10		3.97000 10	1 0 3C	3.63000 40	1 0 4C	011	
3.33000 70		3.09000 20		2.90000 40	1 0 6C	021	
2.80300 50	1 1 0C	2.70700 50	1 1 2C	2.63500 90	1 0 7C	031	
2.49200 80	1 1 4C	2.39000 20	2 0 1C	2.35900 10	2 0 2C	041	
2.30300 30	2 0 3C	2.22500 30	1 1 6C	2.19900 40	2 0 4C	051	
2.12600 90	2 0 5C	2.02400 80	2 0 6C	1.99500 20	1 0 10C	061	
1.84500 20	1 0 11C	1.81900 40	2 1 0C	1.75300 20	2 1 3C	071	
1.72600 20	2 1 4C	1.70700 40	1 0 12C	1.63300 30	2 1 6C	081	
1.62600 30	2 0 10E	1.58500 90	3 0 2C	1.54900 90	3 0 4C	091	
1.52900 30	1 1 12C	1.45400 40	2 0 12C	1.40300100	2 1 10C	101	
1.38800 10	3 0 8C	1.37200 30	0 0 16C	1.32000 70	1 0 16C	111	
1.29200 10	3 0 10C	1.25200 10	3 0 11C	1.23700 60	2 1 13C	121	
1.22100 20	0 0 18C	1.19600 20	4 0 2C	1.18400 20	2 1 14C	131	
1.15200 30		1.14700 20	4 0 6C	1.12100 50	1 0 19C	141	
1.10000 40	3 2 2C	1.05900 40	3 2 6C	1.04800 50	3 1 13C	151	
1.03700 70	2 2 14C					161	
O 1.40/X 2.64/9 2.13/9 1.59/9 1.55/9 2.49/8 2.02/8 3.33/7 1.32/7 1.04/7+							
O 4.19/1 3.97/1 3.63/4 3.33/7 3.09/2 2.90/4 2.80/5 2.71/5 2.64/9 2.49/8*							
		EGS 88/ 2/ 1 4 0 10 86/03/05					K

Appendix B: JC-PDS X-Ray Diffraction Cards (continued)

Calcium Aluminum Oxide
 JC-PDS Card #33-252

5.23	14.45	5.41					N		P1
	0		4		3.480			408.85	P3
			4	3.17A	3.479		214.12	408.85	P4

I
 Calcium Aluminum Oxide P P6
 $Ca_2Al_2O_5$ P7
 CCNRAI 2 291 1972 Aggarwal, P. et al. P9
 o? 36.00 PA

Made by repeated sintering in Pt crucible of a 2:1 mixture of PRC1PB
 \Ca C O3\ and \Al2 O3\. PR 2PB
 Additional lines were seen at 2.66, 2.64 and 2.266 (all very weak). 3PB
 1.00: 0.00 0.00 1.00 / 0.00 -1.00 0.00 / 1.00 0.00 0.00 PC
 5.230 5.410 14.450 90.00 90.00 90.00 408.85 32 PD
 5.410 14.450 5.230 90.00 90.00 90.00 0.3744 0.3619 PE
 DDT S PF
 V II 4.4 0.031 25 186 8.0 1.65 0 PG

7.22000	50	0	2	0	3.60000	40	0	3	1	3.33000	20	1	2	1	01PI
2.70000	60	0	0	2	2.61500	60	2	0	0	2.60400	100	1	4	1	02PI
2.54800	20	0	5	1	2.40500	10	0	6	0	2.16600	50	0	4	2	03PI
2.12000	50	2	4	0	2.03000	40	1	6	1	1.88100	60	2	0	2	04PI
1.82000	40	2	2	2	1.81000	40	1	7	1	1.77300	50	2	6	0	05PI
1.68800	20	0	3	3C	1.54200	40	1	4	3C	1.48700	10	2	8	0C	06PI
1.39200	10	1	6	3C	1.36800	10	2	9	0C	1.35300	10	0	0	4C	07PI
1.32800	10	0	2	4C	1.31900	10	2	5	3C	1.30400	20	1	1	4C	08PI
1.18400	10	3	4	3C											09PI

I 2.60/X 2.70/6 2.62/6 1.88/6 7.22/5 2.17/5 2.12/5 1.77/5 3.60/4 2.03/4P+
 I 7.22/5 3.60/4 3.33/2 2.70/6 2.62/6 2.60/X 2.55/2 2.41/1 2.17/5 2.12/5P*
 02/28/79 07/22/83 tk 84/ 1/26 4 0 07 84/01/19 H-01691 PK

Appendix B: JC-PDS X-Ray Diffraction Cards (continued)

Calcium Aluminum Oxide
JC-PDS Card #33-253

5.552		21.968				N						U1
P63/mmc	194	2	3.840	3.780						586.44		3
P63/mmc	194	2	3.05A	3.782			667.85			586.44		4
I M		mHOG										5
Calcium Aluminum Oxide												P 16
Hibonite-5H, syn												M 26
CaAl12O19												7
												8
OPCOMC		1972 Dyson, British Steel Corp. Swindon Labs.,										C19
		Rotherham, England.										29
OPCOMC		1977 Morgan, P., University of Pittsburgh,										UCC39
		Pittsburgh, Pennsylvania, USA.										UC 49
CRSAAT 242 2845 1956		Curien et al.										OP 59
AMMIAY 42 119 1957												OP 69
hP 64.00												A
Lattice parameters calculated from strong high angle lines 220, 0214.												UCC1B
Ca \$GB-alumina.												UC 2B
To replace 25-122.												3B
A=1.79, B=1.807, Sign=-												AD 4B
Brown-black												OP 5B
Deleted by 38-470.												CL 6B
												DB 7B
1.00: 1.00 0.00 0.00 / 0.00 1.00 0.00 / 0.00 0.00 1.00												C
5.552 5.552 21.968 90.00 90.00 120.00 586.44											12	D
5.552 5.552 21.968 90.00 90.00 120.00 3.9568												E
CoK α 1.7902		M	DDN	G								F
F		IB			8.6 0.085 30 41 11.3-1.59 2							G

10.9000	3L	0	0	2	5.47000	3L	0	0	4	4.82000	3L	0	1	0	01I
4.70000	3L	0	1	1	4.40800	3L	0	1	2	4.01900	5	0	1	3	02I
3.64700	5	0	0	6M	3.64700	5	0	1	4M	3.23900	3L	0	1	5	03I
2.90700	10	0	1	6	2.78100	55	1	1	0	2.73500	15	0	0	8	04I
2.69500	3	1	1	2	2.62200	100	0	1	7	2.47900	100	1	1	4	05I
2.40800	5	0	2	0	2.39400	5	0	2	1	2.37800	20	0	1	8	06I
2.35200	20				2.34700	20	0	2	2	2.28700	30	0	2	3	07I
2.21100	10	1	1	6	2.20400	10	0	2	4	2.18800	10	0	0	10M	08I
2.18800	10	0	1	9M	2.11000	60	0	2	5	2.01000	35	0	2	6	09I
1.90800	3L	0	2	7	1.83800	5	0	1	11M	1.83800	5	0	0	12M	10I
1.80700	5	0	2	8	1.72000	3L	1	1	10	1.71100	5	0	2	9M	11I
1.71100	5	0	1	12M	1.68100	3L	1	2	5	1.62900	3L	1	2	6	12I
1.61900	5	0	2	10	1.61800	5				1.60500	5	0	3	0	13I
1.58900	3L	0	3	2	1.57300	45	1	2	7M	1.57300	45	0	0	14M	14I
1.56300	5	0	3	3	1.54000	15	0	3	4	1.53400	65	0	2	11	15I
1.52500	3L	1	1	12	1.51500	20	1	2	8	1.48700	3L	0	1	14	16I
1.46900	3L	0	3	6	1.45400	5	1	2	9M	1.45400	5	0	2	12M	17I
1.38800	70	2	2	0M	1.38800	70	0	3	8M	1.38000	10	0	2	13M	18I
1.38000	10	2	2	2M	1.34700	3L	2	2	4M	1.34700	3L	1	2	11M	19I
1.31400	20	0	2	14M	1.31400	20	1	3	3M						20I

B 2.62/X	2.48/X	1.39/7	1.53/7	2.11/6	2.78/6	1.57/5	2.01/4	2.29/3	2.38/2+
B 10.9/1	5.47/1	4.82/1	4.70/1	4.41/1	4.02/1	3.65/1	3.24/1	2.91/1	2.78/6*
12/77	07/22/83 tk	86/ 1/21	1	0 10	86/01/06	W-03572			K

Appendix B: JC-PDS X-Ray Diffraction Cards (continued)

Calcium Aluminum Oxide
 JC-PDS Card #9-413

11.982										N	X P	P1
										41E B-		2
I-43d	220		2		2.676						1720.24	3
I-43d	220		2	3.16A	2.677			1386.68			1720.24	4
I M	NBS CP											5
	Calcium Aluminum Oxide											P 16
	Mayenite, syn											M 26
	Ca ₁₂ Al ₁₄ O ₃₃											7
	12CaO · 7Al ₂ O ₃											8
	NBSCAA 9 20 1960											9
	cI 118.00			\12 Ca0.7 Al2 O3\								A
	Colorless											CL 1B
	Sample prepared by Portland Cement Association Fellowship at the NBS.											SMC2B
												SM 3B
	Spectrographic analysis showed the following impurities: 0.1-1.0% each of Na, Si, Sr; 0.01-0.1% Fe, Mg; 0.001-0.01% each of Cu, Mn, Mo.											ANC4B
												ANC5B
												AN 6B
	Pattern made at 25 C.											TM 7B
1.00:	1.00	0.00	0.00	/	0.00	1.00	0.00	/	0.00	0.00	1.00	C
	10.377	10.377	10.377	109.47	109.47	109.47	860.12					5 D
	11.982	11.982	11.982	90.00	90.00	90.00	11.9820					E
CuKα1	1.54056		F Ni	DDX								F
D			SS		51.0	.0159	30 37	57.7-0.95	0			G

4.89000	95	2	1	1C	4.24000	6	2	2	0C	3.79000	16	3	1	0C	01I
3.20400	25	3	2	1C	2.99800	45	4	0	0C	2.68000	100	4	2	0C	02I
2.55600	18	3	3	2C	2.44700	50	4	2	2C	2.35000	10	5	1	0C	03I
2.18900	40	5	2	1C	2.05400	10	5	3	0C	1.94500	30	6	1	1C	04I
1.85000	8	5	4	1C	1.76700	6	6	3	1C	1.73000	12	4	4	4C	05I
1.69500	8	7	1	0C	1.66200	30	6	4	0C	1.63000	10	7	2	1C	06I
1.60100	30	6	4	2C	1.52200	6	6	5	1C	1.49800	6	8	0	0C	07I
1.47500	8	7	4	1C	1.39300	18	7	5	0C	1.35600	4	7	5	2C	08I
1.34000	8	8	4	0C	1.30700	8	8	4	2C	1.29200	6	7	6	1C	09I
1.27700	6	6	6	4C	1.26300	6	9	3	0C	1.23600	4	9	3	2C	10I
1.21000	6	9	4	1C	1.17500	2	10	2	0C	1.14300	4	10	3	1C	11I
1.11200	8	10	4	0C	1.09400	6	10	4	2C	1.08500	4	11	1	0C	12I

S	2.68/X	4.89/X	2.45/5	3.00/5	2.19/4	1.95/3	1.66/3	1.60/3	3.20/3	2.56/2+
S	4.89/X	4.24/1	3.79/2	3.20/3	3.00/5	2.68/X	2.56/2	2.45/5	2.35/1	2.19/4*
			EGS	86/ 8/13	0	0	10	86/03/05		K

Appendix B: JC-PDS X-Ray Diffraction Cards (continued)

Aluminum

JC-PDS Card #4-787

4.0494					N	X P	1
Fm3m	225	4		2.697		66.40	3
Fm3m	225	4	2.70A	2.699	26.98	66.40	4
I MA NBS CP FOR			mGOLsGOL				5
Aluminum						P	16
Aluminum						M	26
Al							7
							8
NBSCAA	1	11	1953	Swanson, Tatge.			9
cF	4.00						A
Tin white						CL	1B
The material used for the NBS sample was a melting point Standard						PRC2B	
Sample of aluminum prepared in the chemistry laboratories of NBS.						PR	3B
The chemical analysis (%): Si 0.011, Cu 0.006, Fe 0.007, Ti						ANC4B	
0.0001, Zr 0.003, Ga 0.004, Mo 0.00002, S 0.0001, Al 99.9 + (by						ANC5B	
difference).						AN	6B
Pattern at 25 C.						TM	7B
Merck Index, 8th Ed., p. 42.							8B
Mineral species of doubtful validity, Am. Mineral., 65, 205 (1980).							9B
1.00: 1.00 0.00 0.00 / 0.00 1.00 0.00 / 0.00 0.00 1.00							C
2.863 2.863 2.863 60.00 60.00 60.00 16.60						1	D
4.049 4.049 4.049 90.00 90.00 90.00 4.0494							E
CuKa1 1.54056		F Ni	DDN				F
D		SS		92.8 .0108	9 9	592.0 0.22 0	G
2.33800100	1 1	1C	2.02400 47	2 0	0C	1.43100 22 2 2	0C 01I
1.22100	24 3 1	1C	1.16900 7	2 2	2C	1.01240 2 4 0	0C 02I
.928900	8 3 3	1C	.905500 8	4 2	0C	.826600 8 4 2	2C 03I
S 2.34/X 2.02/5 1.22/2 1.43/2 0.93/1 0.91/1 0.83/1 1.17/1 1.01/1 0.00/1+							
S 2.34/X 2.02/5 1.43/2 1.22/2 1.17/1 1.01/1 0.93/1 0.91/1 0.83/1 0.00/1*							
			EGS 87/ 7/17	0 0 10	86/03/05		K

Appendix B: JC-PDS X-Ray Diffraction Cards (continued)

Aluminum Chloride
 JC-PDS Card #1-1133

5.93	10.24	6.17		108.00		N	X P	1	
C2/m	12A	4	2.44	2.48			356.32	3	
A2/m	12B	4	2.25A	2.486		133.34	356.32	4	
I								5	
Aluminum Chloride							P	6	
AlCl ₃								7	
								8	
ANCHAM	10	475	1938	Hanawalt et al.				19	
RJRSDK	66	501	1947	Ketelaar et al.				UC 29	
mC	16.00							A	
192.5\$DE								MP 1B	
Colorless								CL 2B	
Dm, melting point and color from Data on Chemicals for Ceramic Use,								C3B	
National Research Council Bulletin 107.								4B	
S.P. 180.2.								5B	
B.P. 182.7 (752 mm).								6B	
1.00: 0.00 0.00	1.00 / 0.00	-1.00	0.00 / 1.00	0.00	0.00			C	
5.917 5.917	6.170	98.91	98.91	119.85	178.16		14	D	
6.170 10.240	5.930	90.00	108.00	90.00	0.6025	0.5791		E	
MoKα1 0.709	F	DD	X 16.0					F	
X	BB	3.5	0.024	19	220	3.3	0.60	0	
5.80000 64	0 0	1C	5.10000 14	0 2	0C	2.93000 40	0 0	2C 01I	
2.80000 64	-1 3	1C	2.46000 100	1 3	1C	1.92000 14	1 3	2C 02I	
1.77000 20	-2 4	2C	1.71000 64	-3 3	1C	1.64000 11	0 6	1C 03I	
1.47000 32	-3 3	3C	1.40000 24	-2 6	2C	1.28000 6	0 8	0C 04I	
1.23000 10	2 6	2C	1.17000 3	-5 1	1C	1.11000 20	-4 6	2C 05I	
1.09000 16	2 6	3C	1.02000 5	-5 5	1C	.990000 8	-6 0	2C 06I	
.970000 10	-6 2	2C						07I	
B 2.46/X	5.80/6	2.80/6	1.71/6	2.93/4	1.47/3	1.40/2	1.77/2	1.11/2	1.09/2+
B 5.80/6	5.10/1	2.93/4	2.80/6	2.46/X	1.92/1	1.77/2	1.71/6	1.64/1	1.47/3*
		EGS 85/	1/13	1	0	08	84/12/13		K

Appendix B: JC-PDS X-Ray Diffraction Cards (continued)

Aluminum Chloride
 JC-PDS Card #22-10

5.93	10.24	6.17		108.00		N	P	P1
C2/m	12A	4		2.490			356.32	3
A2/m	12B	4	2.25A	2.486		133.34	356.32	4
I FOR NBS								5
Aluminum Chloride								P 6
AlCl ₃								7
								8
NBSMA6 9 1971								19
RTCPA3 66 501 1947 Ketelaar et al.								UC 29
mC 16.00								A
Plus 3 lines to 0.963.								LN B
1.00:	0.00	0.00	1.00 / 0.00	-1.00	0.00 / 1.00	0.00	0.00	C
	5.917	5.917	6.170	98.91	98.91	119.85	178.16	14 D
	6.170	10.240	5.930	90.00	108.00	90.00	0.6025 0.5791	E
CuKα1 1.54056								F
DDT C								
C P		CC		55.1	.0094	30	58 63.5-0.51	0 G

5.86000100	0	0	1C	5.12000	12	0	2	0C	4.94000	20	1	1	0C	01I	
4.41000	12	-1	1	1C	3.86000	6	0	2	1C	3.36000	2	1	1	1C	02I
2.93000	30	0	0	2C	2.92000	19	-1	3	0C	2.89000	1	-1	1	2C	03I
2.82000	31	2	0	0C	2.80000	56	-1	3	1C	2.46200	96	1	3	1C	04I
2.44500	50	-2	0	2C	2.20700	1	-2	2	2C	2.08400	1	2	2	1C	05I
1.95600	1	0	0	3C	1.92900	2	0	4	2C	1.92200	11	1	3	2C	06I
1.90700	6	-2	0	3C	1.89500	2	-2	4	0C	1.83600	1	-3	1	2C	07I
1.78700	1	-2	2	3C	1.77700	10	2	0	2C	1.76000	18	-1	3	3C	08I
1.71000	20	-3	3	1C	1.70700	20	0	6	0C	1.67900	1	2	2	2C	09I
1.64700	2	3	3	0C	1.63800	4	-3	3	2C	1.51700	2	1	3	3C	10I
1.50600	1	-2	0	4C	1.48400	3	3	3	1C	1.47500	3	0	6	2C	11I
1.47100	3	-3	3	3C	1.46700	4	0	0	4C	1.46000	3	-2	6	0C	12I
1.42000	1	-4	2	1C	1.41500	2	2	0	3C	1.41000	4	4	0	0C	13I
1.40400	5	-1	3	4C	1.40000	8	-2	6	2C	1.28400	1	3	5	1C	14I
1.27200	1	-2	6	3C	1.23100	3	2	6	2C	1.22300	1	-4	0	4C	15I
1.17400	1	0	0	5C	1.11900	2	3	3	3C	1.11200	2	1	5	4C	16I
1.10800	2	-3	3	5C	1.08900	1	-3	7	3C	1.08700	2	4	6	0C	17I
1.08400	3	1	9	1C	1.08300	2	-5	3	3C	1.08100	2	-4	0	5C	18I
1.00300	1	5	3	1C	.995000	1	-1	9	3C	.994000	1	-4	6	4C	19I
.988000	1	-5	5	0C	.986000	1	-3	9	1C						20I

C 5.86/X 2.46/X 2.80/6 2.45/5 2.82/3 2.93/3 4.94/2 1.71/2 2.92/2 1.76/2+
 C 5.86/X 5.12/1 4.94/2 4.41/1 3.86/1 3.36/1 2.93/3 2.92/2 2.89/1 2.82/3*
 EGS 86/ 8/13 1 0 10 86/03/05 W-00233 K

Appendix B: JC-PDS X-Ray Diffraction Cards (continued)

Calcium

JC-PDS Card #23-430

5.5886									N	P	PP2
Fm3m	225		4			1.525				174.55	3
Fm3m	225		4	1.53A		1.525		40.08		174.55	4
I A NBS											5
Calcium										P	6
Ca											7
											8
NBSMA6	9	68	1971								1 9
ACCRA9	12	419	1959	Berstein, Smith.							UC 2 9
cF	4.00										A
To replace	1-0735,	22-520.									AD B
1.00:	1.00	0.00	0.00 / 0.00	1.00	0.00 / 0.00	0.00	1.00				C
	3.952	3.952	3.952	60.00	60.00	60.00	43.64			1	D
	5.589	5.589	5.589	90.00	90.00	90.00	5.5886				E
CuKα1	1.5405			2DN		C					F
C P			CC	141.8	.0067	17	18	652.8	2.03	0	G
3.22681100	1	1	1C	2.79443	46	2	0	0C	1.97537	23	2 2 0C 01 I
1.68509	23	3	1	1C	1.61321	6	2	2	2C	1.39701	2 4 0 0C 02 I
1.28196	6	3	3	1C	1.24970	5	4	2	0C	1.14077	3 4 2 2C 03 I
1.07550	3	5	1	1C	.987923	1	4	4	0C	.944593	2 5 3 1C 04 I
.931398	1	6	0	0C	.883591	1	6	2	0C	.852250	1 5 3 3C 05 I
.842490	1	6	2	2C	.782521	2	5	5	1C		06 I
C	3.23/X	2.79/5	1.98/2	1.69/2	1.61/1	1.28/1	1.25/1	1.14/1	1.08/1	1.40/1	+
C	3.23/X	2.79/5	1.98/2	1.69/2	1.61/1	1.40/1	1.28/1	1.25/1	1.14/1	1.08/1	*
			EGS	86/	8/13	0	0	10	86/03/05		K

Appendix B: JC-PDS X-Ray Diffraction Cards (continued)

Calcium

JC-PDS Card #10-348

4.486									T	N		X	P	1
Im3m	229		2		1.50	E						90.28		3
Im3m	229		2	1.53A	1.474			40.08				90.28		4
I A														5
Calcium													P	6
Ca														7
														8
JESQAN 103	409	1956	Smith et al.											9
cI	2.00													A
Pattern at	467	C.												TM 1B
Spectroscopic analysis:	C<0.02;	Mg,	N<0.01;	Si<0.005;	Al,	B,	Ba,							ANC2B
Fe<0.001;	Cd,	Li,	K,	Na<0.0001.										AN 3B
Stable above	464	C.												4B
1.00:	1.00	0.00	0.00 / 0.00	1.00	0.00 / 0.00	0.00	1.00							C
	3.885	3.885	3.885	109.47	109.47	109.47	45.14					5		D
	4.486	4.486	4.486	90.00	90.00	90.00	4.4860							E
CuKα1	1.5405		F Ni	DDX										F
D			IB		4.9	0.159	7	9	27.6	0.00	0			G
3.15000	100	1	1	OC	2.23000	20	2	0	OC	1.83000	40	2	1	1C 01I
1.58000	18	2	2	OC	1.41500	12	3	1	OC	1.19700	14	3	2	1C 02I
1.05700	5	3	3	OC										03I
BT3.15/X	1.83/4	2.23/2	1.58/2	1.20/1	1.42/1	1.06/1	0.00/1	0.00/1	0.00/1	0.00/1	0.00/1	0.00/1	0.00/1	+
BT3.15/X	2.23/2	1.83/4	1.58/2	1.42/1	1.20/1	1.06/1	0.00/1	0.00/1	0.00/1	0.00/1	0.00/1	0.00/1	0.00/1	*
		EGS 85/	1/20	1	0	08	84/12/13							K

Appendix B: JC-PDS X-Ray Diffraction Cards (continued)

Calcium Chloride
JC-PDS Card #12-56

		M	X P	1
		110.99	0.00	4
I				5
Calcium Chloride			P	6
CaCl ₂				7
				8
ZAACAB 276	72	1954	Werner.	9
Sample prepared by heating pure Ca with CaCl ₂ at 1000°C and quenched.				PRC1B
Colorless in absence of \N ₂ \.				PR 2B
CuKα 1.5418	F Ni	DD		3B
V	BB			F
				G
2.65000100	2.49300 90	2.39600 90		01I
2.21000 90	2.12500 10	1.64100 40		02I
1.60100 10	1.50600 40	1.40500 20		03I
1.36900 10	1.23100 50	1.20100 40		04I
1.05800 70	1.02800 20	.918000 10		05I
.902000 90				06I
B 2.65/X 2.49/9 2.40/9 2.21/9 0.90/9 1.06/7 1.23/5 1.64/4 1.51/4 1.20/4+				
B 2.65/X 2.49/9 2.40/9 2.21/9 2.13/1 1.64/4 1.60/1 1.51/4 1.41/2 1.37/1*				
	EGS 85/ 1/29	0 0 08 84/12/13		K

Appendix B: JC-PDS X-Ray Diffraction Cards (continued)

Calcium Chloride Hydrate
JC-PDS Card #1-1104

			M	X P	1
			129.00	0.00	4
I	FOR				5
Calcium Chloride Hydrate				P	6
CaCl ₂ · H ₂ O					7
CaCl ₂ H ₂ O					8
ANCHA ^M 10 475 1938 Hanawalt et al.					9
260\$DE				MP	1B
Colorless				CL	2B
Melting point and color from Handbook of Chemistry and Physics.					3B
MoKα1 0.709	F	DD	X 16.0		F
X		BB			G
5.90000 40	4.38000 12	3.41000 12			01I
3.22000 24	3.03000 40	2.81000 24			02I
2.55000 100	2.40000 24	2.26000 60			03I
2.17000 4	2.11000 28	1.93000 12			04I
1.69000 4	1.60000 12	1.53000 8			05I
1.50000 12	1.46000 4	1.41000 4			06I
1.36000 12					07I
B 2.55/X 2.26/6 5.90/4 3.03/4 2.11/3 3.22/2 2.81/2 2.40/2 4.38/1 3.41/1+					
B 5.90/4 4.38/1 3.41/1 3.22/2 3.03/4 2.81/2 2.55/X 2.40/2 2.26/6 2.17/1*					
	EGS 85/ 1/13	0 0 08 84/12/13			K

Appendix B: JC-PDS X-Ray Diffraction Cards (continued)

Calcium Chloride Hydrate
JC-PDS Card #1-989

7.21	5.86		M	X P	1
			147.02	0.00	4
I M CP FOR					5
Calcium Chloride Hydrate					P 16
Sinjarite, syn					M 26
CaCl ₂ · 2H ₂ O					7
CaCl ₂ H ₄ O ₂					8
ANCHAM 10 475 1938 Hanawalt et al.					9
Colorless					CL 1B
Color: Handbook of Chemistry and Physics.					2B
MoKα1 0.709	F	DD	X 16.0		F
X	BB				G
6.10000 40	4.35000 50	3.06000 70			01I
2.83000 100	2.69000 16	2.52000 20			02I
2.35000 20	2.26000 16	2.16000 24			03I
2.12000 60	2.01000 8	1.87000 20			04I
1.78000 12	1.71000 12	1.67000 16			05I
1.62000 4	1.52000 4	1.47800 16			06I
1.40800 4					07I
B 2.83/X 3.06/7 2.12/6 4.35/5 6.10/4 2.16/2 2.52/2 2.35/2 1.87/2 2.69/2+					
B 6.10/4 4.35/5 3.06/7 2.83/X 2.69/2 2.52/2 2.35/2 2.26/2 2.16/2 2.12/6*					
	EGS 85/ 1/13	0 0 08 84/12/13			K

Appendix B: JC-PDS X-Ray Diffraction Cards (continued)

Calcium Chloride Hydrate
JC-PDS Card #25-1035

6.593	6.364	8.557	97.77	93.52	110.56	N		P	P1
0.002	0.005	0.003	0.05	0.04	0.03	47	B-		2
P-1	2		2		1.838			330.78	3
P-1	2		2	1.80A	1.838		183.05	330.78	4
I	NBS CP	FOR							5
	Calcium Chloride Hydrate								P 6
	CaCl ₂ · 4H ₂ O								7
	CaCl ₂ H ₈ O ₄								8
	NBSMA6	11	73	1974					19
	ACBCAR	29	615	1973	Thewalt, Bugg.				UC 29
	aP	30.00							A
1.00:	-1.00	0.00	0.00 / 0.00	0.00	-1.00 / 0.00	-1.00	0.00		C
	6.364	6.593	8.557	93.52	97.77	110.56	330.78	44	D
	6.593	8.557	6.364	97.77	110.56	93.52	0.7705	0.7437	E
				DDN		C			F
C P			CC	102.5	.0073	30	40	46.5-2.22	0 G

6.13000	51	1	0	0C	5.87000	91	0	1	0C	5.31000	29	-1	1	0C	01I
5.25000	27	0	-1	1C	4.70000	28	1	0	1C	4.60000	100	1	-1	1C	02I
4.48000	3	0	1	1C	4.40000	2	-1	1	1C	3.72900	9	0	-1	2C	03I
3.63300	15	1	1	0C	3.56700	53	-1	-1	1C	3.38300	4	1	-1	2C	04I
3.29500	38	1	0	2C	3.24300	4	-2	1	0C	3.22200	16	-1	1	2C	05I
3.18000	22	0	1	2C	3.12900	34	-1	2	0C	3.06400	33	2	0	0C	06I
3.05600	24	1	-2	1C	3.02100	6	-1	-1	2C	2.99600	38	-2	0	1C	07I
2.93800	62	0	2	0C	2.93000	42	0	-2	1C	2.82600	31	-1	2	1C	08I
2.80600	23	0	0	3C	2.77800	4	2	0	1C	2.71500	71	0	-1	3C	09I
2.66700	9	1	-2	2C	2.65700	22	-2	2	0C	2.62900	74	-2	0	2C	10I
2.60900	21	-2	1	2C	2.57200	19	2	-2	1C	2.53500	9	1	-1	3C	11I
2.49800	14	-2	2	1C	2.44500	6	1	0	3C	2.43300	10	-1	1	3C	12I
2.39800	29	-2	-1	1C	2.38200	65	0	1	3C	2.35000	18	2	0	2C	13I
2.30000	17	2	-2	2C	2.23900	22	0	2	2C	2.23400	26	-2	-1	2C	14I
2.22400	16	0	-2	3C	2.21900	30	-1	-2	2C	2.20500	62	2	1	1C	15I
2.19800	60	-2	2	2C	2.19300	25	-3	1	0C	2.15600	30	1	2	1C	16I
2.10500	8	0	0	4C	2.10000	8	-1	3	0C	2.09600	8	0	-1	4C	17I
2.09000	26	2	-1	3C	2.06600	16	-3	2	0C	2.05500	6	1	1	3C	18I
2.04100	6	-3	0	1C	2.00400	30	2	-3	1C	1.99900	18	-3	1	2C	19I
1.99400	6	1	-3	2C	1.98000	6	-2	-1	3C						20I

C 4.60/X 5.87/9 2.63/7 2.72/7 2.38/7 2.94/6 2.21/6 2.20/6 3.57/5 6.13/5+
C 6.13/5 5.87/9 5.31/3 5.25/3 4.70/3 4.60/X 4.48/1 4.40/1 3.73/1 3.63/2*
EGS 86/ 8/13 0 0 10 86/03/05 W-02420 K

Appendix B: JC-PDS X-Ray Diffraction Cards (continued)

Calcium Chloride Hydrate
JC-PDS Card #25-1090

6.593	6.364	8.557	97.77	93.52	110.56	N	X P	1							
						70E C		2							
P-1	2	2	1.850	1.837			330.78	3							
P-1	2	2	1.80A	1.838		183.05	330.78	4							
I								5							
Calcium Chloride Hydrate							P	6							
CaCl ₂ · 4H ₂ O								7							
CaCl ₂ H ₈ O ₄								8							
ANCHAM	10	475	1938	Hanawalt et al.				19							
ACBCAR	29	615	1973	Thewalt, Bugg.			UC	29							
ACBCAR				Ibid.			OP	39							
aP	30.00							A							
A=1.548, B=1.566							OP	1B							
Colorless							CL	2B							
Pattern indexed at Department of Physics, University College, Cardiff, Wales.								C3B							
To replace 1-1080.								4B							
								AD 5B							
1.00: -1.00	0.00	0.00 / 0.00	0.00	-1.00 / 0.00	-1.00	0.00		C							
6.364	6.593	8.557	93.52	97.77	110.56	330.78	44	D							
6.593	8.557	6.364	97.77	110.56	93.52	0.7705	0.7437	E							
Mo	0.70930	E	F	DDN	S 16.0			F							
F			II		3.1	0.032	21 209	1.8-0.27 0							
6.00000	27	0	1	0C	5.20000	20	0 -1	1C	4.70000	42	1	0	1C	01I	
3.58000	27	-1	-1	1C	3.30000	13	1	0	2C	3.02000	13	-1	-1	2C	02I
2.94000	13	0	2	0C	2.81000	42	0	0	3C	2.72000	27	0	-1	3C	03I
2.63000	100	-2	0	2C	2.39000	42	2	1	0C	2.22000	67	-1	-2	2C	04I
2.16000	13	-2	1	3C	2.08000	20	2	-1	3C	2.00000	27	-3	1	2C	05I
1.91000	7	1	2	2C	1.75000	13	0	-3	3C	1.70000	7	1	1	4C	06I
1.62000	7	-4	2	0C	1.57000	7	-3	1	4C	1.49000	13	0	-4	1C	07I
I	2.63/X	2.22/7	4.70/4	2.81/4	2.39/4	6.00/3	3.58/3	2.72/3	2.00/3	5.20/2+					
I	6.00/3	5.20/2	4.70/4	3.58/3	3.30/1	3.02/1	2.94/1	2.81/4	2.72/3	2.63/X*					
			EGS 85/	2/13	1	0	08	84/12/13							K

Appendix B: JC-PDS X-Ray Diffraction Cards (continued)

Calcium Chloride Hydrate
JC-PDS Card #26-1053

7.876		3.9555						N		X P	P1		
								46E B-			2		
P321	150		1	1.712	1.712					212.49	3		
P321	150		1	1.69A	1.712			219.08		212.49	4		
I M	NBS CP	FOR									5		
	Calcium Chloride Hydrate										P 16		
	Antarcticite, syn										M 26		
	CaCl ₂ · 6H ₂ O										7		
	CaCl ₂ · H ₁₂ O ₆										8		
	NBSMA6	12	16	1975							9		
	hP	21.00									A		
	A=1.492, B=1.550, Sign=-										OP 1B		
	Colorless										CL 2B		
	Pattern at 25 C.										3B		
	Isostructural with \Sr Cl ₂ · 6 H ₂ O\ and other hexahydrates of										STC4B		
	alkaline earth halides.										ST 5B		
	Made by slow evaporation at room temperature of \Ca Cl ₂ \ solution.										PR 6B		
	Since sample was hygroscopic intensities varied up to 15%.										7B		
	Merck Index, 8th Ed. p. 181.										8B		
	To replace 1-1220.										AD 9B		
1.00:	1.00	0.00	0.00	/	0.00	1.00	0.00	/	0.00	0.00	1.00	C	
	3.955	7.876	7.876	120.00	90.00	90.00	212.49			22		D	
	7.876	7.876	3.955	90.00	90.00	120.00	0.5022					E	
CuKα1	1.54056		M		DDN		Ag		I			F	
D			SS			39.5	.0161	28	44	57.1	2.41	0	G

6.80000	35	1	0	0C	3.93000	90	1	1	0C	3.42000	65	1	0	1C	01I
2.79200	75	1	1	1C	2.58200	60	2	0	1C	2.27300	60	3	0	0C	02I
2.15900	100	2	1	1C	1.97700	20	0	0	2C	1.89900	12	1	0	2C	03I
1.76700	8	1	1	2C	1.71100	10	2	0	2C	1.70600	25	3	1	1C	04I
1.56900	12	2	1	2C	1.56600	12	4	0	1C	1.49200	20	3	0	2C	05I
1.48800	25	4	1	0C	1.45500	10	3	2	1C	1.39600	9	2	2	2C	06I
1.39290	9	4	1	1C	1.36750	5	3	1	2C	1.31290	3	3	3	0C	07I
1.29460	5	1	0	3C	1.29150	4	4	0	2C	1.25050	2	1	1	3C	08I
1.22950	7	2	0	3C	1.22560	5	4	2	1C	1.18950	5	4	1	2C	09I
1.17430	4	2	1	3C											10I

S	2.16/X	3.93/9	2.79/8	3.42/7	2.58/6	2.27/6	6.80/4	1.71/3	1.49/3	1.98/2+	
S	6.80/4	3.93/9	3.42/7	2.79/8	2.58/6	2.27/6	2.16/X	1.98/2	1.90/1	1.77/1*	
			EGS 86/	8/13	1	0	10	86/03/05			K

Appendix B: JC-PDS X-Ray Diffraction Cards (continued)

Calcium Chloride Hydroxide Hydrate
 JC-PDS Card #2-1099

	M	X P	UI
	203.10	0.00	4
I CP FOR			5
Calcium Chloride Hydroxide Hydrate			P 6
CaCl ₂ · Ca(OH) ₂ · H ₂ O			7
Ca ₂ Cl ₂ H ₄ O ₃			8
OPCOMC Michigan Alkali Company, Wyandotte, Michigan.			9
Laboratory preparation.			B
CuKα 1.541			F
	DD		G
	BB		
4.92000 50	3.32000 20	3.15000 90	01I
2.75000 20	2.46000 20	2.34000 100	02I
1.92000 70	1.79000 30	1.68000 10	03I
1.64000 20	1.52000 30	1.49000 40	04I
1.30000 30	1.27000 20	1.17000 40	05I
B 2.34/X 3.15/9 1.92/7 4.92/5 1.49/4 1.17/4 1.79/3 1.52/3 1.30/3 3.32/2+			
B 4.92/5 3.32/2 3.15/9 2.75/2 2.46/2 2.34/X 1.92/7 1.79/3 1.68/1 1.64/2*			
EGS 85/ 1/13 0 0 08 84/12/13			K

Appendix B: JC-PDS X-Ray Diffraction Cards (continued)

Calcium Chloride Nitride
JC-PDS Card #12-57

			M	X P	1					
			169.70	0.00	4					
I					5					
Calcium Chloride Nitride				P	6					
Ca ₃ NCl					7					
					8					
ZAACAB 276	72	1954	Werner.		9					
CuK α	1.5418	F Ni	DD		F					
V		BB			G					
3.03000	30	2.59900	100	2.46000	10					
2.33600	10	2.14900	40	1.91300	90					
1.77300	70	1.68200	60	1.54100	20					
1.38600	40	1.35100	60	1.31800	10					
1.27300	10	1.13500	20	1.08500	40					
1.04900	10	.949000	20	.937000	90					
.916000	10	.863000	40							
					01I					
					02I					
					03I					
					04I					
					05I					
					06I					
					07I					
B	2.60/X	1.91/9	1.77/7	0.94/9	1.68/6	1.35/6	2.15/4	1.39/4	1.09/4	0.86/4+
B	3.03/3	2.60/X	2.46/1	2.34/1	2.15/4	1.91/9	1.77/7	1.68/6	1.54/2	1.39/4*
			EGS 85/	1/29	0	0	08	84/12/13		K

Appendix B: JC-PDS X-Ray Diffraction Cards (continued)

Calcium Chloride Nitride
JC-PDS Card #17-815

			M	X P	1
			129.62	0.00	4
I					5
Calcium Chloride Nitride				P	6
Ca ₂ NCI					7
					8
ZAACAB 333 99 1964 Emons et al.					9
To be deleted by P-23247.				DB	B
CuK α 1.5418	F Ni	DD			F
V	BB				G
2.64100100	2.44600 80	2.17300 30			01I
2.07800 10	1.92700 50	1.81900100			02I
1.68500 10	1.55400 10	1.49400 50			03I
1.46500 10	1.40300 80	1.36700 50			04I
1.32900 30	1.28800 10	1.18900 10			05I
1.16700 50	1.14800 30				06I
B 2.64/X 1.82/X 2.45/8 1.40/8 1.93/5 1.49/5 1.37/5 1.17/5 2.17/3 1.33/3+					
B 2.64/X 2.45/8 2.17/3 2.08/1 1.93/5 1.82/X 1.69/1 1.55/1 1.49/5 1.47/1*					
	EGS 84/10/11	0 0 08 84/09/26			K

Appendix B: JC-PDS X-Ray Diffraction Cards (continued)

gamma Calcium Nitride
 JC-PDS Card #21-153

17.82	11.56	3.58								N	X P	1			
	0		8	2.63	2.67						737.48	3			
			8	2.44A	2.671					148.25	737.48	4			
I A												5			
Calcium Nitride											P	6			
γ -Ca ₃ N ₂												7			
												8			
RVCMA8	5	1019	1968	Laurent.								9			
o?	40.00	\$GG										A			
Yellow												CL 1B			
Measured density and color given by Moissan, Compt. Rend. Acad. Sci., 127, 497 (1898).												C2B			
1.00:	0.00	1.00	0.00	-1.00	0.00	0.00	0.00	0.00	0.00	1.00		C			
	3.580	11.560	17.820	90.00	90.00	90.00	737.48				32	D			
	11.560	17.820	3.580	90.00	90.00	90.00	0.6487	0.2009				E			
CuK α	1.5418											F			
				IB			1.2	0.102	24	194	1.5-0.20	0			
												G			
8.92000	65	2	0	OC	6.95000	15	2	1	OC	5.94000	15	3	0	OC	01I
3.32000	25	2	0	1C	3.07000	30	3	0	1C	2.97000	15	6	0	OC	02I
2.87000	35	6	1	OC	2.79000	100	4	0	1C	2.77000	10	2	4	0	03I
2.70000	20	3	2	1C	2.58000	30	1	3	1C	2.49000	70	7	1	OC	04I
2.42000	30	4	4	OC	2.27000	70	4	3	1C	2.02000	10	4	4	1C	05I
1.86000	30	8	1	1C	1.79000	25	0	0	2C	1.74000	30	2	1	2C	06I
1.66500	10	2	6	1C	1.64000	20	3	2	2C	1.57500	25	9	3	1C	07I
1.52000	15	6	1	2C	1.48000	20	2	7	1C	1.45000	30	7	1	2C	08I
B	2.79/X	2.49/7	2.27/7	8.92/7	2.87/4	3.07/3	2.58/3	2.42/3	1.86/3	1.74/3+					
B	8.92/7	6.95/2	5.94/2	3.32/3	3.07/3	2.97/2	2.87/4	2.79/X	2.77/1	2.70/2*					
				EGS	84/11/13	1	0	08	84/09/26						K

Appendix B: JC-PDS X-Ray Diffraction Cards (continued)

Calcium Chloryl Nitride Hydrate
JC-PDS Card #21-836

6.86		12.62						N		X P	1	
P31,212	*151									514.33	3	
P31,212	*151							0.00		514.33	4	
I											5	
Calcium Chloryl Nitride Hydrate											P 6	
CaNC1O ₃ · xH ₂ O											7	
RJICAQ 13	508	1968	Kolesnikov.								9	
1.00:	1.00	0.00	0.00 / 0.00	1.00	0.00 / 0.00	0.00	1.00				C	
6.860	6.860	12.620	90.00	90.00	120.00	514.33				12	D	
6.860	6.860	12.620	90.00	90.00	120.00	1.8397					E	
CuKα	1.5418		F Ni	DD		S 57.3					F	
V			BO		0.7	0.188	15	117	1.6	1.95	3#	G

6.00000	60	1	0	0C	3.45000	40	1	0	3C	3.01000	100	1	1	2C	01I
2.78800	100	1	0	4C	2.14700	60	2	0	4C	1.86200	60				02I
1.76300	40				1.71000	40	2	2	0C	1.68400	20	2	1	5C	03I
1.46600	40	3	1	4C	1.40300	10	0	0	9C	1.37500	10	3	1	5C	04I
1.31500	40				1.24500	20	2	2	7C	1.22000	10	3	1	7C	05I
1.19200	10	2	1	9C	1.13000	10	1	0	11C	1.07200	10	2	0	11C	06I

0	3.01/X	2.79/X	6.00/6	2.15/6	1.86/6	3.45/4	1.76/4	1.71/4	1.47/4	1.32/4+	
0	6.00/6	3.45/4	3.01/X	2.79/X	2.15/6	1.86/6	1.76/4	1.71/4	1.68/2	1.47/4*	
			EGS	84/11/13	8	0	08	84/09/26			K

Appendix C: Experimental X-ray Diffraction Data

ALUMINUM NITRIDE POWDER

INITIAL 2 θ = 10.000° Δ 2 θ = 0.050° Δ TIME= 1.00 SEC
SM= 0 BKGR= 0 0 0 K $_{\alpha 2}$ =0 λ =1.540598 Å
SCH= 9 SENS=3.00 C \bar{E} NTR \bar{O} ID= 7 NT= 5

<u>Peak</u>	<u>2θ (°)</u>	<u>d-spacing(Å)</u>	<u>Peak Intensity (%)</u>
1	12.644	6.9954	1.5
2	13.596	6.5076	1.3
3	16.308	5.4310	1.6
4	18.946	4.6803	1.3
5	33.101	2.7041	100.0
6	35.916	2.4984	59.3
7	37.814	2.3772	80.0
8	49.710	1.8326	28.0
9	59.252	1.5583	45.6
10	65.952	1.4152	38.3

Appendix C: Experimental X-ray Diffraction Data (continued)

SPRAY DRIED ALUMINUM NITRIDE POWDER

INITIAL $2\theta = 10.000^\circ$ $\Delta 2\theta = 0.050^\circ$ $\Delta \text{TIME} = 1.00 \text{ SEC}$
 SM= 0 BKGR= 0 0 0 $K_{\alpha 2} = 0$ $\lambda = 1.540598 \text{ \AA}$
 SCH= 9 SENS=3.00 CENTROID= 7 NT= 5

<u>Peak</u>	<u>2θ ($^\circ$)</u>	<u>d-spacing(\AA)</u>	<u>Peak Intensity (%)</u>
1	19.253	4.6064	6.0
2	23.496	3.7833	5.2
3	24.950	3.5660	2.8
4	29.547	3.0208	8.4
5	33.390	2.6814	100.0
6	36.203	2.4792	59.1
7	38.101	2.3600	76.9
8	39.603	2.2739	2.9
9	47.691	1.9054	2.8
10	48.609	1.8715	3.1
11	49.999	1.8227	27.1
12	59.510	1.5521	42.2
13	66.208	1.4104	32.8

Appendix C: Experimental X-ray Diffraction Data (continued)

SINTERED ALUMINUM NITRIDE

INITIAL 2 θ = 10.000° Δ 2 θ = 0.050° Δ TIME= 1.00 SEC
 SM= 0 BKGR= 0 0 0 $K_{\alpha 2}$ =0 λ =1.540598 Å
 SCH= 9 SENS=3.00 CENTROID= 7 NT= 5

<u>Peak</u>	<u>2θ (°)</u>	<u>d-spacing(Å)</u>	<u>Peak Intensity (%)</u>
1	16.440	5.3877	2.7
2	19.889	4.4605	2.7
3	21.254	4.1770	1.8
4	22.647	3.9231	1.7
5	24.597	3.6164	2.4
6	25.233	3.5266	4.1
7	25.861	3.4424	3.5
8	26.150	3.4050	3.3
9	26.688	3.3376	2.2
10	28.842	3.0930	2.2
11	30.048	2.9716	1.5
12	30.893	2.8922	2.2
13	33.105	2.7038	100.0
14	34.407	2.6044	3.1
15	35.186	2.5485	2.8
16	35.942	2.4966	60.9
17	37.818	2.3770	83.8
18	39.139	2.2998	1.4
19	40.708	2.2147	1.9
20	41.502	2.1741	1.3
21	49.719	1.8323	28.4
22	51.886	1.7608	1.2
23	59.264	1.5580	51.1
24	60.511	1.5288	2.0
25	65.967	1.4150	43.6

Appendix C: Experimental X-ray Diffraction Data (continued)

CALCIUM CHLORIDE SALT EXPOSED ALUMINUM NITRIDE CRUCIBLE

INITIAL 2 θ = 10.000° Δ 2 θ = 0.050° Δ TIME= 1.00 SEC
 SM= 0 BKGR= 0 0 0 K $_{\alpha 2}$ =0 λ =1.540598 Å
 SCH= 9 SENS=3.00 CENTROID= 7 NT= 5

<u>Peak</u>	<u>2θ (°)</u>	<u>d-spacing(Å)</u>	<u>Peak Intensity (%)</u>
1	16.501	5.3679	2.9
2	24.002	3.7046	2.0
3	26.148	3.4053	4.3
4	29.060	3.0703	1.7
5	30.144	2.9623	2.8
6	31.040	2.8788	2.6
7	33.300	2.6884	100.0
8	35.268	2.5428	3.0
9	36.133	2.4839	61.0
10	38.032	2.3641	88.0
11	40.908	2.2043	2.8
12	49.908	1.8258	35.1
13	57.598	1.5990	1.5
14	59.448	1.5536	57.3
15	60.756	1.5232	2.0
16	66.146	1.4116	47.3

Appendix C: Experimental X-ray Diffraction Data (continued)

CALCIUM METAL/CALCIUM CHLORIDE SALT EXPOSED ALUMINUM NITRIDE
CRUCIBLE

INITIAL 2 θ = 10.000° Δ 2 θ = 0.050° Δ TIME= 1.00 SEC
SM= 0 BKGR= 0 0 0 K $_{\alpha 2}$ =0 λ =1.540598 Å
SCH= 9 SENS=3.00 CENTROID= 7 NT= 5

<u>Peak</u>	<u>2θ (°)</u>	<u>d-spacing(Å)</u>	<u>Peak Intensity (%)</u>
1	16.460	5.3812	2.9
2	23.856	3.7270	1.9
3	26.151	3.4049	3.3
4	26.428	3.3698	3.3
5	30.152	2.9616	2.9
6	31.138	2.8700	2.1
7	31.480	2.8396	2.1
8	33.310	2.6877	100.0
9	35.309	2.5399	2.8
10	36.147	2.4830	62.8
11	38.043	2.3635	88.7
12	40.913	2.2040	2.5
13	42.830	2.1097	1.5
14	49.916	1.8256	33.0
15	57.639	1.5980	1.5
16	59.458	1.5533	52.7
17	60.795	1.5223	2.2
18	66.152	1.4115	47.7

Appendix C: Experimental X-ray Diffraction Data (continued)

CALCIUM CARBONATE POWDER

INITIAL 2 θ = 10.000° Δ 2 θ = 0.050° Δ TIME= 1.00 SEC
 SM= 0 BKGR= 0 0 0 $K_{\alpha 2}$ =0 λ =1.540598 Å
 SCH= 9 SENS=3.00 CENTROID= 7 NT= 5

Peak	2 θ (°)	d-spacing(Å)	Peak Intensity (%)
1	10.349	8.5410	1.6
2	12.996	6.8067	1.3
3	14.500	6.1039	1.6
4	15.345	5.7696	1.0
5	19.650	4.5142	0.8
6	22.834	3.8914	6.0
7	26.352	3.3794	0.7
8	29.205	3.0554	100.0
9	31.249	2.8601	2.5
10	35.759	2.5090	10.8
11	39.158	2.2987	15.7
12	42.861	2.1083	11.8
13	45.295	2.0005	0.5
14	47.063	1.9294	5.3
15	47.125	1.9270	18.9
16	48.113	1.8897	15.3
17	56.059	1.6392	2.6
18	56.904	1.6168	4.9
19	57.554	1.6001	1.0
20	60.150	1.5371	3.4
21	60.798	1.5223	2.0
22	62.463	1.4856	1.2
23	64.060	1.4524	3.0
24	65.009	1.4335	2.6
25	68.563	1.3676	0.9
26	69.568	1.3503	1.2

Appendix C: Experimental X-ray Diffraction Data (continued)

LOS ALAMOS CALCIUM CHLORIDE SALT

INITIAL 2 θ = 10.000° Δ 2 θ = 0.050° Δ TIME= 1.00 SEC
 SM=15 BKGR= 0 0 0 $K_{\alpha 2}$ =0 λ =1.540598 Å
 SCH= 9 SENS=3.00 CENTROID= 7 NT= 5

Peak	2 θ (°)	d-spacing(Å)	Peak Intensity (%)
1	15.098	5.8634	14.1
2	20.298	4.3715	55.7
3	21.448	4.1397	11.2
4	26.148	3.4053	15.1
5	29.750	3.0007	100.0
6	30.751	2.9052	13.3
7	31.748	2.8162	31.9
8	32.401	2.7609	34.2
9	36.596	2.4535	8.9
10	38.863	2.3154	43.7
11	39.052	2.3047	62.3
12	40.648	2.2178	29.6
13	42.448	2.1278	10.1
14	43.251	2.0902	16.6
15	43.899	2.0608	25.3
16	45.100	2.0087	8.9
17	46.301	1.9593	7.7
18	48.151	1.8883	29.2
19	49.150	1.8522	18.4
20	51.447	1.7748	12.8
21	52.701	1.7355	7.9
22	55.095	1.6656	13.3
23	59.694	1.5478	8.3
24	61.100	1.5155	15.5
25	62.596	1.4828	8.5
26	63.696	1.4598	8.7
27	65.553	1.4229	6.4

Appendix C: Experimental X-ray Diffraction Data (continued)

LOS ALAMOS MOLTEN CALCIUM CHLORIDE SALT

INITIAL 2 θ = 10.000° Δ 2 θ = 0.050° Δ TIME= 1.00 SEC
 SM=11 BKGR= 0 0 0 $K_{\alpha 2}$ =0 λ =1.540598 Å
 SCH= 9 SENS=3.00 CENTROID= 7 NT= 5

Peak	2 θ (°)	d-spacing(Å)	Peak Intensity (%)
1	14.991	5.9050	23.5
2	18.653	4.7532	7.7
3	20.161	4.4009	100.0
4	20.801	4.2670	27.7
5	21.297	4.1687	18.2
6	22.790	3.8989	11.5
7	26.001	3.4242	7.0
8	29.597	3.0158	58.0
9	30.646	2.9149	20.3
10	31.601	2.8290	24.5
11	32.206	2.7772	69.8
12	33.643	2.6618	8.0
13	34.049	2.6310	7.5
14	36.395	2.4666	11.7
15	38.504	2.3362	29.0
16	39.001	2.3076	43.5
17	39.945	2.2552	15.8
18	40.544	2.2232	23.0
19	42.197	2.1399	14.5
20	43.096	2.0973	26.9
21	44.944	2.0153	6.5
22	47.997	1.8940	12.8
23	48.755	1.8663	10.0
24	49.496	1.8401	13.2
25	51.308	1.7793	6.5
26	51.894	1.7605	8.0
27	53.450	1.7129	5.0
28	54.242	1.6897	8.0
29	55.198	1.6627	10.2
30	56.606	1.6247	4.8
31	59.447	1.5536	4.6
32	60.952	1.5188	6.3
33	61.547	1.5055	7.1
34	62.350	1.4881	6.1
35	63.450	1.4649	9.8
36	65.501	1.4239	5.7

Appendix C: Experimental X-ray Diffraction Data (continued)

LOS ALAMOS MOLTEN CALCIUM METAL/CALCIUM CHLORIDE SALT

INITIAL 2 θ = 10.000° Δ 2 θ = 0.050° Δ TIME= 1.00 SEC
 SM=15 BKGR= 0 0 0 $K_{\alpha 2}$ =0 λ =1.540598 Å
 SCH= 9 SENS=3.00 CENTROID= 7 NT= 5

Peak	2 θ (°)	d-spacing(Å)	Peak Intensity (%)
1	14.698	6.0221	29.0
2	19.244	4.6085	11.5
3	19.849	4.4694	25.2
4	20.558	4.3168	39.6
5	21.051	4.2168	22.4
6	22.600	3.9312	7.8
7	24.250	3.6673	7.3
8	27.703	3.2176	28.9
9	28.644	3.1140	16.4
10	29.352	3.0404	72.0
11	30.349	2.9428	20.2
12	31.351	2.8510	15.2
13	32.008	2.7939	100.0
14	32.385	2.7623	34.7
15	33.845	2.6464	15.2
16	36.159	2.4822	18.0
17	38.348	2.3454	24.4
18	38.898	2.3134	20.7
19	39.948	2.2550	16.0
20	41.853	2.1567	19.5
21	42.900	2.1064	36.1
22	44.693	2.0260	9.2
23	45.904	1.9753	16.5
24	47.699	1.9051	10.2
25	48.599	1.8719	14.4
26	49.306	1.8467	17.9
27	51.548	1.7715	11.4
28	53.298	1.7174	8.2
29	54.005	1.6966	13.5
30	54.950	1.6696	13.7
31	61.302	1.5110	9.8
32	63.154	1.4710	13.4
33	66.700	1.4012	6.3

Appendix C: Experimental X-ray Diffraction Data (continued)

ROCKY FLATS TECHNICAL GRADE CALCIUM CHLORIDE SALT

INITIAL 2 θ = 10.000° Δ 2 θ = 0.050° Δ TIME= 1.00 SEC
 SM=0 BKGR= 0 0 0 $K_{\alpha 2}$ =0 λ =1.540598 Å
 SCH= 9 SENS=3.00 CENTROID= 7 NT= 5

<u>Peak</u>	<u>2θ (°)</u>	<u>d-spacing(Å)</u>	<u>Peak Intensity (%)</u>
1	11.898	7.4323	13.7
2	14.816	5.9744	37.9
3	15.529	5.7017	26.9
4	19.396	4.5728	19.8
5	20.001	4.4358	44.0
6	20.746	4.2781	41.5
7	21.257	4.1764	28.2
8	22.143	4.0113	14.7
9	24.397	3.6456	14.0
10	25.858	3.4428	13.2
11	28.701	3.1079	18.0
12	29.493	3.0262	100.0
13	30.541	2.9247	21.3
14	31.669	2.8231	29.7
15	32.141	2.7827	91.4
16	33.493	2.6734	27.5
17	34.001	2.6346	14.8
18	34.644	2.5872	28.8
19	35.603	2.5196	34.4
20	36.336	2.4705	30.5
21	37.006	2.4273	17.8
22	38.451	2.3393	36.9
23	38.805	2.3188	38.2
24	39.502	2.2795	23.2
25	40.494	2.2259	26.4
26	41.303	2.1841	17.0
27	42.055	2.1468	21.6
28	42.393	2.1305	26.5
29	43.043	2.0998	41.8
30	43.606	2.0740	19.1
31	44.806	2.0212	13.3
32	45.689	1.9841	14.2
33	46.603	1.9473	9.1
34	47.813	1.9008	21.3
35	48.852	1.8628	19.4
36	49.412	1.8430	17.3
37	51.107	1.7858	10.2
38	51.697	1.7668	12.9
39	53.435	1.7133	10.2
40	54.104	1.6937	13.8
41	55.006	1.6681	14.2
42	58.033	1.5881	10.9
43	60.892	1.5202	10.7
44	62.295	1.4892	10.0
45	63.250	1.4690	14.3
46	69.254	1.3556	9.4

Appendix C: Experimental X-ray Diffraction Data (continued)

ROCKY FLATS MOLTEN CALCIUM METAL/CALCIUM CHLORIDE SALT

INITIAL 2 θ = 10.000° Δ 2 θ = 0.050° Δ TIME= 1.00 SEC
 SM=0 BKGR= 0 0 0 K $_{\alpha 2}$ =0 λ =1.540598 Å
 SCH= 9 SENS=3.00 CENTROID= 7 NT= 5

<u>Peak</u>	<u>2θ (°)</u>	<u>d-spacing(Å)</u>	<u>Peak Intensity (%)</u>
1	11.498	7.6899	28.4
2	14.750	6.0010	37.9
3	18.006	4.9225	23.6
4	19.991	4.4380	50.0
5	20.649	4.2980	39.7
6	21.186	4.1903	31.2
7	22.935	3.8745	19.3
8	24.304	3.6593	15.6
9	26.453	3.3667	49.5
10	28.295	3.1516	28.4
11	29.441	3.0314	100.0
12	30.443	2.9339	26.6
13	31.452	2.8421	32.2
14	32.058	2.7897	87.9
15	33.090	2.7050	81.2
16	34.508	2.5970	40.5
17	34.913	2.5678	83.2
18	36.201	2.4794	23.6
19	36.985	2.4286	63.3
20	38.496	2.3367	53.0
21	38.756	2.3216	61.3
22	39.957	2.2545	86.2
23	40.394	2.2312	48.2
24	41.305	2.1840	24.4
25	41.944	2.1522	24.1
26	42.949	2.1042	39.9
27	43.554	2.0763	18.3
28	46.100	1.9674	23.4
29	47.929	1.8965	29.6
30	48.696	1.8684	25.9
31	49.391	1.8437	24.1
32	52.692	1.7357	15.8
33	54.085	1.6943	24.9
34	54.954	1.6695	20.9
35	55.452	1.6557	24.9
36	58.184	1.5843	13.6
37	60.663	1.5253	26.6
38	61.594	1.5045	22.6
39	65.264	1.4285	14.8
40	66.254	1.4095	19.3